MASTER

The design of an aluminium jam of noise barriers along (motor) ways

Duru, E.

Award date:
2016

Graduation project:	**'**The design of an aluminium jam of noise barriers along (motor) ways'
Report:	Master thesis
Date:	February 2016
Student:	Eren Duru | 0755686
	Department of the Built Environment
	Unit Structural Design
Graduation committee:	prof. dr. ir. J. Maljaars
	Ir. Hove, B.W.E.M. van
	Ir. R. Blok
Supervisor from Graduation Company:	R.C. van Kemenade

TU/e Technische Universiteit
Eindhoven
University of Technology

Table of contents

Graduation report of E. Duru for a Master thesis submitted to the Department of the Built Environment at Eindhoven University of Technology in partial fulfillment of the requirements for the degree of Master of Science.

'The design of an aluminium jam of noise barriers along (high) ways'

Name: Eren Duru | 0755686

Address: Urkhovenseweg 34
                       5641 KG Eindhoven

Phone number: +31 6 81 94 12 02

TU/e Technische Universiteit Eindhoven University of Technology

1. Introduction

Most noise barriers near roads or rail tracks consist of jams (vertical members) and posts (horizontal members) supporting the shields. In present day systems the posts are, in most cases, made of aluminium whilst the jams are still made of steel. It may be beneficial to construct the entire structure out of aluminium for reasons such as simplifying the assembly and creating a system with a lower self-weight. Therefore, the aim of the project is the development of a detailed design and validation thereof through calculation, of an aluminium noise barrier, focusing on the jam and its connections to the post and to the foundation. Important issues are the ease of erection, minimization of material needs, series production, fatigue and ultimate resistance, and dynamic response.

Figure 1.1.1 shows the elements of the IPG modular noise barriers, which are designed and applied by Van Campen Industries B.V. for the HSL at A12 between Gouda and Moerdijk. Blue indicates the jams, red for the posts.
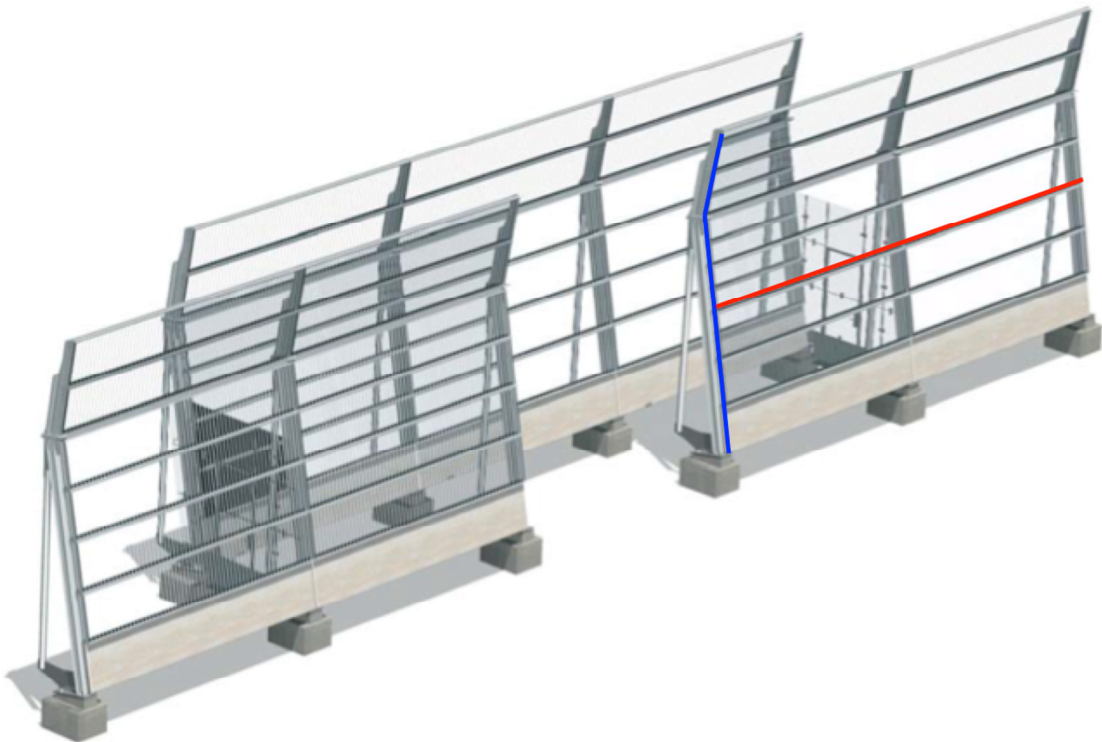
Figure 1.1.1: IPG Modular noise barrier Van Campen Industries B.V.

The project will be carried out in collaboration with Van Campen Industries. The thesis is submitted to the Department of the Built Environment at the Eindhoven University of Technology in partial fulfillment of the requirements for the degree of Master of Science.

The main reason I have chosen this topic is my interest in subjects where it is possible to combine a cross-sectional design with structural calculations. The second reason is my curiosity in the phenomenon of dynamics. Designing a cross-section and dynamics are not a part of my current study and specialization. Therefore, I see these topics as a challenge to complete my study with. I also see this subject as an opportunity to develop an out of the box specialization.

1.1. Reading guide

In first part of this report, the problem (section 2), and the goal (section 3) of this research will be described. Section 4 gives the project analysis of present day noise barriers, in this section also the conclusions and opportunities for the aluminium design will be briefly discussed based on the literature survey. The following section, section 5, will be about aluminium alloys. In section 6 some design principles of aluminium jams will be considered, at the end of this section a choice will be made for one design principle, which will be considered during this report. Section 7 gives some aluminium cross-sections, which are considered in the cross-section design process.

Afterwards, the static (section 8) and the dynamic calculations (section 9) of the jams will be provided. The static fatigue calculations are based on the design guide Eurocode [1][2][3][4] and GCW-2012 [5]. The Eurocode is a design guideline that is used in Europe and GCW-2012 is a design guideline for designing a noise barrier that is only used in the Netherlands. The dynamic fatigue analysis is based on a power spectral density analysis, which makes use of Dirlik's approach [6].

Section 10 gives the comparison between the noise barrier with a steel jam and a noise barrier with an aluminium jam. In the last part of this report recommendations are given.

2. Problem

2.1. Problem description

If the loads vary over time, the stresses and displacements will vary over time as well. As a rule, for buildings and most civil engineering structures, these variations are assumed to happen slowly over time. Under these circumstances, a statistical analysis suffices when it comes to the calculations, as considered in section 8.

But in some civil engineering structures, especially in light structures, it is possible for the loads to fluctuate much more over a much smaller period of time. The fluctuating behaviour of wind is shown in Figure 2.1.1. This causes an increase in the stresses and can cause damaging vibrations within the structure. Wind is one of these loads. Given the fact that the steel jams will be replaced by a lighter alternative, it is possible that the problem described earlier may occur. In such situations an additional dynamic analysis is necessary, this will be provided in section 9.
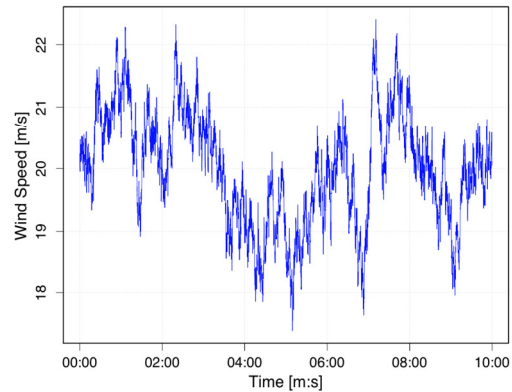
Figure 2.1.1: Fluctuating behaviour of wind

The fatigue endurance limit

This problem is caused by the phenomenon called fatigue. In a steel structure, fatigue is normally not considered for general structure (fatigue is not usually the limiting criteria). Aluminum however, is subject to fatigue failure (referred to as its endurance limit) more readily than steel, as compared in Figure 2.1.2. Fatigue failure is classified as an ultimate limit state. Regular static ultimate limit design involves a check of the extreme value of the load against the ultimate resistance of a structural element. In fatigue design, however, the occurring load fluctuations must be checked against the fatigue resistance. In the latter case, the stress range, i.e. the difference between the maximum and minimum occurring stress, is essential for fatigue design.

In this specific case, the ratio between the fatigue strength and ultimate resistance of the aluminium connection is low. In addition due to the low self-weight the life load consumes a large portion of the total load. This makes that fatigue is relatively important for aluminium structures and it may govern the design. Fatigue should always be checked in case of a structure subjected to fluctuating loads.
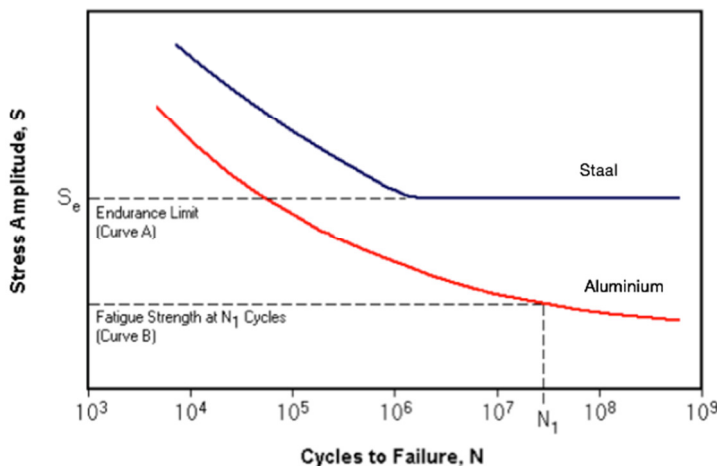
Figure 2.1.2: Endurance limit

2.2. Problem statement

The problem statement is as follow: is it possible to develop a viable aluminium alternative to replace the existing steel jam of noise barrier, which has a fatigue life of 50 years?

The three most important sub-questions are formulated as follows:

- How do the frequencies of the stress responses of the structure relate to the frequencies of the dynamic wind loads?
- How to the dynamic- and statistical fatigue calculations compare, and what is the reliability of the methods?
- Should it be mandatory for structural engineers to conduct a dynamic analysis, or does it suffice to perform the analysis as described in Eurocode [1]?

3. Goal

The goal of this research project is to develop a viable aluminium jam which meets the following requirements:

- Requirement regarding load: the jam's light dead load allows the jam to be installed manually, with a maximum of two employees, at the construction site. The maximum lifting weight for one employee according to the Europe guideline NEN-EN 1005-2:2003+A1:2008 is 25 kg. Based on this rule, the maximum allowable dead load of the jam can be easily calculated, namely: 2x25 = 50 kg;
- Requirement regarding assembly: using extrusion techniques several functionalities have been integrated in the cross section of the jam, which reduces the assembly time compared to the steel alternative;
- Maintenance: a maintenance free period of 30 years is desired. During this period the aluminium jam will remain resistant to structure damaging corrosion;
- Requirements regarding strength, stiffness, and stability: the structure may not buckle or show undesired behavior due to fluctuating loads during its life –time of 50 years.

4. Project analysis

In this section the conclusions and opportunities for the aluminium design will be briefly discussed based on the literature survey (Annex B).

In the project analysis and literature survey four different structures of noise barriers have been discussed. The purpose of this project analysis was to acquire insights in the connections between the jams and the posts, and the connections between the jams and the foundation. In order to clearly mark the weaknesses of the connections of the steel jam.

Briefly, the building principles of different connections of the reference projects will be discussed. Also the opportunities for an aluminium alternative will be given in this section.

4.1. Building principles

Connection between the jam and the post

First the connection between the jam and the post will be considered. In the first three variants it is not possible to make a direct connection between these two elements, for this connection a connecting element (e.g. kikker profile, clamping profile or a side-post) is required as shown in Figures 4.1.1 – 4.1.3.

Figure 4.1.1: ''kikker profile''   Figure 4.1.2.: Clamping profile   Figure 4.1.3: side-post
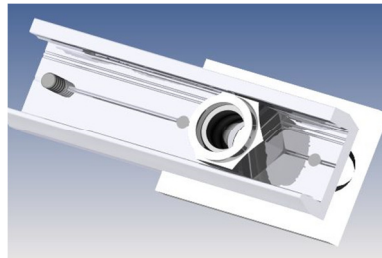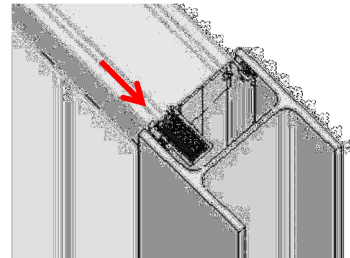
In variant 4, which is a prototype of an aluminium jam, the connection between the jam and the post can be made without using a connecting element. This is possible because of the space between the flanges of the profile. Through extrusion it is possible to produce very complex aluminium cross-sections with relative ease.

Connection between the jam and the foundation

The second connection is the connection between the jam and the footing plate. The jams of variants 1, 2 and 3 are connected to the concrete barrier using footing plate, anchors, and nuts. The footing plates are welded to the jams. The holes in the footing plate are aligned with the anchors sticking out from the concrete barrier. The footing plate is placed on the concrete barrier and then secured and set using the nuts. Reinforcements can be welded onto the jam and footing plate if deemed necessary.

As opposed to the previous variants, in variant 4 this connection is not realized through welding. In this variant the choice has been made to extrude screw-tubes in the longitudinal direction of the jam. Afterwards screwing the bolts into the screw-tubes (with a special design) leads to a manually inserted thread in the aluminium profile that fits the thread of the bolt. The footing plate can then be attached to the jam by sticking bolts through the holes in the footing plate into these screw-tubes and can then be tightened. After the footing plate has been attached to the jams the resulting

structure can then be attached to the concrete barrier in a similar fashion as the previously discussed variants (by means of anchors and nuts).

4.2. Opportunities

Because of the two different materials steel (jams) and aluminium (posts), which are used in the structure (variant 1, 2, 3), it is not possible to connect the elements without using additional connecting elements. By designing the jams in aluminium, a direct connection of the posts with the jams will be made possible using the extrusion technique. This way the assembly will be simplified and also the assembly time will be faster compared to the steel design.

Additionally, the almost unlimited range of shapes using extrusion technique makes welded joints unnecessary. This also simplifies the assembly and reduces the assembly time.

The extrusion technique is considered in Annex B.

5. Aluminium alloys

Pure aluminium is a relatively soft metal. The predominant reasons for alloying a metal are to increase strength, hardness, resistance to wear, creep, stress relaxation, and fatigue. The low strength of pure aluminium limits its commercial usefulness, therefore aluminium alloys are developed. The tensile yield strength of high-purity aluminium is roughly 10 MPa while some heat-treated commercial high strength alloys have yield strengths greater than 550 MPa. With respect to 'non-heat treatable' aluminium alloys, by definition, these are alloys that do not gain an appreciable increase in strength with heat treatment, and this is primarily because these alloys do not experience precipitation hardening. This is related to their composition.

Choosing the correct aluminium alloy is a crucial passage that might determine the success of a product. According to NEN-EN 1999-1-1 article C.2 [4] the following aluminium alloys have suitable extrusion properties and are suitable for structural design:

- from 6xxx series EN AW-6082, EN AW-6061, EN AW-6005A, EN AW-6106, EN AW-6063, EN AW-6060;
- from 7xxx series EN AW-7020.

The alloys are internationally registered under an ID that consists of a four-digit number. In Europe, the relevant European Standard EN 573-1 requires the following format:

EN AW-xxxx with: EN = European Standard, A = Aluminium, W = Wrought

In addition, a temper must be added, this follows the four-digit number separated by a hyphen, the format is thus as follows: EN AW-xxxx-Xxx.

In this section a brief summary will be given of the chosen aluminium alloys for the structure (jam + footing plate). In the Annex B a detailed description of different alloys, the meaning of the tempers and comparisons between alloys are given.

The jam

As mentioned before, the 7xxx and 6xxx series are both alloys which are suitable for aluminium extrusions. In this section, a brief conclusion regarding the material of the structure will be given.

The 7xxx series was not chosen for the design of the jam, despite its high yield stress. This is due to the fact that this alloy is very tough which makes it hard to extrude. Also, a profile extruded from a 7020 alloy is very rough which makes it unsuitable for anodization. This alloy is mostly used for hidden structures.

The 6xxx alloys are heat treatable, and have moderately high strength coupled with excellent corrosion resistance. They are easily welded. A unique feature is the alloy's extrudability, making them the first choice for architectural and structural members where unusual or particularly strength- or stiffness-criticality is important. The material properties of the 6xxx – Al-Mg-Si alloy are given below [7]:

- Heat treatable;
- High corrosion resistance, excellent extrudability, moderate strength;
- Building & construction, highway, automotive, marine applications;
- Representative alloys: 6061, 6063, 6111;
- Typical ultimate tensile strength range: 18-58 ksi.

Different applications of the 6xxx series are shown below, taken from other projects.

Figure 5.1.1: The power of extruded Al-Mg-Si alloys is the ''pit-the-metal-where-you need-it'' flexibility that these alloys and the extrusion process provide.

Figure 5.1.2: Roof structures for arenas and gymnasiums are usually 6063 or 6061 extruded tube covered with a 5xxx alloy sheet.

Figure 5.1.3: Geodesic domes, such as this one made originally to house the ''Spruce Goose'', a prototype heavy strategic airlift military transport aircraft, in Long Beach CA, the largest geodesic dome ever constructed at around 305 m across and 122 m high.

Figure 5.1.1: Extruded profiles   Figure 5.1.2: Roof structures   Figure 5.1.3: Geodesic dome

In accordance with NEN-EN 1999-1-1 Table 3.2b [4] a choice has been made for the aluminium alloy which will be used for the Jams. Because of the suitable mechanical properties and very suitable extrusion properties aluminium EN AW-6063-T6 is selected, see Annex B for a detailed description.

The footing plate

Because there is no formability needed in the design of the footing plate, it is not useful to use the same alloy for the footing plate as used for the jams. In this case, it is useful to select an alloy which has better mechanical properties. The alloy from the 5xxx series is non heat-treatable and exhibits the best combination of high strength with resistance to corrosion.

Alloys 5052, 5086, and 5083 are the work horses from the structural standpoint, with increasingly higher strength associated with the increasingly higher Mg content. The material properties of the 5xxx – Al-Mg alloy are given below [7]:

- Strain hardenable;
- Excellent corrosion resistance, toughness, weldability, moderate strength;
- Building & construction, automotive, cryogenic, marine applications;
- Representative alloys: 5052, 5083, 5754;
- Typical ultimate tensile strength range: 18-51 ksi.

In accordance with NEN-EN 1999-1-1 Table 3.2a [4] a choice has been made for the aluminium alloy which will be used for the footing plate. Because of the highest value for the yield stress in comparison with other 5xxx series alloys, alloy EN AW 5083 H14 is selected for the material of the footing plate. As such, the required strength of the footing plate can be met with a minimum usage of material.

6. Design principles of the system

Based on the reference project analysis a couple of design principles have been determined for the aluminium variant, as shown in Figure 6.1.1 below. The design of the cross-section of the jam will be discussed in section 7. The principles, advantages, and disadvantages of each of the philosophies will be considered in this section. Finally, a design principle shall be chosen.
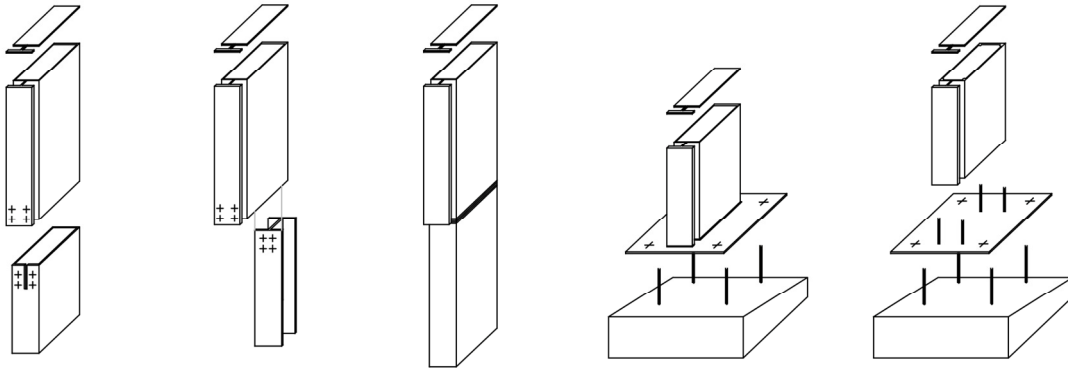
Figure 6.1.1: design principles of the aluminium jam

6.1. Design principle 1

The structure in this design consists entirely of aluminium, as shown in Figure 6.1.2. The extruded profile is partially rammed into the ground. The top part, also an extruded element, can then be slit into the bottom part via a telescope connection. Using bolts both elements can be fixed to each other. By using extrusion additional flanges are extruded, which allows the shield to be slid into the profile. Thermal expansion is also taken into consideration. As long as the gap between the end of the shield and then web of the flange is large enough, this will not be a problem. Extrusion can also be used to create a profile for the base part, which fits over the jam (telescope connection).

Advantages:

- Because of the lightweight structure of the top and bottom element, the entire structure can be moved manually without using cranes. However, it should be mentioned that the maximum weight of an element does not exceed 50 kg (see starting point 3);
- Using extrusion techniques space between the flanges are created which reduces the assembly time compared to the steel alternative;
- A system which consist only of aluminium.
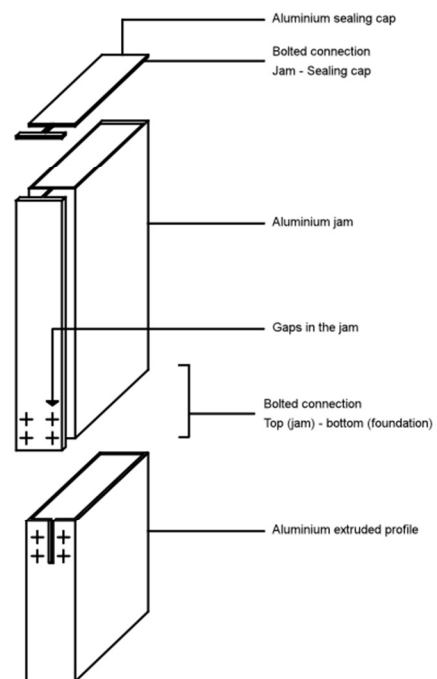
Figure 6.1.2: Design 1, Aluminium top + Aluminium bottom element

Disadvantages:

- Application relies on the strength of the subsurface. This design principle is not uniformly applicable in every situation;
- Slim profiles may lead to stability issues;
- The part that is rammed into the ground and the connection (bolted connection) must to be treated specifically with regard to corrosion;
- It is not realistic to assume that there are no machines needed for the installation of the structure, because without machines the bottom element cannot be rammed into the ground. Therefore, it is not necessary to design the bottom element of aluminium.

6.2. Design principle 2

This design is similar to design principle 1, as shown in Figure 6.1.3. However, in this case, the bottom part consists of a steel I-profile. Similar to the previous design, the top and bottom element have to be connected mechanically to be able to transfer forces from the jam (top element) to the foundation (bottom element). In order to be able to realise this bolt connection, gaps will be made throughout the jam.

Advantages:

- A cheaper alternative compared to design principle 1 because it is possible to use a standardized steel profile as a bottom element;
- Also in this design the assembly time is reduced compared to the steel alternative because of the space between the flanges.

Disadvantages:

- Application relies on the strength of the subsurface. This principle is not uniformly applicable in every situation;
- Slim profiles may lead to stability issues;
- The part that is rammed into the ground and the connection (bolted connection) must to be treated specifically with regard to corrosion;
- The connection between the aluminium and steel needs to be handled carefully duet o the phenomenon of galvanic corrosion.
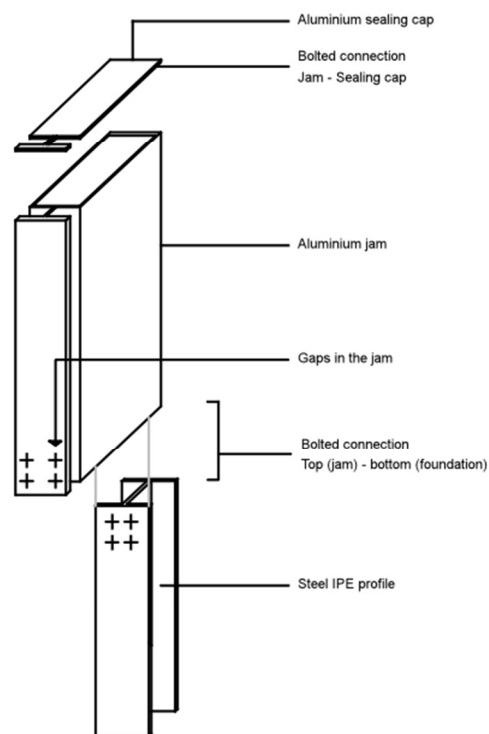
Figure 6.1.3: Design 2, Aluminium top + Steel bottom element

6.3. Design principle 3

The difference between this design principles and previous design principles is the welded connection between the top and the bottom element. The structure in this design consists entirely of aluminium as design principle 1 is. The structure is shown in Figure 6.1.4. The rectangular aluminium profile is partially rammed into the ground, subsequently the aluminium top part, an extruded element, can then fixed to the bottom element using welding technique.

Advantages:

- Because of the lightweight structure of the top and bottom element, the entire structure can be moved manually without using cranes. However, it should be mentioned that the maximum weight of an element does not exceed 50 kg;
- Also in this design the assembly time is reduced compared to the steel alternative because of the space between the flanges;
- A system consisting only of aluminium;

Disadvantages:

- Application relies on the strength of the subsurface. This principle is not uniformly applicable in every situation;
- Slim profiles may lead to stability issues;
- The part that is rammed into the ground and the connection (bolted connection) must to be treated specifically with regard to corrosion;
- In this design, there is not made optimal use of the possibilities of extrusion technique;
- Welded connection present in the system. The strength of the aluminium jam will be reduced because of the weld.

Aluminium sealing cap

Bolted connection
Jam - Sealing cap

Aluminium jam

Welded connection
Top (jam) - bottom (foundation)

Aluminium extruded profile
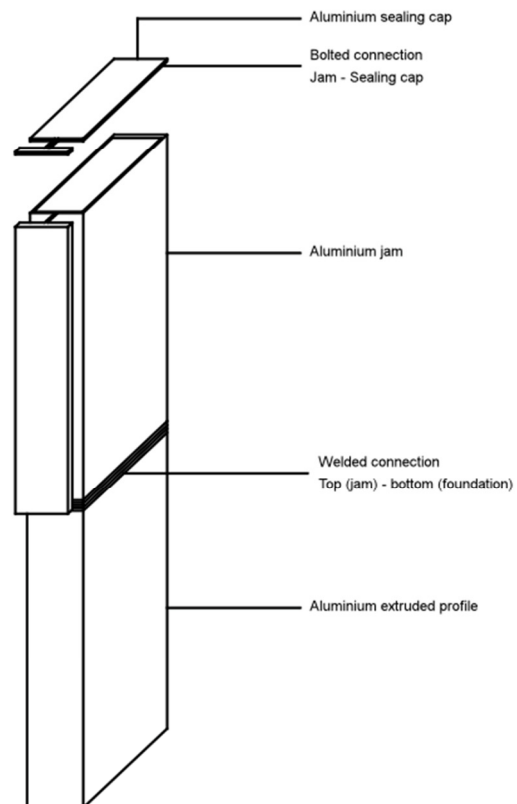
Figure 6.1.4: Design 3, Aluminium top + Aluminium bottom element

6.4. Design principle 4

First, the post and the footing plate will be attached to each other by welding them together. This can be done before the posts are transported to the location (in fabric). Afterwards, the posts which are welded to the footing plate, will be attached to the concrete barrier using nuts. According to GCW-2012 [5] the diameter of the gaps in the footing plate should be at least 5 mm bigger than the anchor diameter to avoid any problems with the installation. The sealing cap will be used in order to avoid water accumulation in the profile. With a simple screw the sealing cap will be fixed to the post. The structure is shown in Figure 6.1.5.

Advantages:

- Independent of the subsurface, applicable in any situation;
- Construction can be positioned and installed using a light crane;
- The jam can be moved manually without using cranes. However, it should be mentioned that the maximum weight of an element does not exceed 50 kg;
- Using extrusion techniques space between the flanges are created which reduces the assembly time compared to the steel alternative;
- A system which consist only of aluminium.

Disadvantages:

- Heavy crane equipment needed to place the concrete barrier;
- Welded connection present in the system.
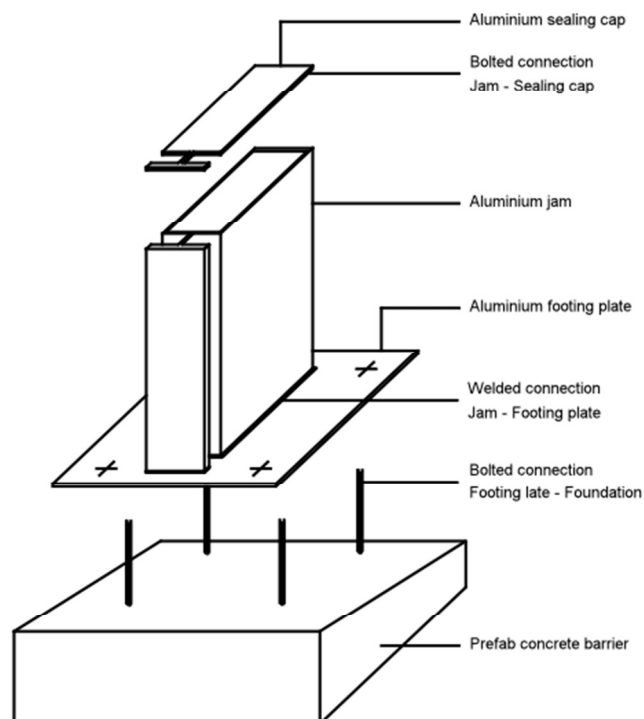
Figure 6.1.5: Design 4, Aluminium top element + Aluminium footing plate

6.5. Design principle 5

This variant is based on an existing modern day variant. The total system consists of a concrete barrier, a footing plate, and a jam as shown in Figure 6.1.6.

In this variant the jam is extruded with a screw-tube in its longitudinal direction, screw thread is then manually formed in the screw- tube by screwing bolts into the tubes. The footing plate can then be easily attached to the jam by bolts which are passed through the footing plate into the screw- tubes. The bolts should be strong enough to handle the force transfer between the jam and the footing plate.

After the footing plate has been attached to the jam the resulting construction can be set and fixed to the anchors which stick out of the concrete barrier.

Advantages:

- Independent of the subsurface, applicable in any situation.
- Construction can be positioned and installed using a light crane;
- The jam can be moved manually without using cranes. However, it should be mentioned that the maximum weight of an element does not exceed 50 kg;
- Using extrusion techniques several functionalities have been integrated in the cross section of the jam, such as the space between the flanges and the screw-tubes which reduces the assembly time compared to the steel jam in modern day systems;
- No welding required, as opposed to the traditional method.

Disadvantages:

- Heavy crane equipment needed to place the concrete barrier;
- Because of the usage of screw tubes, a special focus should be put on the connection between the footing plate and the jam.
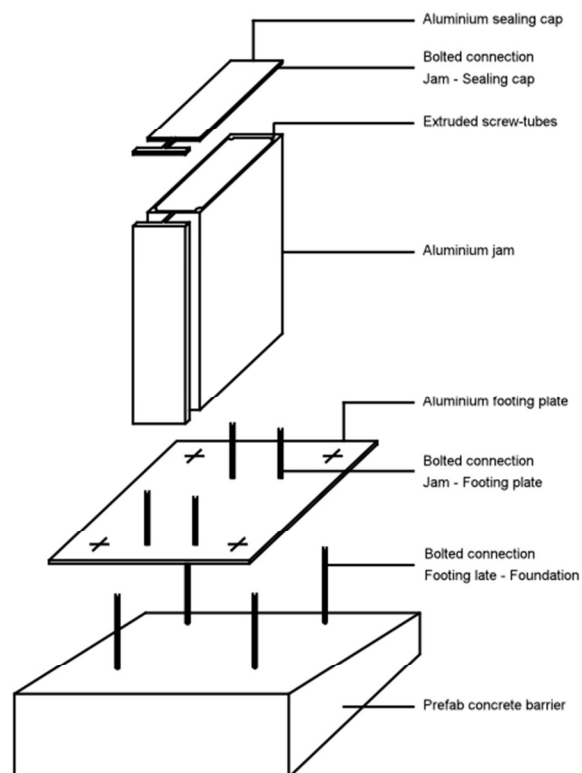
Figure 6.1.6: Design 5, Aluminium top element + Aluminium footing plate

18

6.6. Conclusion design principles

From the five design scenarios a design is selected in collaboration with the company at which the internship takes place.

Because the first three principles are heavily reliant on the composition of the subsurface they are not uniformly applicable in every situation. There is also a risk for instability problems due to the slim profiles. The most important advantage in these principles is that no heavy machinery is required during the installation process. This is only possible if the aluminium bottom part is dimensioned light enough such that it can be manually installed, or using simple cranes.

Principle 4 is not suitable due to the fact that the welded connection is a weather-dependent process and reduces the strength of the material at the welded point in the structure. Therefore, principle 5, that makes the most use of the advantages of aluminium, is chosen as the system which will be used during this research project.

7. Cross section analysis

The versatility of aluminium as a metal is complemented by the versatility of the extrusion process. Other metals can be extruded but few with the ease of aluminium and its alloys. Aluminium's high strength-to-weight ratio, and its ability to be extruded into any shape – no matter how complex, with tight tolerances, make it an ideal material for design applications which require maximum versatility from a cross-sectional area.

One of the most important design aspects that influence the material use is not a material property, but is related to section geometry. In general, most section geometries that work for steel will also work for aluminium. However, using extrusion techniques it is possible to integrate functionalities in the cross section which can reduce the assembly time of the system. To add functionalities in the cross-section it is important to gain more insight on the link between material use of the section geometry and the second moment of area (also known as the moment of inertia of a shape). Figure 7.1.1. shows some simple geometry designs, the Figure compares the second moment of areas of various aluminium cross-sections.
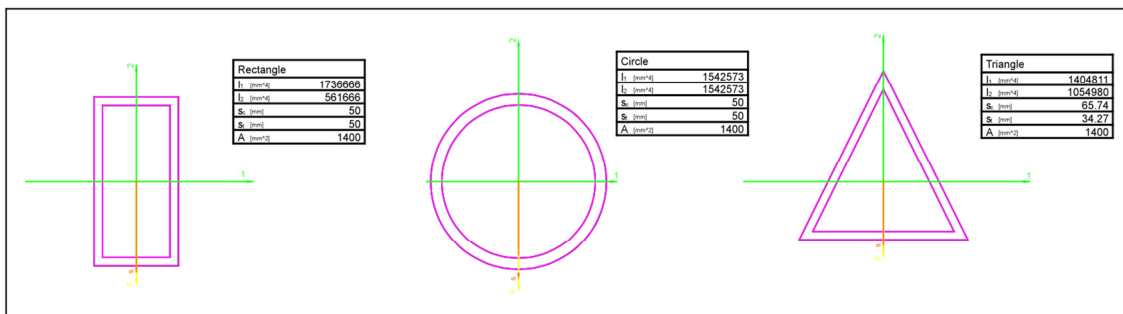
Figure 7.1.1: Simple geometry designs of aluminium cross-sections

For the various geometry sections an equal area, namely 1400 mm^2, of aluminium is used to make a realistic comparison of second moment of area possible. It can be seen that the rectangle has the highest value for the second moment of area. This is because most of the area, in comparison of the other geometries, is concentrated as far away as possible away from the centroid (middle of area). To deal with minimum material use to design the lightest possible jam, the rectangle principle will be used in the design phase.

7.1. Cross-section designs

Based on this simple analysis, some cross-sections are designed using AutoCAD mechanical. In this section the different designs will be given and explained briefly. The dimensions of the cross-section designs are based on the static calculation of the definitive design in section 8. Also the choices of different aspects during the design process will be considered in more detail in section 8.

In every Figure the following aspects are given:

- Cross-sectional properties;
- Dimensions;
- Thicknesses;
- The suitable press of the extrusion process based on the circumscribing circle diameter (CCD), see Figure 7.1.2.
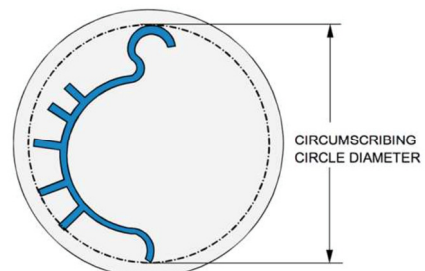
Figure 7.1.2: Cylindrical billet with an exemplary cross-sectional area of an extrusion
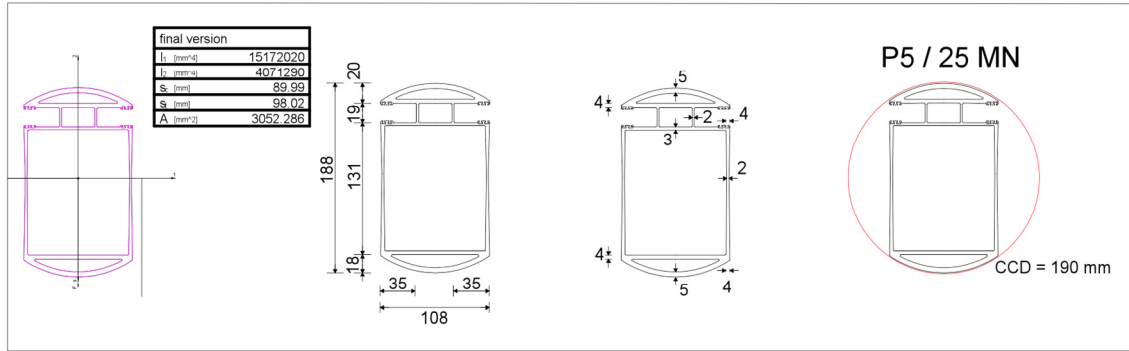
Figure 7.1.3: Design 1

Based on static calculations, the conclusion can be given that design 1 is applicable in situations where low noise barriers are used, in this case up to a maximum of 2 meters. Because of the small CCD of the cross-section, it is possible to extrude this jam with the smallest press available at Nedal B.V. The dimensions of the presses is shown in Figure 7.1.7.
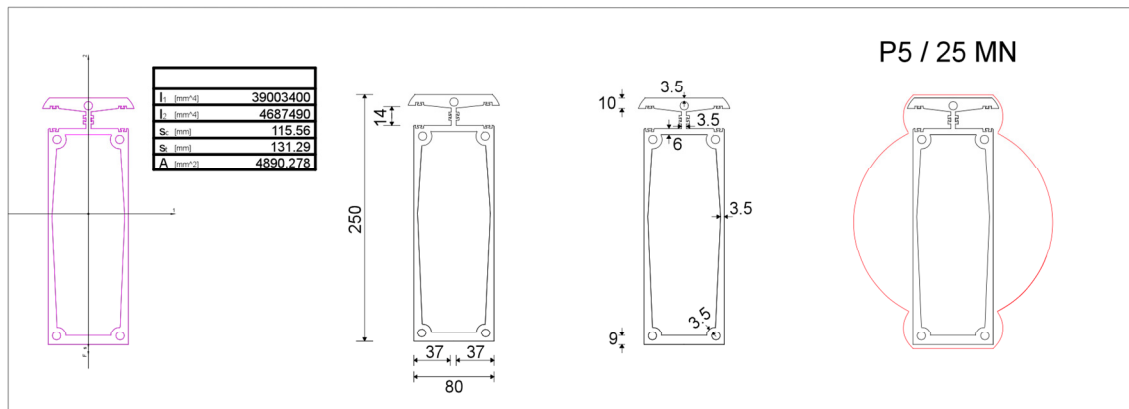
Figure 7.1.4: Design 2

Similar to design 1, design 2 is also applicable in situations where low noise barriers are used. Also, this cross-section fits within the boundaries of the smallest press. Because this variant protrudes the circle diameter of the press, it is important to have this variant checked by professionals' to make sure that the profile does not break during the extrusion process and that its strength is not affected.
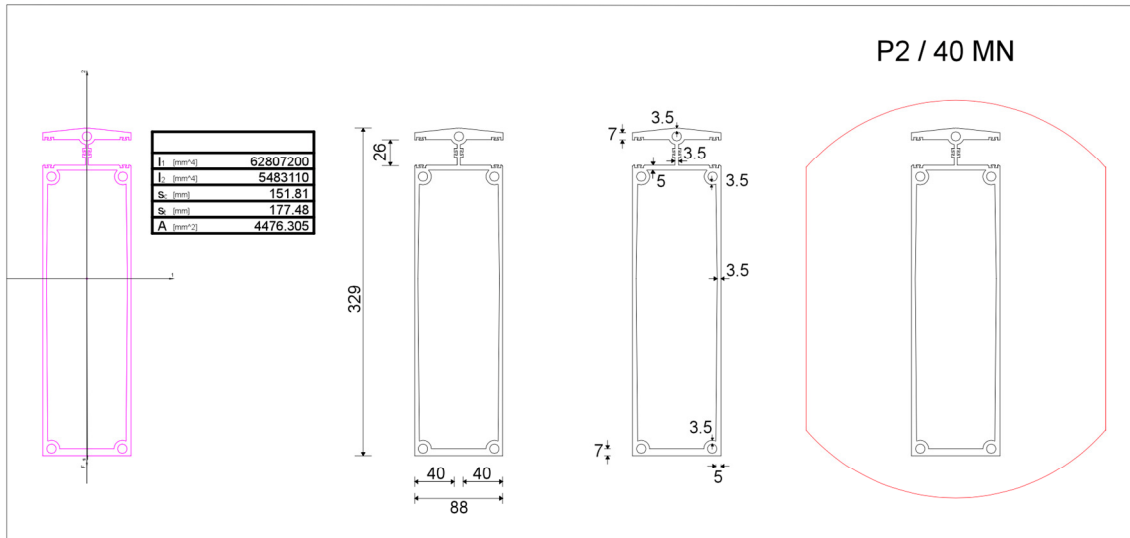
Figure 7.1.5: Design 3

Because of the high value of the second moment of area of design 3, this variant is applicable for situations where high noise barriers (in this case up to a maximum of 4 meters, see section 8) are required. Because of the high value of the second moment of area it's evident that a bigger press is used.
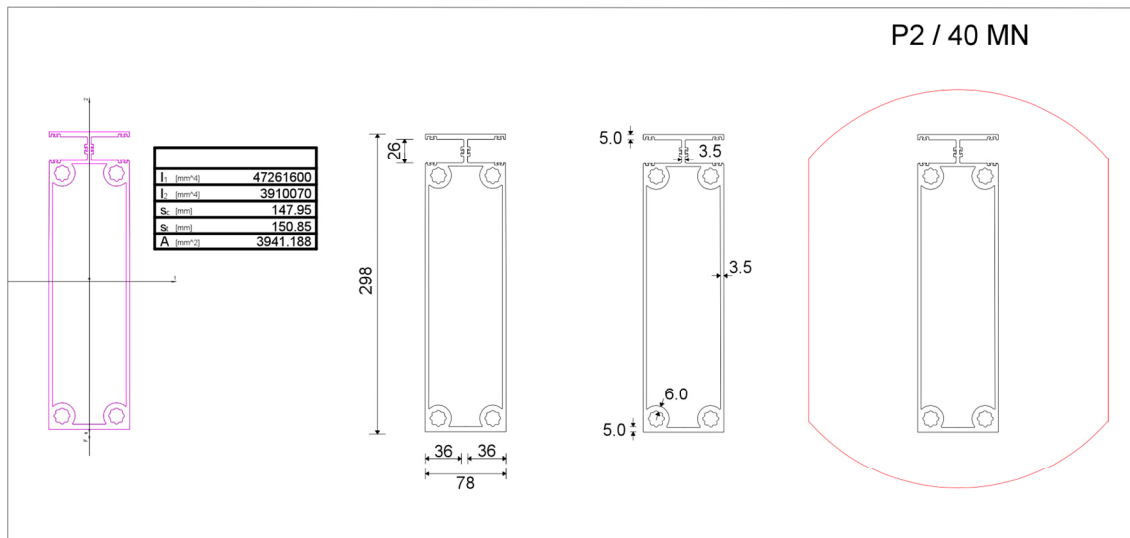
Figure 7.1.6: Design 4

The different cross-section designs are considered in the literature survey, in the following section, only the definitive design will be discussed in more detail.
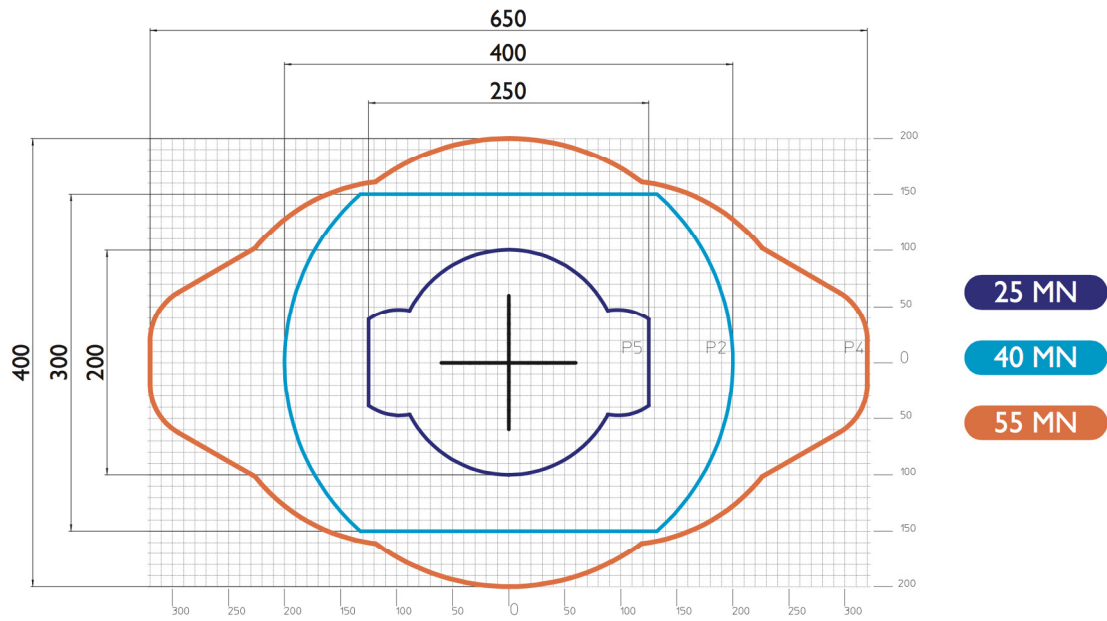
Figure 7.1.7: Dimensions of the available presses at Nedal Extrusions B.V.

7.2. The design

In this chapter, the choices made during the ''design process of the aluminium jams'' will be explained, and how the cross-section meets the requirements of aluminium extrusion profiles will be shown. First, each aspect of the cross-section will be considered briefly. Afterwards the building sequence of the system will be considered.

7.2.1. Circumscribing Circle Diameter (CCD)

As mentioned in section 8.1 starting point 5, the measurements of the cross section must be based on the measurement limits that most extrusion plants can supply of aluminium extrusions, based on the circumscribing circle diameter (CCD). In this case we assumed the measurements based on the press P2/40 MN of the company 'Nedal Extrusions'. As shown in Figure 7.1.8 the cross-section meets this requirement.

P2 / 40 MN
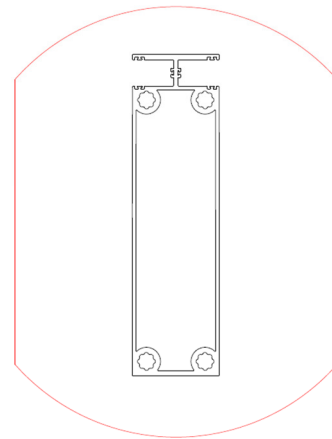
Figure 7.1.8: CCD of the cross-section

7.2.2. Neutral axis

It is possible to create a high value for 'the second moment of area ' without exceeding the requirement explained in section 8.1. The second moment of area is a measure of the 'efficiency' of a cross-sectional shape to resist bending caused by loading. The high value is created by concentrating most of the area (weight/thicknesses) as far as possible from the neutral axis; the neutral axis is given in Figure 7.1.9. The measurements and the increasing thickness of the elements from the neutral axis are given in below in the Figures 7.1.10. and 7.1.11.

$I1 = 47261600$ mm^4
$I2 = 3910070$ mm^4
$S1 = 147.95$ mm
$S2 = 150.85$ mm
$A = 3941$ mm^2
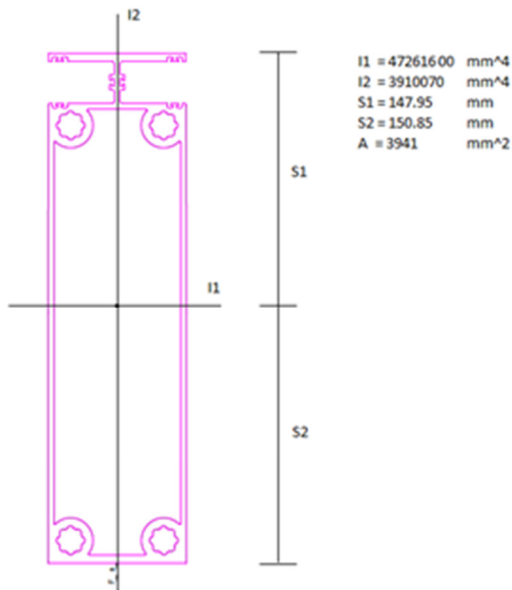
Figure 7.1.9: Values of the cross-section   Figure 7.1.10: measurements   Figure 7.1.11: thicknesses
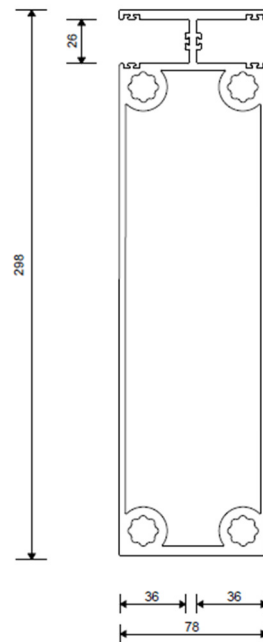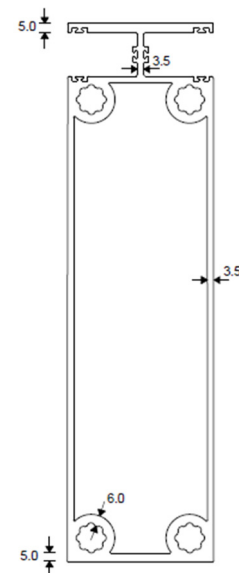
7.2.3.   Recommended wall thickness according to Sapa's design Manual

Factors which will influence the wall thickness are: the extrusion force, the extrusion speed, the selected alloy, the shape of the profile, the requirements for the surface, and the tolerances. In Figure 7.1.12 below, the graph is given which is used to determine the minimum wall thickness for the used aluminium alloy (namely: EN AW-6063) when designing the cross-section. In this case, a minimum thickness of 3.5 mm is used.
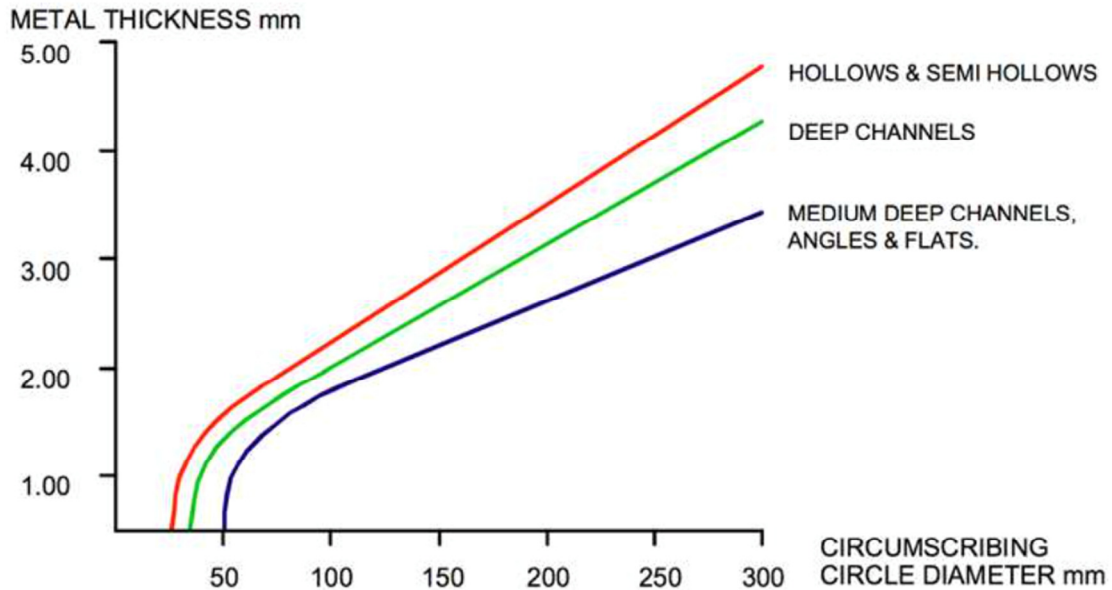
Figure 7.1.12: Minimum section thickness for 6063 alloy extrusions

7.2.4. Space for the glass-panels

In section 8.1. starting point 4 the possibility to slide the glass panels between the jams without any connector is mentioned. The cross-section is provided with holders in which rubber elements can be pushed. Per jam 6 rubbers are needed as shown in Figure 7.1.13. This way the glass panels with a thickness of 16 mm can slide between the jams without using any other connector element.
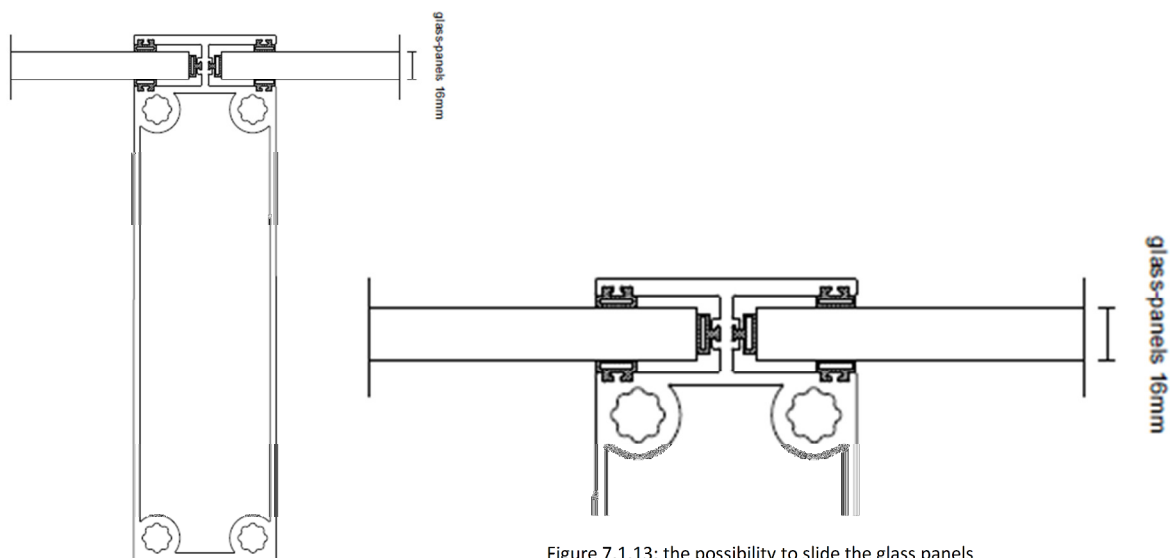
Figure 7.1.13: the possibility to slide the glass panels

7.2.5. Main element " rectangular tube"

The main element of the cross-section consists of a rectangular tubing profile. Flexural buckling needs not be checked due to the usage of a rectangular tubing profile in the cross-section.

7.2.6. Total weight

In section 8.1 starting point 3 it is mentioned that the structure of the jams must have a maximum weight of 50 kg. Using the density of aluminium, the area of the cross section, and the height of the structure, the total weight of the jam can be calculated as follows:

$$2700 \cdot 3941 \cdot 10^{-6} \cdot 4 \approx 44.56 \text{ kg}$$

However, the calculation of the footing plate is still missing. Because the footing plate is a part of the structure, the weight of the plate must be added to the total weight of the jams. This calculation will be given in section 8.6.6.

7.2.7. Other requirements of aluminium extrusions which have been met

To optimize the production process of aluminium extrusions, a profile's design should always be as production-friendly as possible. To optimize the production process, the requirements shown in table 7.1.1. have been met:

Table 7.1.1: requirements of aluminium extrusions

Requirements	Explanation
The cross-section have radiuses corners (with radius 0.50 mm)	It is not possible to produce razor-sharp corners by extrusion. Corners should be rounded. A radius of 0.5 – 1 mm is often sufficient.
The cross-section is symmetrical	Due to the symmetry the pressing speed will be the same over the entire cross-section. As a result of this, an equal strength will be obtained in the parts of the cross-section.
The cross-section has a small circumscribing circle diameter	Cost typically increases as the circumscribing circle diameter increases.
The cross-section has not deep, narrow channels	For profiles that have pockets or channels, the rule of thumb is that the ratio between width and height should be roughly 1:3. This is to ensure that the strength of die is not jeopardized.

7.2.8. Exploded view

The exploded view of the structure is given in Figure 7.1.14. The system consists of a cap to seal off the jam, an aluminium jam, an aluminium footing plate, 4 bolts to fix the jam to the footing plate, and 4 nuts to fix the structure (jam + footing plate) to the anchors that are sticking out the concrete barrier. The system is based on design principle 5 as shown in section 6.

First, the jam and the footing plate will be attached to each other by using the bolts. This can be done before the jams are transported to the location (at production plant). Afterwards, the jam that is connected to the footing plate will be attached to the concrete barrier using nuts. The sealing cap can attach to the jam anytime; it does not depend on building sequence. The sealing cap will be used in order to avoid water accumulation in the profile. With a simple screw the sealing cap will be fixed to the jam.
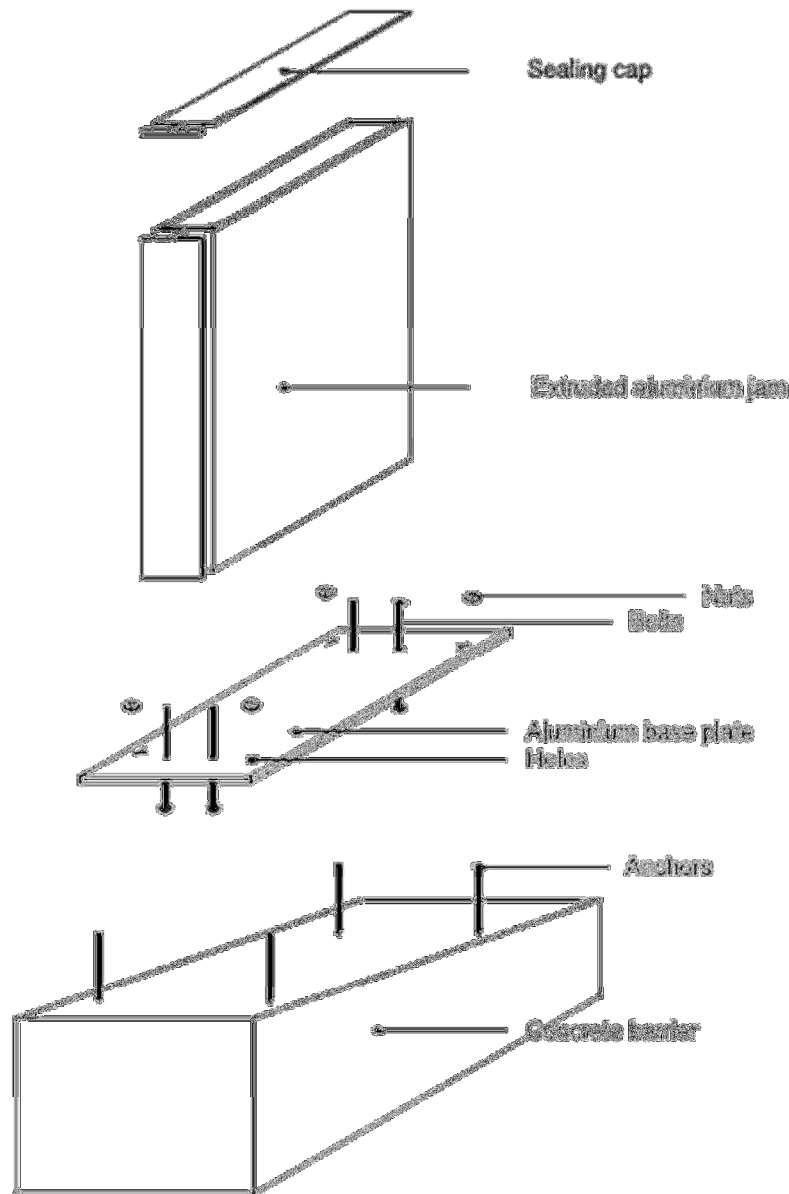
Figure 7.1.14: exploded view of the system

7.2.9. The connection between the footing plate and the concrete barrier

The issue of corrosion poses an extreme concern in the design. One of the first questions a designer must address when analysing a fastener application is whether the fastener will be subjected to a corrosive attachment. It is important to understand that there are several different types of corrosion.

One must however keep in mind that since different materials come in contact (steel, aluminium and concrete) at the bottom of the structure, galvanic corrosion might occur. Galvanic corrosion is prevented by electrically insulating these materials from each other. The insulation has to break all contact between the metals.

Connection between the anchors and the footplate
In order to protect the aluminium from the effects of being directly in contact with the concrete, the aluminium footing plate will be provided with a layer of bitumen at the bottom. To separate the aluminium footing plate from the anchors (steel) that are sticking out of the concrete, a rubber ring will be used to break all the contact between the aluminium and steel, as shown in Figure 7.1.15.

Dacrolit-coated steel nut
Aluminium base plate
Bitumen layer
Ring (electrically insulating element)
Concrete barrier
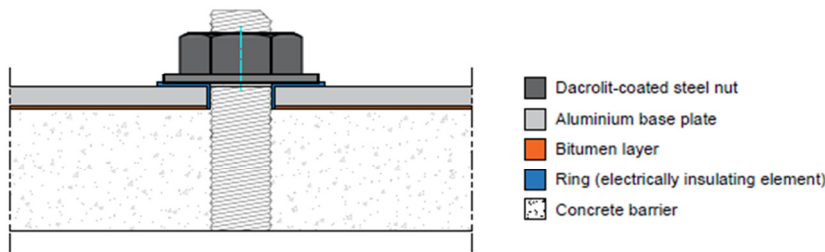
Figure 7.1.15: breaking all contact between materials
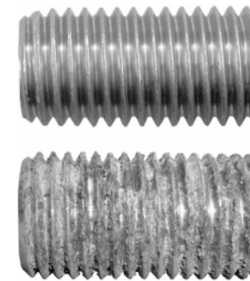
Figure 7.1.16: Without and with a barrier of protection

Connection between the screws and the footplate
In order to prevent galvanic corrosion between the anchors and the footing plate, this connection will be considered in this section.

Without any barrier of protection, steel will quickly succumb to the effects of corrosion as shown in Figure 7.1.16. A plating compatibility chart [8] is provided in Figure 7.1.17. that may be used to aid with fastener selection based on galvanic reaction.

Fastener Metal → Base Metal ↓	Zinc & Galvanized Steel	Aluminum & Aluminum Alloys	Steel & Cast Iron	Brasses, Coppers, Bronzes & Monel	Martensitic Stainless Type 410	Austenitic Stainless Type 302/304, 303, 305
Zinc & Galvanized Steel	1	2	2	3	3	3
Aluminum & Aluminum Alloys	1	1	2	3	Never Recommended	2
Steel & Cast Iron	1, 4	1	1	3	3	2
Brasses, Coppers, Bronzes & Monel	1, 4, 5	1, 5	1, 5	1	1	2
Martensitic Stainless Type 410	1, 4, 5	1, 5	1, 5	1	1	1
Austenitic Stainless Type 302/304, 303, 305	1, 4, 5	1, 5	1, 5	1, 5	1	1

Figure 7.1.17a: galvanic reaction of the fastener – base metal

Plating Compatibility Chart KEY:	
1	The corrosion of the base metal is not increased by the fastener.
2	The corrosion of the base metal is marginally increased by the fastener.
3	The corrosion of the base metal is considerably increased by the fastener.
4	The plating on the fastener is rapidly consumed, leaving the bare fastener metal.
5	Corrosion of the fastener is increased by the base metal.
Note: Surface treatment and environment can significantly alter activity.	

Figure 7.1.17b: Compatibility chart keys of galvanic reaction of the fastener – base metal

Conclusion: As mentioned before, the base metal consists of aluminium EN-AW 6063-T6. Using Figure 8.5.10a and Figure 8.5.10b the choice has been made to apply galvanized steel in order to prevent galvanic corrosion.

8. Static analysis

In this part of the report the static calculations will be done for the jams of the sound barrier. The sound barriers consist of aluminium jams with a maximum c.t.c. of 2.00 m and a length of 3.00 m. Glass panels are placed in between the jams. All glass panels are 8.8.3 toughened and laminated. The thickness of a glass panel is 16mm.

The following calculations will be done:

- Aluminium jam;
- Fixations jam on concrete foundation.

8.1. Data, conditions, specifications and starting points

In this chapter the data, specifications and starting-points, which are relevant for the calculations, are discussed.

Material properties

- Density   2700 kg/m^3;
- Young's modulus   70000 MPa;
- Shear modulus   26000 Mpa;

Alloy of the jams: AW EN-6063 T6:

- Yield strength: 250 N/mm^2 for $t \leq 25$
                                        260 N/mm^2 for $5 < t \leq 15$

Alloy of the footing plate: AW EN-5083 H14:

- Yield strength: 280 N/mm^2 for $t \leq 25$

Steel 8.8 quality anchor bolts in concrete:

- Ultimate tensile stress   800 N/mm^2;
- Ultimate yield stress   640 N/mm^2.

Galvanized steel 8.8 quality bots in jam:

- Tensile stress area $xxx \ mm^2$
- Ultimate yield stress   640 N/mm^2.

Prefab concrete foundation (C25/30)

- Maximum compression stress: 0.6 x 30 = 18.0 N/mm^2.

Starting-points

1. The jam has a length of 4.00 meters and a c.t.c. of 2.00 meter, this has to do with the maximum dimensions of the glass panels that can be realized (2 meters in height or width).

2. The jams are rotated under an angle of 15 degrees;

3. The jam including the footing plate has a maximum dead load of 50 kg;

4. There is a possibility to slide the glass panels between the jams without the use of additional connectors;

5. The measurements of the cross section must be based on the measurement limits; most extrusion plants supply aluminium extrusions based on the diameter of the circumscribing circle (DCC). According to [12] the presses available at the company '' Nedal Extrusions'' has been selected.

6. A factor of 3 is allowed between the minimum and the maximum plate-thickness (b) of the cross-section;

7. The calculation of the wind force is based on wind area II, built location;

8. The calculation does not apply to heightened applications such as an overpass or embankments;

8.2. Determining the loads acting on the jams

The load acting on the jams can be split into the dead load of the panels, the dead load of the jams and the wind load.

Dead load of the glass-panels

As mentioned before, the sound barriers consist of aluminium jams with a maximum c.t.c. of 2 m with a length of 3 m. The glass panels are placed in between the jams. All glass panels are 8.8.3. toughened and laminated. The glass panels have the following dimensions: 2000 x 3000 x 16 mm (l x h x t). The glass panels have a weight of 0.016 x 2500 = 40.0 kg/m^2 (received data from van Campen Industries).

Dead load of the jams

The jams have a maximum weight of 36 kg/unit.

Wind pressure on surfaces according to NEN EN-1991-1-4 [1]

The governing load case on a sound barrier is the wind load. In this section the calculation of the wind pressure is given. From the calculations below, determined according to NEN-EN 1991-1-4 [1], it shows that the wind speed on the sound barrier equals 1.70 kN/m^2.

The wind force F_w acting on the structure may be determined directly by using the following expression:

$$F_w = c_s c_d \cdot \sum_{elementen} c_f \cdot q_p(z_e) \cdot A_{ref}$$

Where:

$- c_s c_d$ is the structural factor;

$- c_f$ is the force coefficient for the structure or structural element;

$- q_p(z_e)$ is the peak velocity pressure at reference height z_e, for z_e 6 meter q_p is equal to 580 N/m^2;

$- A_{ref}$ is the reference area of the structure, in this case A_{ref} is equal to 6x2=18 m^2.

Below, the unknown variables will be determined step by step.

Peak velocity pressure $q_p(z_e)$ at reference height 6 meter

Table 8.2.1: properties of the jams

Length jams	Design value	Peak velocity pressure q_p
4.00 meter	4.00 meter	580 N/m^2

Force coefficient for the structural element c_f

The force coefficient for the structural element can be determined using article 7.4. NEN-EN 1991-1-4 [1]. For free-standing walls and parapets the resulting pressure coefficients c_f should be specified for the zones A,B,C and D as shown in Figure 8.2.1. According this article, the following values can be used to determine the force coefficient for the structural element:

- - Zone A: 3.4 [-]
- - Zone B: 2.1 [-]
- - Zone C: 1.7 [-]
- - Zone D: 1,2 [-]
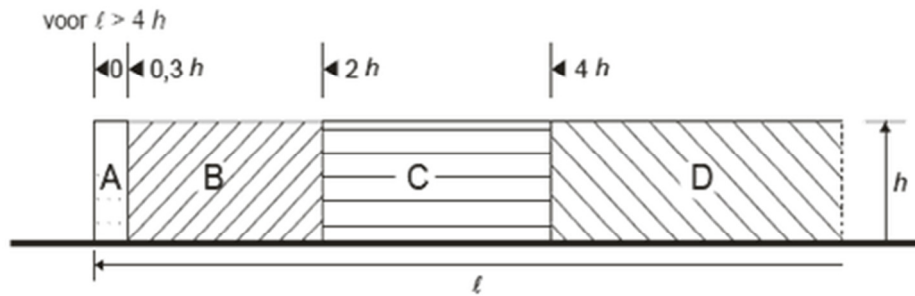
Figure 8.2.1: Zones of the noise barrier

The structural factor $c_s c_d$

The structural factor $c_s c_d$ should take into account the effect of wind actions from the non-simultaneous occurrence of peak wind pressures on the surface (c_s) together with the effect on the vibrations of the structure due to turbulence (c_d).

For structures with a height less than 50 m the value may be taken as 1 according to NEN EN-1991-1-4 article 6 [1].

Wind force F_w

All of the unknown variables are now known. The wind force acting on the structure can be determined directly by using the following expression:

$$F_w = c_s c_d \cdot \sum_{elementen} c_f \cdot q_p(z_e) \cdot A_{ref}$$

F_w Zone A = $\quad 1 \cdot 3.4 \cdot 580 = \quad 2.0 \; kN/m^2$
F_w Zone B = $\quad 1 \cdot 2.1 \cdot 580 = \quad 1.2 \; kN/m^2$
F_w Zone C = $\quad 1 \cdot 1.7 \cdot 580 = \quad 0.9 \; kN/m^2$
F_w Zone D = $\quad 1 \cdot 1.2 \cdot 580 = \quad 0.7 \; kN/m^2$

Although the value for zone A is higher; the value of zone B will be used for further calculation of the worst-case situation. This is because the jam behind zone A is an edge element, which supports a smaller area of the panels.

Safety factors

There are two key conditions, which must be considered: Ultimate limit state (ULS) at failure and the serviceability limit state (SLS) under working loads. Safety factors, which are given in table 8.2.2, are required for the calculation of the ULS.

Table 8.2.2 Safety factors

	Wind load	Dead load	
		Favourable	Unfavourable
ULS	1.3	0.9	1.2

8.3. Total acting loads on the jams

As mentioned in section 6 the panels are not attached to the jams, but are slid between the profiles of the jam. This means that the dead load of the panels does not act on the jams directly. However, it must be mentioned that because the noise barrier is rotated under an angle of 15 degrees, the dead loads of the elements of the noise barrier needs to be resolved in the perpendicular direction. Because of this angle, also the wind load needs to be resolved, see Figure 8.3.1. Note that the resolved loads are different in the favourable and unfavourable situation. The forces which occur due to the wind and dead load must be calculated. The calculations are given in Figures 8.3.2 – 8.3.4.
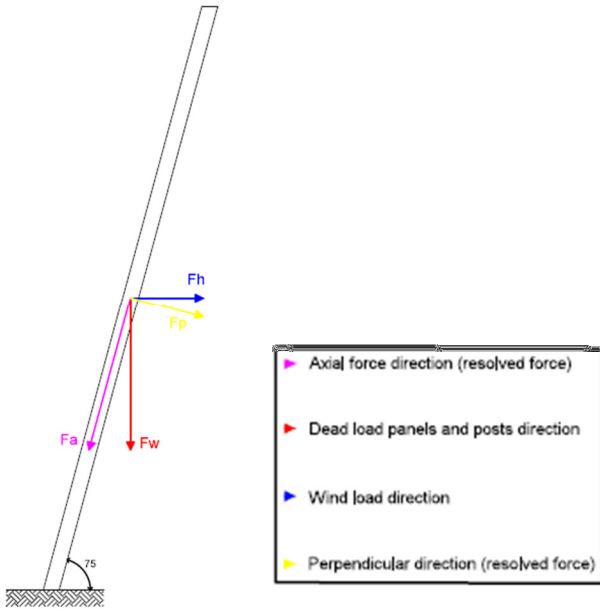
Figure 8.3.1: schematic view of the forces acting on the jam
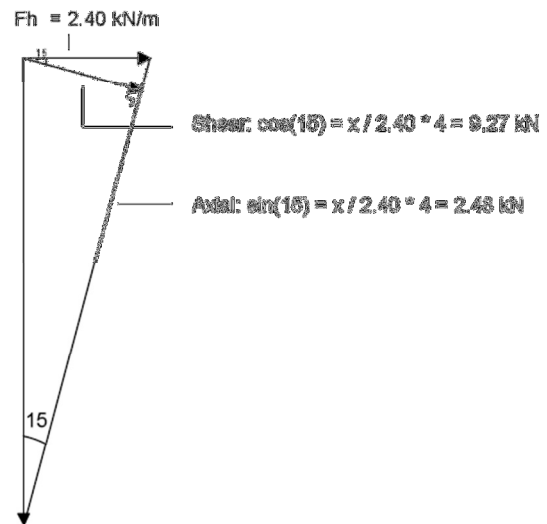
Figure 8.3.2: resolved forces wind load
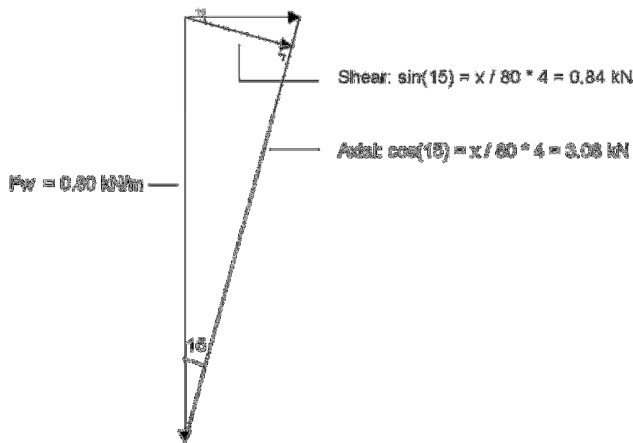
Figure 8.3.3: Resolved forces panels
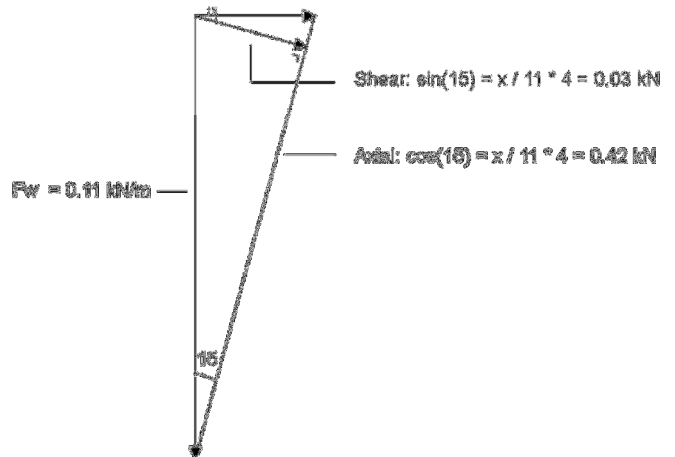
Figure 8.3.4: Resolved forces jam

The total values of the forces acting on the structure in the SLS and the ULS are shown in table 8.2.3. (only the resolved direction will be considered in the calculations!).

Table 8.2.3.: the forces acting on the structure

	SLS (worst case)	ULS	
		Favourable	**Unfavourable**
Total shear force (V)	**10.22 kN**	9.20 kN	**12.26 kN**
Total axial force (N)	**5.99 kN**	5.39 kN	**7.19 kN**
Total line load (kN/m)	**2.56 kN/m**	2.30 kN/m	**3.07 kN/m**

The Maximum moment as result of the loads can calculated with:

(SLS): $M_{cr} = \frac{1}{2} \cdot 2.56 \cdot 4.00^2 = 20.48 \, kNm$

(ULS): $M_{Ed} = \frac{1}{2} \cdot 3.07 \cdot 4.00^2 = 24.56 \, kNm$

For further calculations, the unfavourable situation will be considered (to take the worst case situation into account).

8.4.   Maximum deflections (SLS)

Table 8.4.1. below gives the maximum deflections of the jams according to GCW-2012 [5].

Table 8.4.1: Requirements on the maximum deflection of the jams

Element	Vertical noise barrier	Horizontal noise barrier
Jams	Exclusive deflection of the foundation: L/150	Exclusive deflection of the foundation: L/300
	Inclusive deflection of the foundation: L/75 (or L/50)	Inclusive deflection of the foundation L/150 (or L/100)

The permissible deflection for the vertical noise barrier are given by: 4000/150 = 26.67 mm

8.5. Static calculations for the stability and strength (checks)

In this chapter the static calculations of the jams will be considered in detail.

8.5.1. The stability of the jam

For the stability of the structure, only the local buckling resistances should be checked. As mentioned before, flexural buckling needs not to be checked because the cross section is rectangular tubing profile.

To account for cross-sectional instability, the cross-section of a member is often schematized as being built up out of plate elements. It is assumed that connections between plate elements act as hinges. When a plate is subjected to compression, bending or shear, or a combination of loads, the plate may buckle locally before the whole structural member becomes unstable.

Local buckling not only influences the strength of the structure, but also limits its deformation capacity. This deformation capacity is important in the design of structures. It determines the possibility to apply the elastic or plastic moment resistance and to allow redistribution of forces and moments. Therefore, NEN EN-1999-1-1 [4] provides a classification system of cross-sections [9].

In this section, according to NEN-EN 1999-1-1 article 6 [4] the structure will be checked on local buckling. Figure 8.6.1 gives the dimensions of critical part of the cross-section which will be checked on local buckling.
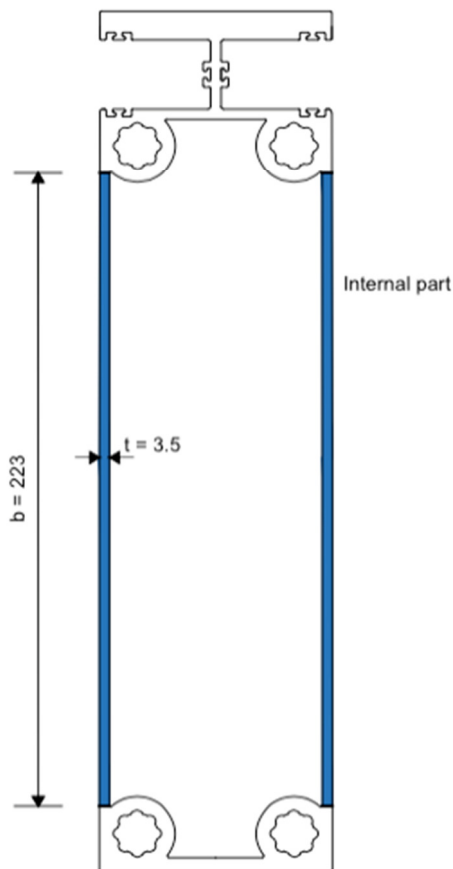
Figure 8.6.1: cross-section with the critical part of the aluminium design

The local buckling check consist of the following subject which will be discussed in this section:

- 8.6.1.1. Slenderness parameter;
- 8.6.1.2. Classification of the elements of the cross-section;
- 8.6.1.3. Local buckling check (bending and compressive stresses);
- 8.6.1.4. Conclusions.

8.5.1.1. Slenderness parameter according to NEN-EN 1999-1-1, art. 6 [4]

The susceptibility of the unstiffened plate to local buckling is defined by the slenderness parameter β, which has the following values:

a. Internal parts with stress gradient and outstands with peak compression at root $\beta = \eta \, b/t$

where
- b is the width of a cross-section part;
- t is the thickness of a cross-section;
- η is the stress gradient factor given by the expressions:

$\eta = 0.70 + 0.30\psi$ $(1 \geq \psi \geq -1)$
$\eta = 0.80/(1 - \psi)$ $(\psi < -1)$, see Figure 8.6.2.

where
ψ is the ratio of the stresses at the edges of the plate under consideration related to the maximum compressive stress. In general the neutral axis should be the elastic neutral axis, but in checking whether a section in class 1 or 2 it is permissible to use the plastic neutral axis. Figure 8.6.2. shows the values η of flat internal parts under stress gradient.

NOTE   All cross section parts are considered simply supported when calculating the parameters β even if the cross section parts are elastically restrained or clamped.
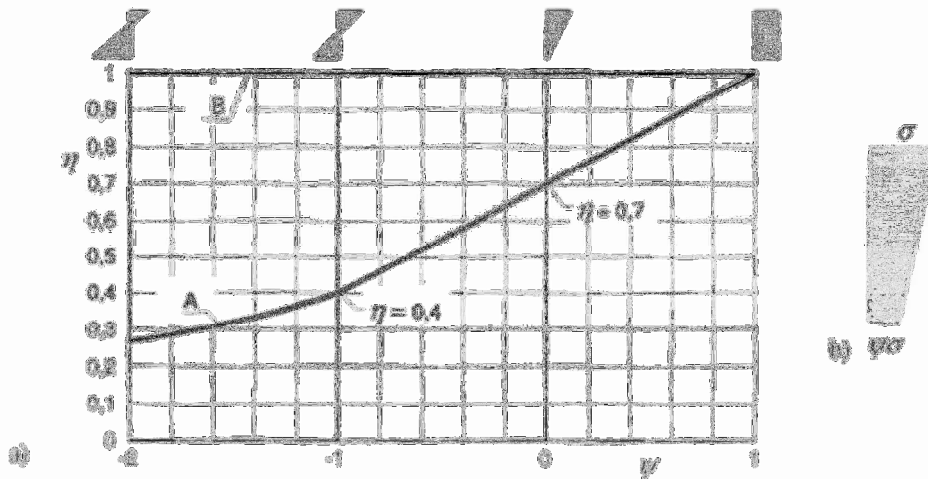
Figure: 8.6.2: Flat internal part under stress gradient, values of η. For internal parts or outstands (peak compression at root) use curve A. For outstands (peak compression at toe) use line B.

Before we can classify the cross-section, we need to determine the stress gradient factor as given in the formula above. After this the classification of the cross-section will be determined as described in NEN-EN 1999-1-1, article 6.1.4 [4], where plates with longitudinal edges simply supported, elastically restrained, or completely fixed are taken to correspond to ''internal parts'', and plates with one longitudinal edge free correspond to ''outstands''.

Figure 8.6.3. shows the critical parts of the cross-section with the distances of the edges to the neutral axis. First, the section modulus of the edges must be determined. Hereinafter, the

compressive stresses and the ratio of the stresses at the edges of the plate (being considered) related to the maximum compressive stress can determined.

The properties of the cross-section are given in Figure 8.5.2.
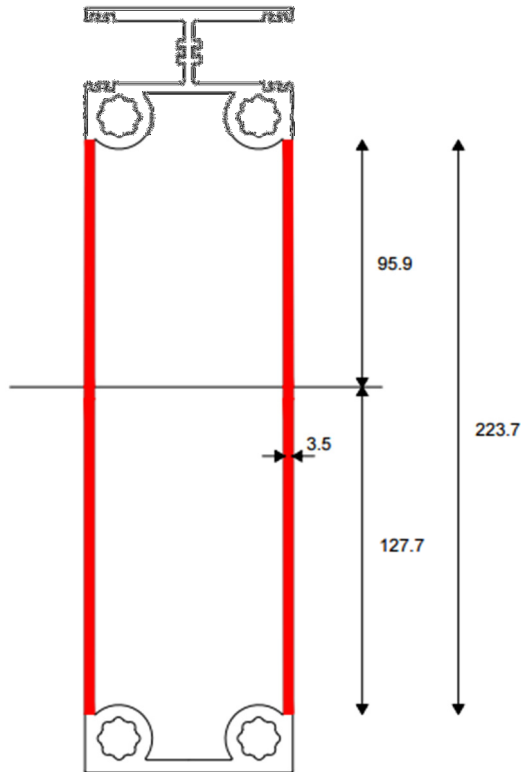
Figure 8.6.3: the critical part of the cross-section with the distances of the edges to the neutral axis

Determining the ratio of the stresses at the edges of the plate

1. Section modulus above the neutral axis:

$$W_{above} = \frac{I_{yy}}{z_{above}}$$

2. Section modulus below the neutral axis:

$$W_{below} = \frac{I_{yy}}{z_{below}}$$

Where z_{below} has a negative value.

The maximum value of the stresses in the upper edge as a result of the bending moment can be given by:

$$\sigma_{max;1} = \frac{M \cdot z_{boven}}{I_{yy}} = \frac{M}{W_{above}}$$

The maximum value of the stresses in the lower edge as a result of the bending moment can be given by the formula:

$$\sigma_{max;2} = \frac{M \cdot z_{below}}{I_{yy}} = \frac{M}{W_{below}}$$

The second moment of area without reducing the thicknesses is:

$$I_{yy} = \sum \left(\frac{1}{12} \cdot b \cdot h^3 + A \cdot y^2\right) = 47261600 \ mm^4$$

The values of z are given in Figure 4.3.2, namely: $z_{above} = 95.9 \ mm$ and $z_{below} = 127.7 \ mm$

Now, the section modulus can be determined:

$$W_{above} = \frac{I_{yy}}{z_{above}} = \frac{47261600}{95.9} = 492821.7 \ mm^3$$

$$W_{below} = \frac{I_{yy}}{z_{below}} = \frac{47261600}{-127.7} = -370098.7 \ mm^3$$

The maximum stresses including the normal stresses can be determined using the following formula:

$$\sigma_{max} = \frac{N}{A_{eff}} + \frac{M}{W_{el}}$$

Where $N = 7190 \ N$ (section 8.3) and $A_{eff} = 3188.8 \ mm^2$ (section 8.5)

1. Maximum stress in point upper edge:

$$\sigma_{max;1} = \frac{7190}{3188.8} + \frac{-24560000}{492821.7} = -47.6 \ N/mm^2$$

2. Maximum stress in lower edge:

$$\sigma_{max;2} = \frac{7190}{3188.8} + \frac{-24560000}{-370098.7} = 68.6 \ N/mm^2$$

The ratio ψ between the maximum stresses is:

$$\psi = \frac{68.6 + -47.6}{-47.6} - 1 = -1.44$$

Now, using the following formula, the stress gradient factor can be determined:

$$\eta = 0.80/(1 - \psi) = 0.80/(1 - -1.44) = 0.33$$

The slenderness parameter β of the part of the cross-section is given in table 8.6.1.

Table 8.6.1: Slenderness parameter β

Part	$\eta \cdot b/t$	β
Internal part	$0.33 \cdot 223.7/3.5$	21.1

8.5.1.2. Classify the cross-section according to NEN-EN 1999-1-1, article 6 [4]

According to NEN-EN 1999-1-1 table 3 [4], the aluminium alloy EN AW-6063 T6 can be classified in class A of the durability rating.

The classification of the cross-section is given in NEN-EN 1999-1-1 article 6.5.2 [4], where plates with longitudinal edges simply supported, elastically restrained, or completely fixed are taken to corresponds to ''internal parts'', and plates with one longitudinal edge free correspond to ''outstand''. Table 8.6.2 shows this classification system:

Table 8.6.2. The classification system

$\beta \leq \beta_1$	class 1	$\beta_2 \leq \beta \leq \beta_3$	class 3
$\beta_1 < \beta \leq \beta_2$	class 2	$\beta_3 < \beta$	class 4

The values of β_2 and β_3 are given in table 8.6.3.

Table 8.6.3: slenderness parameters $\beta_1/\varepsilon, \beta_2/\varepsilon, \beta_3/\varepsilon$

Material classification according to Table 3.2	Internal part			Outstand part		
	β_1/ε	β_2/ε	β_3/ε	β_1/ε	β_2/ε	β_3/ε
Class A, without welds	11	16	22	3	4,5	6
Class A, with welds	9	13	18	2,5	4	5
Class B, without welds	13	16,5	18	3,5	4,5	5
Class B, with welds	10	13,5	15	3	3,5	4
$\varepsilon = \sqrt{250/f_0}$, f_0 in N/mm²						

with $f_0 \, AW \, EN - 6063 \, T6 = 160 \, N/mm^2$

The slenderness parameters $\beta_1, \beta_2 \, and \, \beta_3$ are shown in table 8.6.4.

Table 8.6.4: slenderness parameters $\beta_1, \beta_2, \beta_3$

Material class:	Internal part		
	β_1	β_2	β_3
Class B, without welding	13.8	20	27.5

Using the classification system, we can classify the critical part of the cross-section. Because $\beta \leq \beta_3$ we can conclude that this part belongs to cross-section class 3. Logically, the reduction factor ρ_c is in the case equal to 1. Hence, replacing the true section by an effective section is not needed.

8.5.1.3. Local buckling check (bending and compressive stresses)

In this section, the presented parts of the cross-section will be checked on local buckling. For this check, the following unity check (UC) will be used:

$$\frac{\sigma_{cr}}{f_o} < 1$$

where:

- $\sigma_{cr} = the\ elastic\ critical\ buckling\ stress$;
- $f_o = yield\ strength\ -\ 160\ N/mm^2\ for\ EN\ AW\ 6063\ T6$

The elastic critical buckling stress may be find according to:

- $\sigma_{cr} = k_{cr} \cdot \frac{\pi^2 E}{12(1-v^2)} \cdot \left(\frac{t}{b}\right)^2$

Where

- t is the plate thickness;
- b width of the plate;
- v Poisson ratio (in this case 0.3).

According to [9] the values of the buckling factor k_{cr} can be found for the calculation of the critical stress for the internal parts and the outstands. Figure 8.6.4. gives the minimum values for k_{cr} for plates with simply supported edges and various supports of the sides with $v = 0,3$.
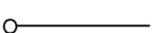
Type of plates	Boundary conditions		k_{cr}
Internal parts	Both sides simply supported	○————○	4.00
	One side clamped, other side simply supported	⌇————○	5.50
	Both sides clamped	⌇————⌇	7.00
Outstands	One side simply supported, other side free	○————	0.425
	One side clamped, other side free	⌇————	1.25

Figure 8.6.4: Minimum values for k_{cr} for plates with $v = 0,3$.

According to Figure 8.6.4. the buckling factor can be determined, namely $k_{cr} = 4.00$. The critical stress follows from the following formula:

- $\sigma_{cr} = 4.00 \cdot \frac{\pi^2 \cdot 70000}{12(1-0.3^2)} \cdot \left(\frac{3.5}{223.7}\right)^2 = 62\ N/mm^2$

8.6.1.4. Conclusion

Conclusion: Because the elastic critical stress is lower than the yield strength of EN AW 6063-T6 we may conclude that the plate will not buckle, see UC below.

- $\frac{62}{160} = 0.4$

8.5.2. Strength and stiffness of the jam

The maximum c.t.c.-distance for the 4.00 m jam is 2.00 m on both sides. The relevant geometry and properties of the cross-section is given in Figure 8.5.2. The determination of the load distribution is determined below.

8.6.2.1. Serviceability Limit State (SLS; deflection check):

The maximum deflection of the jam can be calculated with:

- $\delta_{max} = \frac{M_{max} \cdot l^2}{8 \cdot E \cdot I} = \frac{2.56 \cdot 4000^4}{8 \cdot 70000 \cdot 47261600} = 24.76 \; mm$

The maximum allowed top deflection equals $\frac{4000}{150} = 26.67 \; mm \geq 24.76 \; mm$

Conclusion: the structure meets the requirements given in section 8.4.

8.5.2.2. Resistance under combined load (ULS; strength check)

A plate subjected to combined, axial force and in-plane moment, under factored loading should be given a separate classification for the separate actions in accordance with NEN-EN 1999-1-1 article 6.5.2 [4]. In so doing, the value of β should be based on the pattern of edge stress produced if the force (N_{Ed}) and the moment (M_{Ed}) act separately.

If the combined action includes the effect of a coincident shear force, V_{Ed}, then V_{Ed} may be ignored if it does not exceed $0.5V_{Ed}$. If $V_{Ed} < V_{Rd}$ the following condition should be satisfied:

$$\frac{N_{Ed}}{N_{c,Rd}} + \frac{M_{Ed}}{M_{c,Rd}} + \left(\frac{2V_{Ed}}{V_{Rd}} - 1\right)^2 \leq 1.00$$

The values of N_{Ed}, V_{Ed} and M_{Ed} are presented in section 8.3. The values for $N_{c,Rd}$, $M_{c,Rd}$ and V_{Rd} will given below.

<u>Resistance under uniform compression</u>

Because the axial force is in this case very low, it is usual to ignore the axial force. However, for the completeness of the calculation the resistance under uniform compression will also considered in this section.

The susceptibility of the unstiffened plate to buckling is defined by the parameter β**,** where $\beta = b/t$. Using the same classification system presented in section 8.6.1, we can classify the part hatched in Figure 8.6.3. Because $\beta > \beta_3$ $(with \; \beta = 223.7/3.5 = 63.9)$ we can conclude that this part belongs to cross-section class 4.

Hence, the actual cross-section must be replaced by an effective cross-section. The effective cross-section is obtained by multiplying the thicknesses by a reduction factor ρ_c.

- $\rho_c = 1,0$ $for \quad \beta \leq \beta_3$
- $\rho_c = \frac{C_1}{(\beta/\varepsilon)} - \frac{C_2}{(\beta/\varepsilon)^2}$ $for \quad \beta > \beta_3$

Table 8.6.5 (given in NEN-EN 1999-1-1 table 6.4 [4]) shows the values of the constants C_1 and C_2.

Table 8.6.5: Constants C_1 and C_2 in expressions for ρ_c

Material classification according to Table 3.2	Internal part		Outstand part	
	C_1	C_2	C_1	C_2
Class A, without welds	32	220	10	24
Class A, with welds	29	198	9	20
Class B, without welds	29	198	9	20
Class B, with welds	25	150	8	16

Table 8.6.7. shows the reduction factor and the effective thickness of the parts of the cross-section.

Table 8.6.7: reduction factors ρ_c and effective thicknesses t_{eff} of the elements

Part	ρ_c	t_{eff}
Critical part	$\dfrac{32}{51.12} - \dfrac{220}{2613.25} = 0,52$	$0,54 \cdot 3.5 = 1.9 mm$

Using Autodesk AutoCAD Mechanical, the thicknesses of the critical parts are reduced. Some properties of the reduced cross-section are given in Figure 8.6.5.

Subsequently, the resistance under uniform compression can be determined using the following formula:

$$N_{o,Rd} = A_{eff}\, f_o / \gamma_{M1}$$

This formula leads to the following value of the resistance under uniform compression:

- $N_{o,Rd} = A_{eff}\, f_o / \gamma_{M1} = 3188.8 \cdot 160/1.1 = 463825\ N = 436.8\ kN$

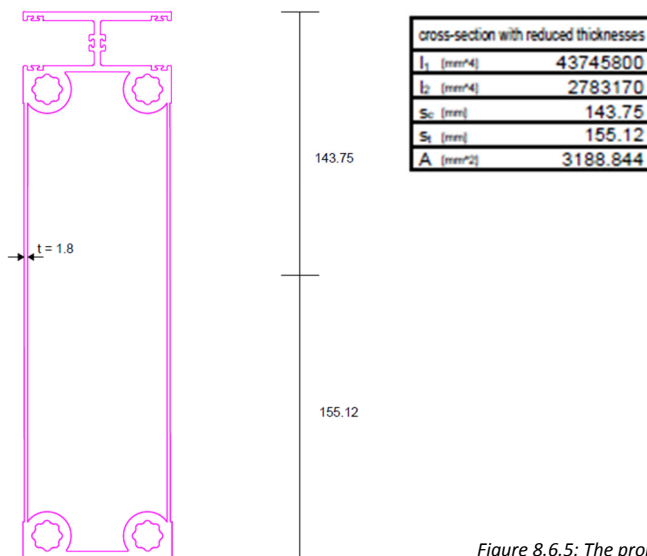| cross-section with reduced thicknesses	
I_1 (mm^4)	43745800
I_2 (mm^4)	2783170
S_c (mm)	143.75
S_t (mm)	155.12
A (mm^2)	3188.844

Figure 8.6.5: The properties of the cross-section with reduced thicknesses

NOTE: The contribution of the axial force will be minimal in the check of the resistance under combined load because the very low ratio $N_{Ed}/N_{o,Rd}$.

Resistance under shear

The susceptibility to shear buckling is defined by the parameter β, where $\beta = b/t$ and b is the shorter of the side dimensions. For all edges conditions the plate in shear is classified as slender or non-slender as follows:

- $\beta \leq 39\varepsilon$ non-slender plate;
- $\beta > 39\varepsilon$ slender plate.

Where ε is calculated in the same way as in section 8.6.1: $\varepsilon = \sqrt{250/f_o}$, where $f_o = 160 \ N/mm^2$

This classification system indicates that the two-hatched parts given in Figure 8.6.3. are slender plates. For these plates the resistance has to be determined using the following expression:

$$V_{Rd} = v_1 bt \ f_o/(\sqrt{3} \ \gamma_{M1})$$

where

- $v_1 = 17t\varepsilon\sqrt{k_\tau}/b$ but not more than: $v_1 = k_\tau \frac{430t^2\varepsilon^2}{b^2}$ and $v_1 \leq 1,0$
- $k_\tau = 5,34 + 4,00(b/a)^2$ if $a/b \geq 1$
- $k_\tau = 4,00 + 5,34(b/a)^2$ if $a/b < 1$
- $a = \ the \ length \ of \ the \ plate \ in \ the \ direction \ of \ tension$

This results in the following value for the resistance under shear for the slender plates:

- $k_\tau = 5,34 + 4,00(223.7/223.7)^2 = 9,34$
- $v_1 = 17t\varepsilon\sqrt{k_\tau}/b = 17 \cdot 3.5 \cdot 1.25 \cdot \sqrt{9.34}/223.7 = 1,0$

Because the value $v_1 = 1.0$, it is unnecessary to calculate the resistance separately. For this reason, following formula will be used:

$$V_{Rd} = A_{total} \ f_o/\sqrt{3} \ \gamma_{M1}, \ \ \text{where } A_{total} \text{ is the total area of the cross-section}$$

This formula leads to the following resistance under shear:

$$V_{Rd} = A_{total}\frac{f_o}{(\sqrt{3} \ \gamma_{M1})} = 3941.1 \cdot \frac{160}{(\sqrt{3}\cdot 1.10)} = 330958 \ N = 331.0 \ kN$$

Because $V_{Rd} > 2V_{Ed}$, the effect of a coincident shear force may be neglected. Now, the formula for the check of the resistance under combined load can be rewritten:

$$\frac{N_{Ed}}{N_{C,Rd}} + \frac{M_{Ed}}{M_{C,Rd}} \leq 1.00$$

Resistance under transverse stress gradient

As mentioned before, the applied actions at the end of the rectangular plate result in a transverse stress gradient. The stresses are transferred into an axial force and bending moment treated separately. The axial force is already treated. The bending moment will treated in this section according to NEN-EN 1999-1-1 article 6.5.3 [4].

The susceptibility to buckling is defined by the parameter β, where $\beta = 0.40bt$. The classification for the cross-section is already carried out in section 8.6.1 In this section it is clearly shown that the two hatched parts given in Figure 8.6.7 are class 3 cross-sections. The other plates of the cross-section are class 1 cross-sections.

The bending moment resistance $M_{o,Rd}$ can determined using the following formulas:

- $M_{o,Rd} = W_{pl}\, f_o/\gamma_{M1}$ for class 1 and 2 cross-sections;

- $M_{o,Rd} = \left[W_{el} + \frac{\beta_3-\beta}{\beta_3-\beta_2}\left(W_{pl} - W_{el}\right)\right] f_o/\gamma_{M1}$ for class 3 cross-sections.

First the elastic and plastic moduli will be determined of the hatched parts. The plastic modulus can be determined by multiplying the area A by the distance from the neutral axis to the centroid a:

$$W_{pl} = A_1 \cdot a_1 + A_2 \cdot a_2 = 2 \cdot (335.7 \cdot 47.5 + 447.0 \cdot 63.9)$$
$$= 89018.1\ mm^3$$

Because the rectangle geometry of the plates, the elastic moduli of the hatches parts can be determined using the following expression:
$W_{el} = W_{pl}/1.5 = 89018.1/1.5 = 59345.4\ mm^3$.

The bending moment resistance of the class 3 cross-sections is:

- $M_{o,Rd} = \left[43253.4 + \frac{27.5-21.1}{27.5-20}(89018.1 - 59345.4)\right] 160/1.10$

  $= 9974415.1\ Nmm = 9.97\ kNm$

Subsequently, the bending moment resistance of the other parts must be determined.

The maximum value of the elastic section modulus of the whole cross-section can be defined by:

$$W_{el} = I_y/s_{max}$$

Figure 8.6.7: parts of class 3

Where s_{max} is the largest distance from the neutral axis to outermost fiber. The moment of inertia I of the cross-section is $55527300\ mm^4$ the distance from the neutral axis to outermost fibre is $164.79\ mm$. The total elastic section modulus is:

- $W_{el,total} = \frac{47261600}{150.85} = 313302.0\ mm^3$

Reducing this value by the elastic section modulus of the class 3 cross-sections, we get:

- $W_{el,reduced} = 313302.0 - 59345.4 = 253956.6\ mm^3$

Assuming $\frac{W_{pl}}{W_{el}} = 1.5$ we can calculate the plastic section modulus W_{pl}, namely:

- $W_{pl,reduced} = 1.5 \cdot 253956.6 = 380934 \ mm^3$.

The bending moment resistance can be determined by substituting $W_{pl,reduced}$ in the formula of class 1 or 2 cross-sections, as given below:

- $M_{o,Rd} = 380934 \cdot 160/1.10 = 26317672.7 \ Nmm = 26.3 \ kNm$.

By summing the bending moment resistances of class 1 and 3, the total bending moment resistance of the cross-section can be determined:

- $M_{o,Rd,total} = 10.0 + 26.3 = 36.3 \ kNm$

Check of the resistance under combined load

As mentioned before, the following condition should be satisfied:

$$\frac{N_{Ed}}{N_{c,Rd}} + \frac{M_{Ed}}{M_{c,Rd}} + \left(\frac{2V_{Ed}}{V_{Rd}} - 1\right)^2 \leq 1.00$$

As mentioned before, the shear force may be ignored because it does not exceed $0.5V_{Rd}$. Now, the condition can be rewitten as:

$$\frac{N_{Ed}}{N_{c,Rd}} + \frac{M_{Ed}}{M_{c,Rd}} \leq 1.00$$

This leads to the following unity check of the resistance of the cross-section under combined load:

$$\frac{7.2}{463.8} + \frac{24.6}{36.3} \leq 1 \quad \rightarrow \quad 0.69 < 1.00$$

Conclusion: the cross-section meets the requirements given in NEN-EN 1999-1-1 article 6.5 [4].

8.5.3. Supporting plate (ULS; strength check)

In this section, the bending moment resistance M_{Rd} of the ''glass-panel supporting'' plate of the cross-section will be determined and checked. The following condition should be satisfied:

$$(M_{Ed}/M_{Rd}) \leq 1,0$$

The ''glass-panel'' supporting part is shown in Figure 8.6.8a. It should be noted that only the most critical wind direction will be considered, see Figure 8.6.8b. As a result of the presented loading, the panels will bend as shown in Figure 8.6.8c. Due to the bending, the glass-panels will create pressure points at the end of each supporting plate, see Figure 8.6.8d.

Figure 8.6.8a: the glass-panel supporting plates
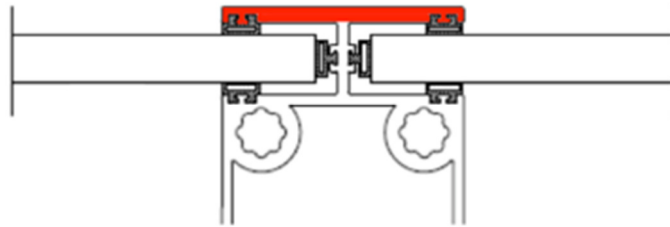
Figure 8.6.8b: wind direction in the worst-case situation
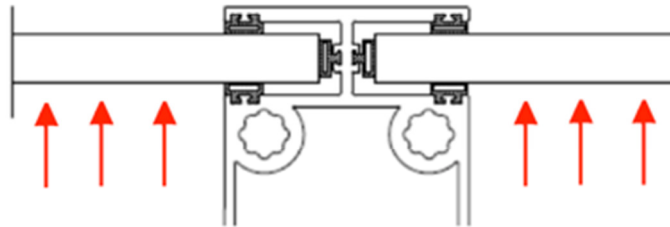
Figure 8.6.8c: bending of the panels due the wind loading
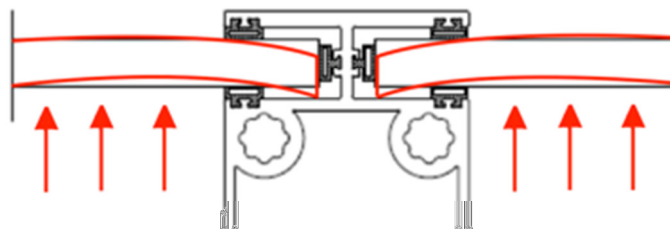
Figure 8.6.8d: pressure points through the glass-panels
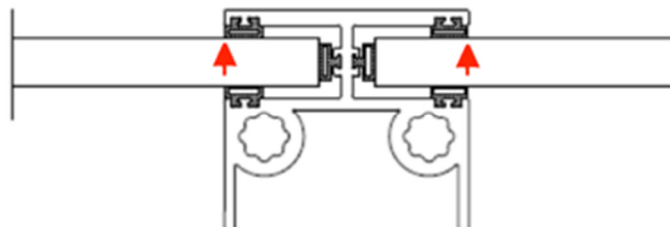
Assuming that the plate is anchored at only one end to a vertical support from which it is protruding, we can consider it to be a cantilever beam/plate, as shown in Figure 8.6.9. The total loading on the glass-panels is given in section 8.3: 3.07 kN/m. Because of the symmetry of the cross-section, it is allowed to consider only half of the supporting plate. Because of this, the acting force should be divided by 2.
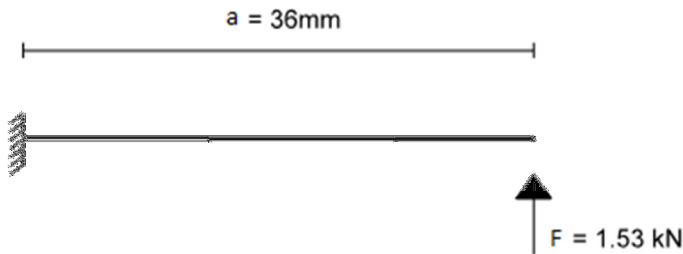
Figure 8.6.9: Cantilever beam principle of the supporting part

The maximum moment in the ultimate limit state can be determined using the following formula:

- $M_{Ed} = F \cdot a = 1.53 \cdot 10^3 \cdot 36 = 55080 \, Nmm$

The bending moment resistance M_{Rd} for class 1 and 2 cross-sections can be determined using the following formula:

- $M_{Rd} = W_{pl} \, f_o / \gamma_{M1}$

where

- $W_{pl} = (39.00 \cdot 5.00) \cdot (147.95 - 2.50) = 28362 \, mm^3$

Substituting the value of W_{pl} in M_{Rd} gives the bending moment resistance of this part, namely:

- $M_{Rd} = 28362 \cdot 160/1.1 = 4125490 \, Nmm$

Conclusion: The "glass-panel" supporting part of the cross-section satisfies the condition given in this section, namely:

$$\frac{M_{Ed}}{M_{Rd}} = \frac{55080}{4125490} = 0.01 \leq 1.0$$

8.5.4. Designing bolts in the jams

In order to prevent failure of the system, it is important that the bolt in the jam can transfer the forces to the footplate. According to NEN-EN 1993-1-8 article 3.6 [3] the resistance of bolt will be determined. Because the structure is loaded in shear and tension, the design resistance of the bolted joints loaded in shear and tension must be determined.

8.5.4.1. Check resistance of bolt joint loaded in shear

The shear resistance of steel bolts is given by:

- $F_{V,Rd} = \frac{\alpha_v \cdot f_{ub} \cdot A_s}{\gamma_{M2}}$

Where $A_s = 245 \ mm^2$ according to [13] for M20 bolts. The selected bolt should satisfy the following condition:

- $\frac{F_{V,Ed}}{F_{V,Rd}} \leq 1.00$

The shear resistance is thus determined as follows:

- $F_{V,Rd} = \frac{0.6 \cdot 800 \cdot 245}{1.25} = 84.08$ kN

The maximum value of the shear force $F_{V,Ed}$ (at the bottom of the jam) is given in section 8.3, namely $12.26 \ kN$. This means that the selected screw satisfies the given condition, namely:

- $\frac{12.26}{84.08} = 0.15 \leq 1$

8.6.4.2. Check resistance of bolt joint loaded in tension

The design tension resistance of bolts is given by:

- $F_{t,Rd} = \frac{k_2 \cdot f_{ub} \cdot A_s}{\gamma_{M2}}$

Where $A_s = 245 \ mm^2$ according to [10]. The selected screw should satisfy the following condition:

- $\frac{F_{t,Ed}}{F_{t,Rd}} \leq 1.00$

The tension resistance is thus determined as follows:

$F_{t,Rd} = \frac{0.63 \cdot 800 \cdot 245}{1.25} = 98.78 \ kN$

The design tensile force in each bolt as a result of bending moment can be calculated by dividing M_{Ed} by the distance between the bolt and the pressure point. This value is shown in Figure 8.6.10.

- $F_{t,Ed} = \frac{24.56}{2 \cdot 0.256} = 47.87 \ kN$

Also the resistance against tension satisfies the given condition, namely:

- $\frac{47.87}{98.78} = 0.48 \leq 1.00$
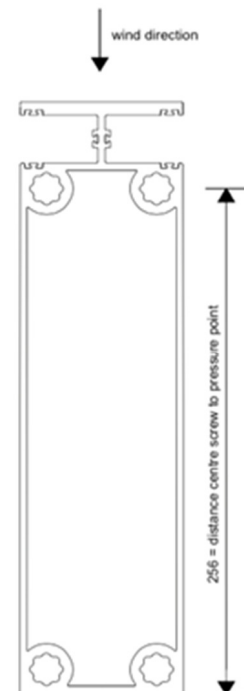
Figure 8.6.10: distance between the bolt and the pressure point

8.5.4.3. Check resistance of bolt joint loaded in combined loading
The resistance against the combined loading should satisfies the following condition:

- $\dfrac{F_{V,Ed}}{F_{V,Rd}} + \dfrac{F_{t,Ed}}{1.4\,F_{t,Rd}} \leq 1.00$

Also the resistance against the combined loading satisfies the given condition, namely:

- $\dfrac{12.26}{84.08} + \dfrac{47.87}{138.29} = 0.49 \leq 1.00$

8.5.4.4. Determining the effective embedment length L_e

In Figure 8.6.11 the geometry and the assumed symbols with particular reference to the definition of the embedment length are given. The total length of the bolt inside the aluminium slot is called the nominal embedment length (L_n), but the length parameter that influences the joint response is the effective embedment length (L_e). The effective embedment length is the one used in the formulation for the pull-out strength ($F_{o,Rd}$) prediction. Dr. Craig C. Menzemer, University of Akron [11] found an expression for the pull-out strength from pull-out test results of different bolt slots. From the data analysis, a predictive model for pull-out strength is proposed as:

$$F_{o,d} = 0.29 \cdot D \cdot L_e \cdot f_u$$

In which $F_{o,d}$ is the predicted pull-out strength in N, D is the nominal diameter of the bolt, L_e is the effective embedment length in mm, f_u is the tensile ultimate strength (is in this case 186 MPa) of the extrusion.
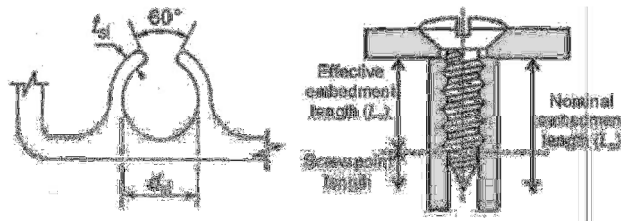
Figure 8.6.11: definition of screw-groove joints geometry

Now, the minimum embedment length can be solved using the following expression:

$$61400 = 0.29 \cdot 14.28 \cdot x \cdot 186 \quad \rightarrow \quad x = 7.9 \; cm$$

8.5.4.5. Designing the amount of material in jam near the bolts

In this section, the amount of material that is required in the jam (near the bolts) to be able to transmit the forces from the jam to the screws will be determined.

The design value $F_{Ed} = 50.53 \; kN$ in each bolt is given in section 8.6.4.1. Dividing this force by the yield strength $f_{0.2}$ of the alloy gives the minimum required Area A_{min}:

$$A_{min} = \frac{F_d}{f_{0.2}} = \frac{47870}{160} = 299.2 \; mm^2.$$

The minimum diameter near the anchors in the jam can be determined using the following formula:

$$299.2 \leq \frac{\pi}{4} \cdot ((20 + 2t)^2 - 20^2) => t > 4.2 \; mm$$

This leads to the following minimum diameter: $D_{min} = 20 + 2 \cdot t = 20 + 2 \cdot 4.2 = 28 \; mm$
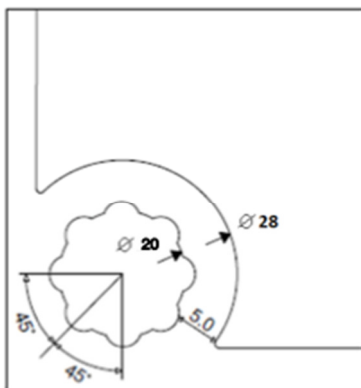
Figure 8.6.12: Minimum required diameter

51

8.5.5. Fixation on concrete foundation (anchors)

Footplates will realize the fixation of the jams to the concrete foundation and anchor bolts. Assuming that the anchors will be placed by means of drilling and non-shrink cement grout. Using NEN-EN 1993-1-8 article 3 [3], the anchors will be designed.

8.5.5.1. The resistances of the anchors

If shear is present, the design shear force $F_{V,Ed}$ should not exceed the design shear resistance $F_{V,Rd}$ given in the following expression:

$$F_{V,Rd} = \frac{\alpha_v \, f_{ub} \, A_s}{\gamma_{M2}}$$

In the same manner this applies also to tension. The design tensile force $F_{t,Ed}$ should not exceed the design tension resistance $F_{t,Rd}$ given in the following expression:

$$F_{t,Rd} = \frac{k_2 \, f_{ub} \, A_s}{\gamma_{M2}}$$

Note: For the combined shear and tension load, the following condition should be satisfied:

$$\frac{F_{V,Ed}}{F_{V,Rd}} + \frac{F_{t,Ed}}{1.4 \, F_{t,Rd}} \leq 1.0$$

A M16 5.6 quality anchor bolt with a tensile stress area of $A_s = 156 \, mm^2$ is considered. The values of α_v and k_2 are given in NEN-EN 1993-1-8 Table 3.4 [3], namely $\alpha_v = 0.6$ and $k_2 = 0.9$. The nominal value of the ultimate tensile strength $f_{ub} (= 500 \, N/mm^2 \, for \, 5.6 \, quality)$ is given in NEN-EN 1993-1-8 Table 3.1 [3].

Now, the following resistances can be determined:

Shear resistance: $\quad F_{V,Rd} = 0.6 \cdot 500 \cdot 156/(1.25 \cdot 1000) = 37.4 \, kN/anchor$

Tension resistance: $\quad F_{t,Rd} = 0.9 \cdot 500 \cdot 156/(1.25 \cdot 1000) = 56.2 \, kN/anchor$

The design shear force is presented in section 8.3, namely $F_{V,Ed} = 12.26 \, kN$. The design tensile force in presented in section 8.3, namely $F_{t,Ed} = 47.87$. Now, the bolts can be checked:

$$\frac{12.3}{37.4} + \frac{47.9}{78.7} \leq 1.0 \;\; \rightarrow \;\; 0.9 \leq 1.0$$

8.5.5.2. Basic anchorage length

According to NEN-EN 1992-1-1 article 8 [2], the basic required anchorage length $l_{b,rqd}$ in a straight bar assuming constant bond stress equal f_{bd} can be determined:

$$l_{b,rqd} = (\phi/4)(\sigma_{sd}/f_{bd})$$

where σ_{sd} is the design stress of the bar at the position from where the anchorage is measured from. The values of f_{bd} are given in NEN-EN 1992-1-1 article 8.4.2 [2]. The design value of the ultimate bond stress, f_{bd}, for ribbed bars may be taken as:

$$f_{bd} = 2.25 \, \eta_1 \, \eta_2 \, f_{ctd}$$

The values and the calculation:

- $f_{ctd} = \alpha_{ct} \, f_{ctk,0.05} \, / \, \gamma_c$ where: $\alpha_{ct} = 1$, $\gamma_c = 1.5$ and $f_{ctk,0.05} = 1.5 \, N/mm^2$
- $\eta_1 = 1$
- $\eta_2 = 1$
- $\phi = 16$
- $f_{bd} = 2.25 \, N/mm^2$
- $f_{yd} = 240 \, N/mm^2$
- $l_{b,rqd} = 2(16/4)(240 \, /2.25) = 852 mm$
- Shape anchor = hook

The design anchorage length l_{bd} can be determined using:

$$l_{bd} = \alpha_1 \, \alpha_2 \, \alpha_3 \, \alpha_4 \, \alpha_5 \, l_{b,rqd} \geq l_{b,min}$$

The values of α_n are given in NEN-EN 1992-1-1 table 8.2 [2]. The choice has been made for a hook anchor. The design anchorage length in this case is equal to:

- $l_{bd} = 0.7 \cdot 1 \cdot 1 \cdot 1 \cdot 1 \cdot 852 = 596 \, mm$.

The applied anchor with minimum cover of 100mm is shown in Figure 8.6.13.
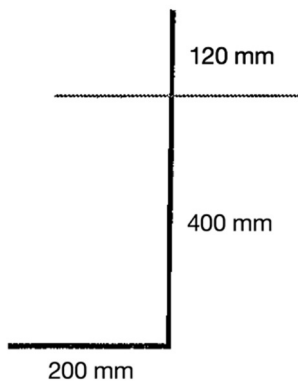
Figure 8.6.13.: Anchor in the concrete barrier

8.5.6. Fixation on concrete foundation (footplate)

In this section, we will calculate the dimensions of the footplate. First we will calculate the maximum stress in the footplate that occurs due to the loading. Subsequently we will choose an aluminium alloy from NEN-EN 1999-1-1 table 3.2a [4]. In this table, the characteristic values are given for wrought aluminium alloys.

The tension force in the screws are presented in section 8.6.4.1. In order to calculate the M_{Ed} for the anchors, the distance from the centre of the anchor to the centre of the bolt in the jam has to be known, shown in Figure 8.6.14. We assume a spreading in one borehole in the footplate of 1:1. The diameter of the boreholes are 20mm. This gives an effective working width of $b_{eff} = 2 \cdot 20.0 = 40 \ mm$. The bending moment in the footing plate is $M_{Ed} = 47.9 \cdot 0.040 = 1.8202 \ kNm$.

Hence:

$$\sigma_{Ed} = \frac{M_{Ed}}{W} = \frac{1.916 \cdot 10^6}{1/6 \cdot 2 \cdot 40 \cdot 23^2} = 271 \ N/mm^2$$

The wrought aluminium alloy EN AW-5083 H14 will be used as footplate with a yield strength of $f_{0.2;d} = 280 \ N/mm^2$. The dimensions of the footplate are given in Figure 8.6.14.
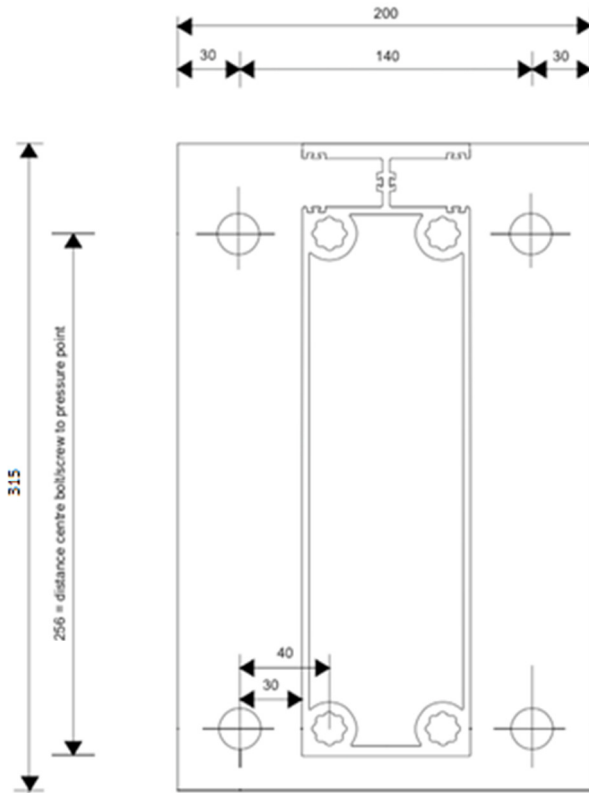
Figure 8.6.14: Fixation of footing plate on concrete barrier

Now, the weight of the footplate can be calculated as follows:

- $A_{footplate,netto} = (200 \cdot 315) - 4(\pi \cdot 10^2) = 61743 \ mm^2$
- $m_{total} = m_{footplate} + m_{jam} = (41743 \cdot 23 \cdot 2700 \cdot 10^{-9}) + 44.6 = 47.2 \ kg$

Conclusion: The total weight of the structure meets requirement 3 given in section 8.1.

8.5.7. Fatigue resistance

A check regarding the fatigue of the structure must be done. NEN-EN 1999-1-3 [4] and GCW-2012 [5] specify that the calculations to perform this check must be done according to Miner's rule using different stress magnitudes in a spectrum. From GCW-2012 [5] one must refer to the 'safe life design' scenario as opposed to the 'damage tolerant design' scenario.

For the safe life design the damage D_L for all cycles using Miner's summation should fulfill the condition:

$$D_L \leq D_{lim}$$

Where:

$D_L = \sum n_i/N_i$ is calculated in accordance with the procedure given in NEN-EN 1999-1-3 annex 2.A [4].

8.6.7.1. Fatigue loading

In accordance with NEN-EN 1999-1-3 article 2.4. [4] a partial factor should be applied to the fatigue loads F_{Ek} to obtain the design load F_{Ed}:

$$F_{Ed} = \gamma_{Ff} F_{Ek}$$

where:

γ_{Ff} is the partial factor for fatigue loads.

In this case, the recommended value of $\gamma_{Ff} = 1.0$ should be applied according to ''NOTE 1'' of the given article. The tensile force in each screw as a result of bending moment can be calculated by dividing the characteristic value of the moment M_{cr} by the distance between the screw and the pressure point, as given below:

- $F_{t,Ed} = \frac{20.48}{2 \cdot 0.256} = 40.0 \ kN$

Dividing the tensile force by the tensile stress area ($A_s = 245 \ mm^2$) the maximum value of the stress can be determined:

- $\sigma_{max} = \frac{F}{A_s} = \frac{40.0 \cdot 10^3}{245} = 163 \ N/mm^2$

8.5.7.2. Number of cycles according to S-N curve with range $\Delta\sigma_i$ (resistance)

In this section the threads of the steel bolt and the threads of the aluminium (section 8.6.4) that is caused by screwing the bolts into the jam will be checked.

The characteristic value of N depends on the detail of the structure. The detail categories and the $\Delta\sigma - N$ relationships for steel plain members and mechanically fastened joints of steel are given in NEN-EN 1993-1-9 table 8.1. [3].

Because the fatigue strength of aluminium threads in tension is not given in NEN-EN 1999-1-3 [4], it should be noted that the following estimation will be used for the estimation of the fatigue strength:

$$\Delta\sigma_{c,aluminium} = 0.3 \cdot \Delta\sigma_{c,steel}$$

Figure 8.6.15. shows the detail category and the constructional detail which will be used for the fatigue analysis of the steel screw-threads.
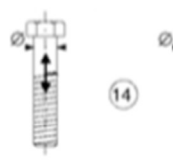
Detail category	Constructional detail		Description	Requirements
50	size effect for $\iota > 30mm$: $k_s = (30/\iota)^{0.25}$	(14)	14) Bolts and rods with rolled or cut threads in tension. For large diameters (anchor bolts) the size effect has to be taken into account with k_s.	14) $\Delta\sigma$ to be calculated using the tensile stress area of the bolt. Bending and tension resulting from prying effects and bending stresses from other sources must be taken into account. For preloaded bolts, the reduction of the stress range may be taken into account.

Table 8.6.15: Detail category for bolts and rods with rolled or cut threads in tension

The fatigue strength curves for the calculation of the direct stress ranges are shown in Figure 8.6.16.
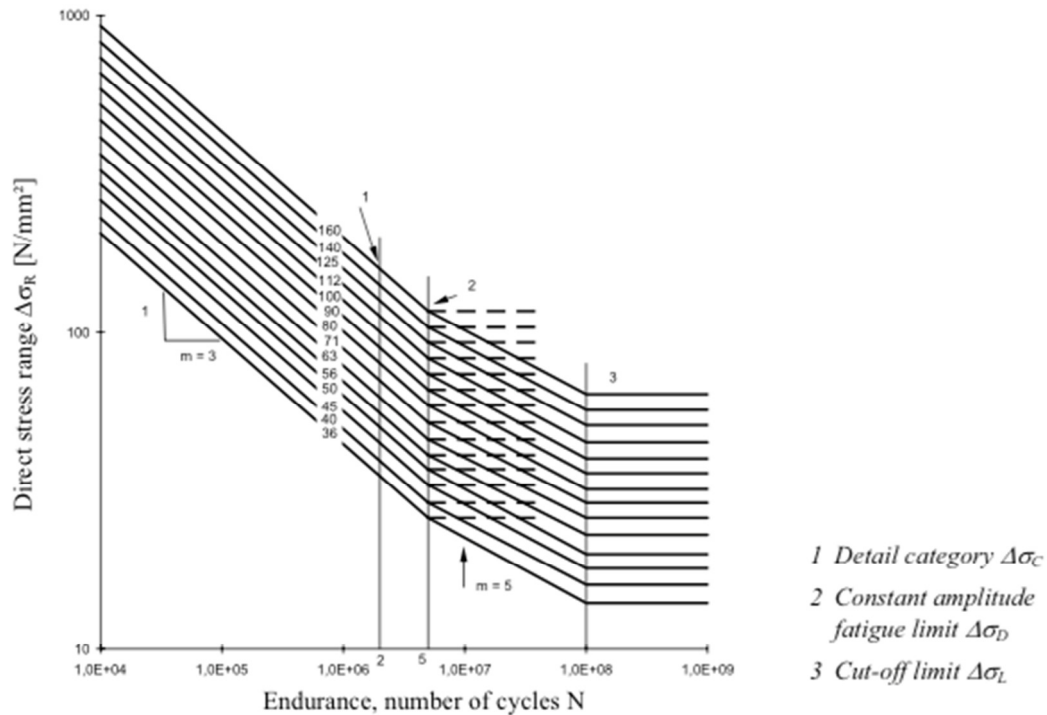
Table 8.6.16: Detail category for bolts and rods with rolled or cut threads in tension

8.5.7.3. Number of loads for dynamic response (load)

In this section, two different methods for determining the fatigue damage will be compared. The first method is in accordance with NEN-EN 1991-1-4 Annex B.3 [1] as shown in Figure 8.6.17. This method does not clearly describe the ratios ($\Delta S/S_k$), which should be taken into account when determining N_i. The second method shows clearly the ratios that have to be taken into account when determining N_i, as shown in table 8.6.8. Both methods use a life-time of 50 years. After the comparison, the choice will be made for the method that will be used to determine the fatigue damage.

(1). Figure 8.6.17. shows the number of times N_g, that the value ΔS of an effect of the wind is reached or exceeded during a period of 50 years. ΔS is expressed as a percentage of the value S_k, where S_k is the effect due to a 50 years return period wind action.
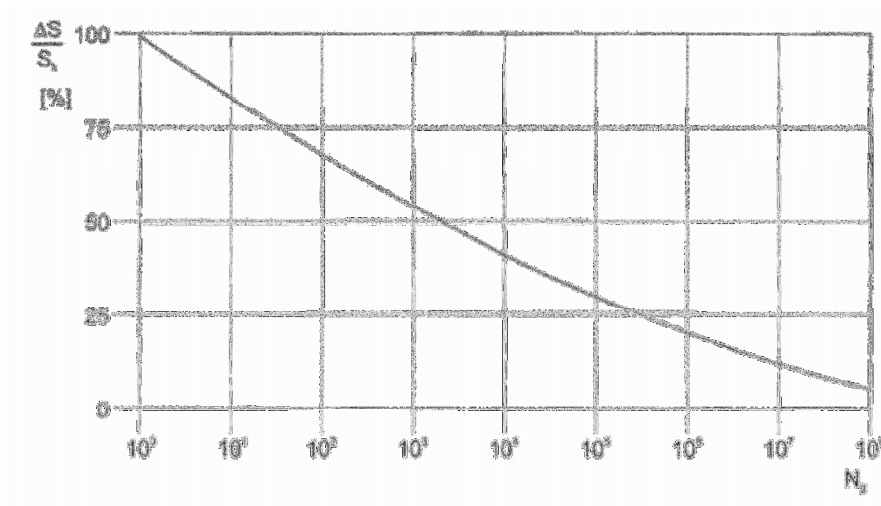
Figure 8.6.17: Number of gust loads N_g for an effect $\Delta S/S_k$ during a 50 years period

The relationship between $\Delta S/S_k$ and N_g is given by the following expression:

$$\frac{\Delta S}{S_k} = 0.7 \cdot \left(\log(N_g)\right)^2 - 17.4 \cdot \log(N_g) + 100$$

(2). The number of cycles according to GCW-2012 [5] is given in table 8.6.8 below.

Table 8.6.8: value α with the matching number of cycles n_i according to GCW-2012

Value α	Number of cycles n_i
1.00	1
0.85	6
0.73	60
0.60	600
0.48	6.000
0.26	60.000
0.12	600.000
0.03	6.000.000

(3). Comparison methods (1) and (2).

To compare the two methods to each other, the numbers of cycles given in table 8.6.8 are implemented in the formula of the fist method. In this way, the values are calculated for $\Delta S/S_k$. Dividing these values by 100, the factors of α are obtained as shown in table 8.6.9.

Table 8.6.9: value α with the matching number of cycles n_i according to NEN-EN 1991-1-4 Annex B.3

$value\ \alpha$	Number of cycles n_i
1.00	1
0.87	6
0.71	60
0.57	600
0.44	6.000
0.33	60.000
0.23	600.000
0.14	6.000.000

Figure 8.6.18. shows the comparison of the two methods.
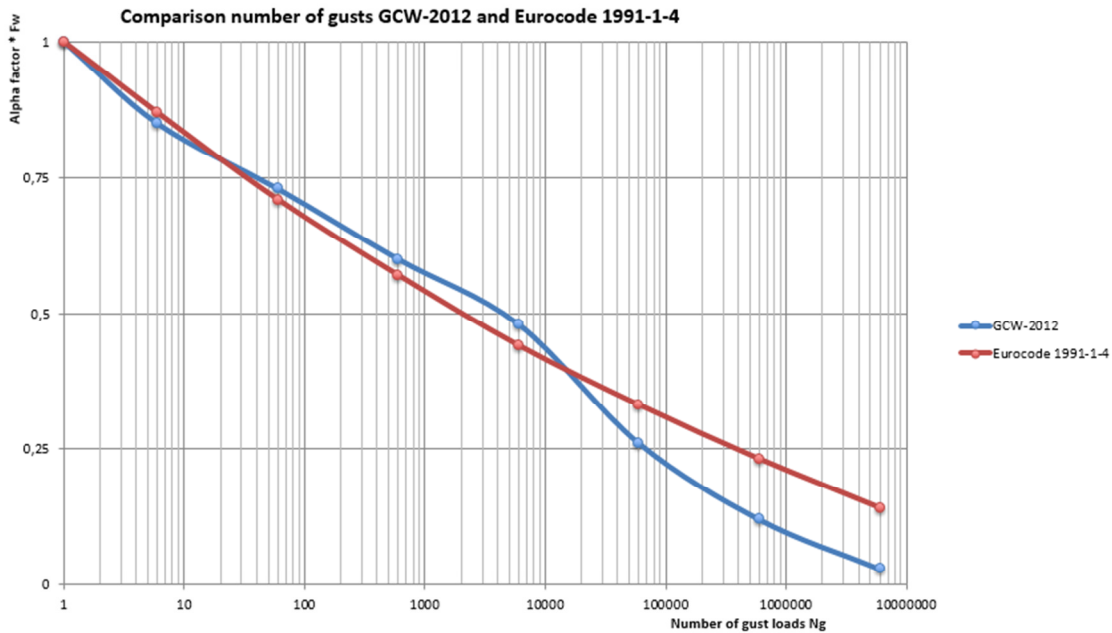
Figure 8.6.18: comparison of method (1) and (2) of gust loads N_g for an effect $\Delta S/S_k$ during a 50 years period

Conclusion: The comparison shows that the two methods do not differ too much from each other for high enough alpha values. However, the difference grows larger if lower alpha values are used. We can see that the second method (NEN-EN 1991-1-4 Annex B.3 [1]) is more conservative. Due to these differences we are unable to apply the same factors α for the maximum windload as is specified in the second method (GCW-2012 [5]). Additionally, NEN EN 1991-1-4 Annex B.3 [1] lacks sufficient documentation regarding the factors α of the maximum wind loads that need to be considered. As opposed to method 1, the second method does provide a clear specification of the factors α regarding the maximum wind loads for noise barriers. There is insufficient amount of information available, and the GCW-2012 [5] is the only source suitable for this specific situation and widely used

by structural engineers who design noise barriers. Therefore, the GCW-2012 [5] factors with its gusts cycles will be used when determining the fatigue damages. In the next phase of this study the integrity of this method will be tested using a dynamical analysis.

This dynamic analysis will be done according to the power spectral density (PSD) method. This method is briefly considered in [12]. As opposed to the fatigue analysis given in this chapter, the PSD method will incorporate the dynamic behaviour of the structure. By studying the dynamic behaviour of the structure we will be able to draw conclusions regarding the necessity of including the dynamic response in our calculations, and whether other structural engineers should do the same in the future.

It must however be mentioned that further research is required to be able to explain the differences between the two methods.

8.5.7.4. The fatigue check of the steel screws-threads

The detail category is given in section 8.6.7.2, namely $\Delta\sigma_C = 50$. The partial factor γ_{Mf} for fatigue strength safe life, according to GCW-2012 [5], can be determined using NEN-EN 1999-1-3 Table L.2 [4] and is equal to 1.00. The S-N curve to use follows from:

- $\frac{\Delta\sigma_C}{\gamma_{Mf}} = \frac{50}{1.00} = 50\ MPa$

Subsequently, the cut off limit and the constant amplitude fatigue limit can be given as follows:

Cut off limit:

- $\Delta\sigma_L = \left[\frac{5}{100}\right]^{\frac{1}{5}} \cdot \Delta\sigma_D = 0.405\Delta\sigma_c = 20.25\ MPa$

Constant amplitude fatigue limit:

- $\Delta\sigma_C = \left[\frac{2}{5}\right]^{\frac{1}{3}} \cdot \Delta\sigma_C = 0.737\Delta\sigma_C = 38.85\ MPa$
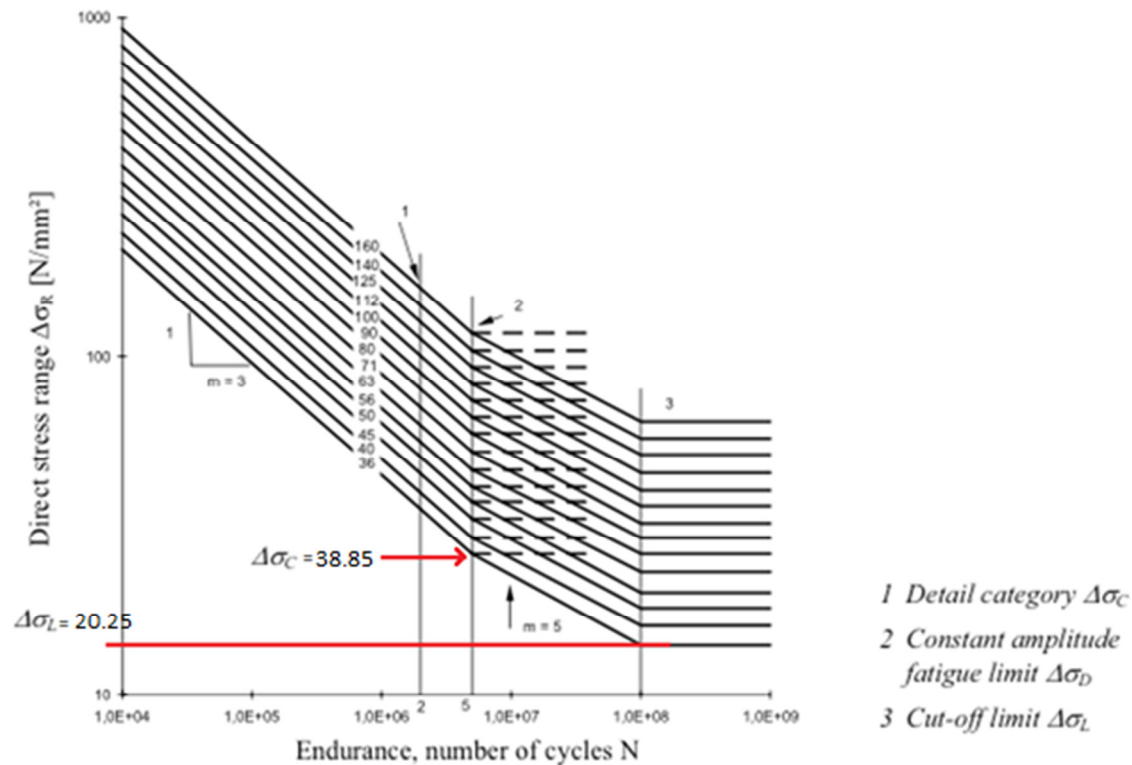
Table 8.6.19: the cut-off limit and the constant amplitude fatigue limit for the S-N curve

For nominal stress spectra with stress ranges above and below the constant amplitude fatigue limit the fatigue strength should be based on the extended fatigue strength curves as follows:

- $\Delta\sigma_R{}^m \cdot N_R = \Delta\sigma_C{}^m \cdot 2 \cdot 10^6$ with   m=3   for $N \leq 5 \cdot 10^6$
- $\Delta\sigma_R{}^m \cdot N_R = \Delta\sigma_C{}^m \cdot 5 \cdot 10^6$ with   m=5   for $5 \cdot 10^6 \leq N \leq 10^8$

The total damage according to GCW-2012 [5]

Table 8.6.10: the damage according to GCW-2012

Value α	n_i	$\Delta\sigma$ N/mm^2	N_i	n_i / N_i
1.00	1	163	27079	3.69283E-05
0.85	6	138	44623	0.000134458
0.73	60	118	71377	0.000840609
0.60	600	98	124601	0.004815334
0.48	6.000	73	301463	0.019902919
0.26	60.000	42	1582906	0.037904961
0.12	600.000	18	234186898	0.000000000
0.03	6.000.000	5	infinite	0.000000000
Total damage D:				0.063635209
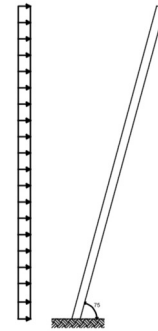
The red line in the table indicates the difference between the m-value by determining the number of cycles N; $m = 3$ for values of the direct stress range $\Delta\sigma_R$ more then the detail category $\Delta\sigma_C$ and $m = 5$ for values of the direct stress range $\Delta\sigma_R$ lesser then the detail category $\Delta\sigma_C$.

Conclusion: According to the design guide of noise barriers (GCW-2012 [5]) the fatigue satisfies the following condition:

$$Total\ damage\ = \sum \frac{n_i}{N_i} < 1.0 \rightarrow 0.06 < 1.0$$

The total damage according to NEN-EN 1991-1-4 [1]

Table 8.6.11: the damage according to GCW-2012

Value α	n_i	$\Delta\sigma$ N/mm^2	N_i	n_i / N_i
1.00	1	163	27079	0.000123094
0.85	8	138	44623	0.000448129
0.73	48	118	71377	0.002802031
0.60	350	98	124601	0.016051113
0.48	2.800	73	301463	0.066343062
0.26	350.000	42	1582906	0.126349871
0.12	12.000.000	18	234186898	0.008540187
0.03	120.000.000	5	infinite	0.000000000
Total damage D:				0.220657551
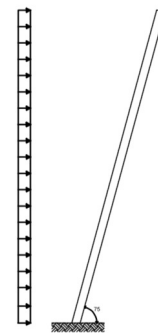
Conclusion: According to NEN-EN 1991-1-4 [1] the fatigue satisfies the following condition:

$$\sum \frac{n_i}{N_i} < 1.0 \rightarrow 0.22 < 1.0$$

8.5.7.5. The fatigue check of the aluminium screws-threads

As mentioned before, the fatigue strength of aluminium threads in tension is not given in the design guide. Therefore, the following expression was given for the estimation of the fatigue strength:

- $\Delta\sigma_{c,aluminium} = 0.3 \cdot \Delta\sigma_{c,steel} = 0.3 \cdot 50 = 15 \; Mpa$

In the same way as given in the previous section, the fatigue strength and subsequently the fatigue damage will be considered below.

The S-N curve to use follows from:

- $\frac{\Delta\sigma_C}{\gamma_{Mf}} = \frac{15}{1.00} = 15 \; MPa$

Subsequently, the cut off limit and the constant amplitude fatigue limit can be given as follows:

Cut off limit:

- $\Delta\sigma_L = \left[\frac{5}{100}\right]^{\frac{1}{5}} \cdot \Delta\sigma_D = 0.405\Delta\sigma_c = 8.24 \; MPa$

Constant amplitude fatigue limit:

- $\Delta\sigma_C = \left[\frac{2}{5}\right]^{\frac{1}{3}} \cdot \Delta\sigma_C = 0.737\Delta\sigma_C = 11.06 \; MPa$
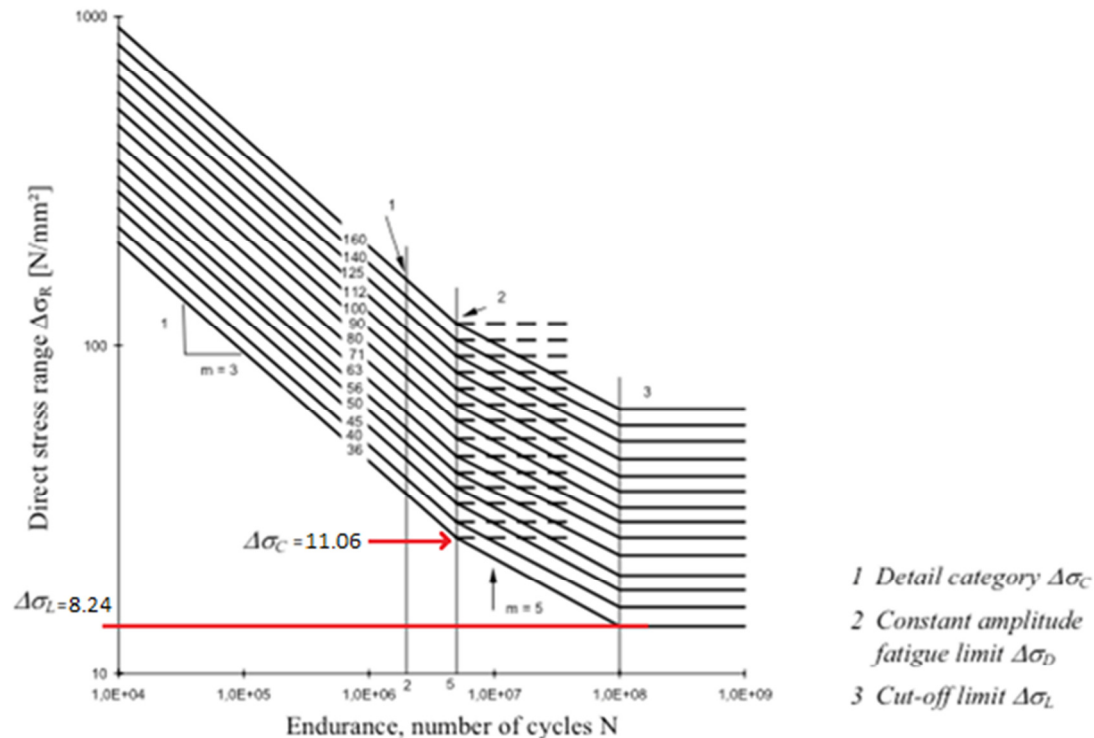
Figure 8.6.20: the cut-off limit and the constant amplitude fatigue limit for the S-N curve

For nominal stress spectra with stress ranges above and below the constant amplitude fatigue limit the fatigue strength should be based on the extended fatigue strength curves as follows:

- $\Delta\sigma_R{}^m \cdot N_R = \Delta\sigma_C{}^m \cdot 3 \cdot 10^6$ with   m=3   for $N \leq 5 \cdot 10^6$
- $\Delta\sigma_R{}^m \cdot N_R = \Delta\sigma_C{}^m \cdot 5 \cdot 10^6$ with   m=5   for $5 \cdot 10^6 \leq N \leq 10^8$

The total damage according to GCW-2012 [5];

Table 8.6.12: the damage according to GCW-2012

Value α	n_i	$\Delta\sigma$ N/mm²	N_i	n_i/N_i
1.00	1	163	8123	0.000123094
0.85	6	138	13387	0.000448192
0.73	60	118	21413	0.002802031
0.60	600	98	37380	0.016051113
0.48	6.000	73	90439	0.066343062
0.26	60.000	42	47872	0.126349871
0.12	600.000	18	70256069	0.008540187
0.03	6.000.000	5	Infinite	0.000000000
Total damage D:				0.220657551
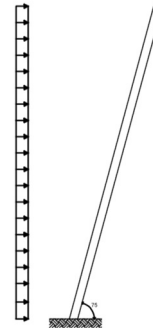
The red line in the table indicates the difference between the m-value by determining the number of cycles N; $m = 3$ for values of the direct stress range $\Delta\sigma_R$ more then the detail category $\Delta\sigma_C$ and $m = 5$ for values of the direct stress range $\Delta\sigma_R$ lesser then the detail category $\Delta\sigma_C$.

Conclusion: According to the design guide of noise barriers (GCW-2012 [5]) the fatigue damage satisfies the following condition:

$$\sum \frac{n_i}{N_i} < 1.0 \ \rightarrow 0.23 < 1.0$$

The total damage according to NEN-EN 1991-1-4 [1];

Table 8.6.13: the damage according to GCW-2012

Value α	n_i	$\Delta\sigma$ N/mm²	N_i	n_i/N_i
1.00	1	163	8123	0.000123094
0.85	8	138	13387	0.000597589
0.73	48	118	21413	0.002241625
0.60	350	98	37380	0.009363149
0.48	2.800	73	90439	0.030960096
0.26	350.000	42	47872	0.737040912
0.12	12.000.000	18	70256069	0.170803748
0.03	120.000.000	5	Infinite	0.000000000
Total damage D:				0.951130214
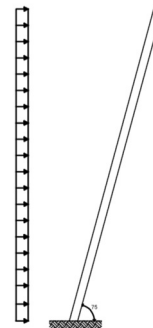
Conclusion: According to NEN-EN 1991-1-4 [1] the fatigue damage satisfies the following condition:

$$\sum \frac{n_i}{N_i} < 1.0 \ \rightarrow 0.95 < 1.0$$

9. Dynamic analysis

In this section the dynamic analysis according to Dirlik's [6] approach will be given and discussed. In the literature survey this method is explained in more detail. In the introduction, section 9.1, the method will be discussed briefly. After the introduction, the calculations and the results of the dynamic analysis will be given in section 9.2.

9.1. Introduction

If the load varies throughout time the displacements and stresses will also vary throughout time. Figure 9.1.1. visualizes this principle. In this Figure it is clearly shown that the wind loading varies over time. As a result, the structural response will also vary over time.
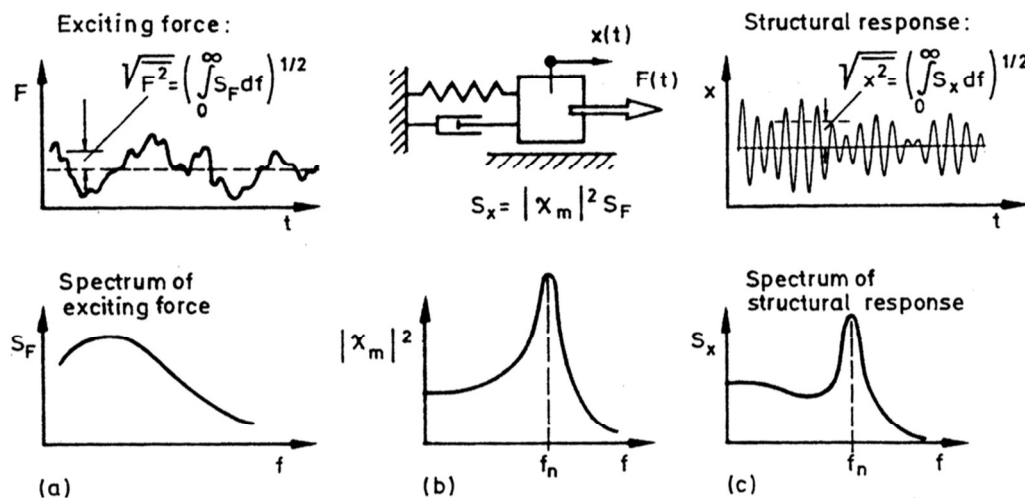
Figure 9.1.1: fluctuating wind loading

Similar to the literature survey, two dynamic analysis options will be considered briefly, namely the time domain and the frequency domain analysis.

Time domain S-N Fatigue Life Estimation
Traditionally, the Rainflow cycle counting method is widely used to describe the stress range to decompose a variable amplitude time signal of stress into fatigue cycles. The damage from each cycle is computed using a Wöhler curve and the damage over the entire signal is calculated by summing up the damage from all the individual cycles. This approach is satisfactory for periodic loading but requires very large time records (a set of static wind measurements) to accurately describe a random loading process. The accumulated damage is expressed as a proportion of the damage required for the material to succumb. According to [13] the overall process for fatigue life estimation in the time domain is shown in Figure 9.1.2.

Figure 9.1.2: Time domain calculation

The Fourier transform
Primarily, the frequency domain is another way of representing a time history. Certain information about a random process becomes apparent in a frequency domain plot, which is difficult to see in the time domain. Using the Fourier Transformation and Inverse Fourier Transformation, it is easy to flip back and forth between the two domains, as shown in Figure 9.1.3. In this way an engineer can see both time and frequency domain representations of a signal in the same way as he would flip a graph between log and linear axes to gain a different perspective.
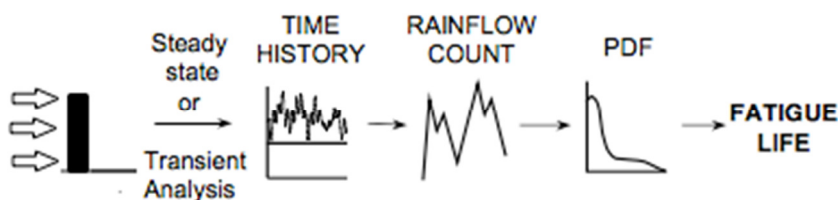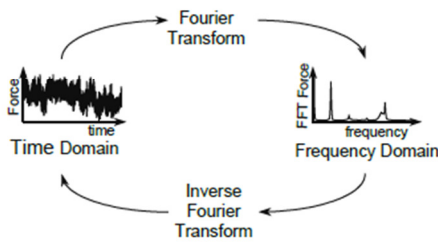

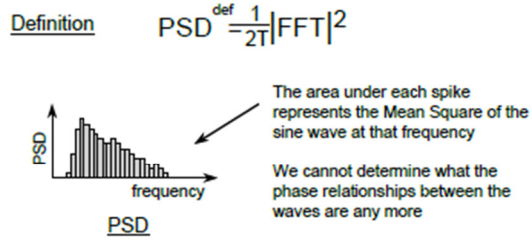Figure 9.1.3. The Fourier Transformation   Figure 9.1.4. PSD and FFT

Frequency domain Fatigue Life estimation
Alternatively, a compact frequency domain fatigue calculation can be utilized where the random loading and response are categorised using Power spectral density (PSD) functions and the dynamic structure is modelled as a single degree of freedom (SDOF) system with linear structural behaviour. The real load distribution varies randomly in space and time. Nevertheless, the equivalent static load is largely adequate as long as the structural behaviour can be assumed as linear. A non-linear analysis provides a more realistic description of the structural response, but only if at the same time a realistic gust load pattern is applied.

The PSD's are obtained by taking the modulus squared of the FFT (Figure 9.1.4.) and describes the frequencies of the wind fluctuations which is important to assess the dynamical effects of wind. In other words, the PSD is a common statistical function that describes the loads. The structure can resonate if the frequency of the wind loading is close to the natural frequency of the system. As a result, the structure can be damaged.

The PSD of a stress-time history has been receiving more attention as a result of increased use of Finite Element methods to analyse structures. Given a set of dynamic input forces, a Finite Element program will predict PSD plots at any point on a component or structure. In this section the methods will be given for computing fatigue life, or damage, directly from a PSD as opposed to a time signal. According to [13] the overall process for fatigue life estimations in the frequency domain is shown in Figure 9.1.5.
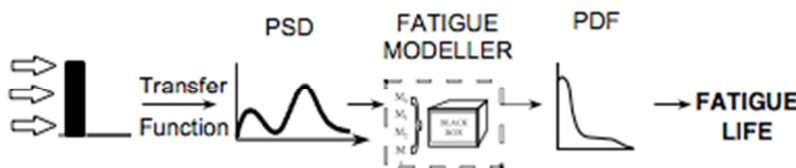

Figure 9.1.5: Frequency domain calculation

The total amount of expected stress cycle counts during the design lifetime
Section 9.2.11. describes the final step of the PSD analysis, namely the stress range spectra $N(\Delta\sigma)_{Life}$. The stress range spectra can be computed by the following expression:

$$N(\Delta\sigma)_{Life} = \int_0^{\bar{u}} \frac{T_{Life}}{T_{ref}} \cdot f(\bar{u}) \cdot N(\Delta\sigma, u)du$$

Where:

- T_{Life} is the designed Lifetime;
- T_{ref} is the average time of the mean wind speed;
- $f(\bar{u})$ is the probability density function of the mean wind speed (Weibull distribution function);
- $N(\Delta\sigma, u)$ is the stress range spectra for a given mean wind speed within the average time period.

The total amount of expected stress cycle counts during the design life-time of a structure can be derived based on the Palmgren-Miner's hypothesis, usually referred as Miner's Rule. This widely accepted rule, assumes that if n_i cycles of load are applied to a component at a level of stress which would cause failure at N_i cycles in a constant amplitude test, then the fraction of life used is exactly proportional to n_i. Or it can be stated as, that failure occurs when:

$$\sum \frac{n_i}{N_i} = 1$$

Where

- n_i is the number of applied load cycles of type i;
- N_i is the pertinent fatigue life;

The principle of the steps of the dynamic fatigue analysis, which will be discussed in this section, is given in Figure 9.1.6 below.
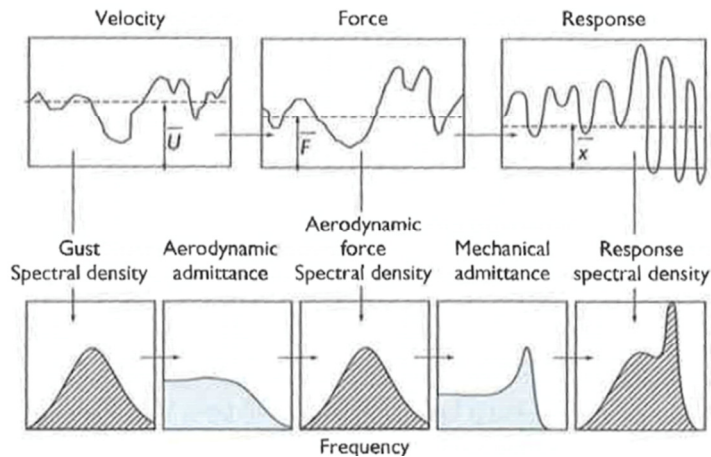
Figure 9.1.6: relation between the velocity of the wind and response of the structure

For a realistic determination of the fatigue damage due to wind exerted vibrations it is important to consider all aspects which can influence the response of the structure. This involves the aerodynamic and mechanic parameters. The parameters can be considered by using transfer functions, also called as admittance functions. The aerodynamic admittance functions will considered in section 9.2.4 and the mechanic admittance function will be considered in section 9.2.5.

9.2. Dynamic analysis

In this section the steps described earlier in the literature survey for the determination of reliable cycle count spectra for the expected design life are computed for exemplary single degree of freedom system with different dynamic properties. For this analysis the program MATLAB is used. The associated structural properties are listed in table 9.2.1. This section is separated into the following sections:

- 9.2.1. Natural frequencies of the structure;
- 9.2.2. The Gaussian distribution function;
- 9.2.3. Power spectral density function of the wind gusts;
- 9.2.4. Power spectral density function of the wind force;
- 9.2.5. Mechanical admittance function;
- 9.2.6. Power spectral density function of the displacements;
- 9.2.7. Comparison of the frequency of the loading and the response;
- 9.2.8. Power spectral density function of the stresses;
- 9.2.9. Weibull distribution function;
- 9.2.10. PSD cycle counting method;
- 9.2.11. The total amount of stress cycles and the total damage of the aluminium and steel;
- 9.2.12. Comparison of the static and dynamic analysis;

The numerical calculations were done with a MATLAB script. There are two variables, the frequency f (or the angular velocity $\omega = 2\pi f$) and the velocity u, which need to be discretized. The frequency f runs from 0 to 10 Hz, and the velocity u from 0 to 30 m/s. Both variables were implemented as grids with a step size of 0.1. The associated parameters of the wind conditions and structural properties are given in table 9.2.1.

Table 9.2.1: The associated parameters of the wind conditions and structural properties

Parameter	Value	Unit
Mean velocity v_m	17	m/s
Turbulence Intensity I_{ref}	16.5	%
Integral Length Scale L_k	29.89	m
Standaard deviation σ	3.1	m/s
Shape parameter k	1.83	$-$
Scale parameter A	5.6	m/s
Density air ρ	1.25	kg/m^3
Force coefficient c_f	2.1	$-$
Loaded area A	4	m^2
Angular frequency $\omega_1 = \omega_0$	58.17	rad/sec
Damping ratio ξ	$0.01, 0.1 \ and \ 1$	$-$
Mass of the structure m	47.2	kg

The calculation of the Angular frequency ω_0 and the damping ratio ξ will be considered below.

9.2.1. Natural frequencies of the structure

Using general formulas of a cantilever beam [14], the first three undamped natural frequencies of the jams can be determined. The principle is given in Figure 9.2.1.
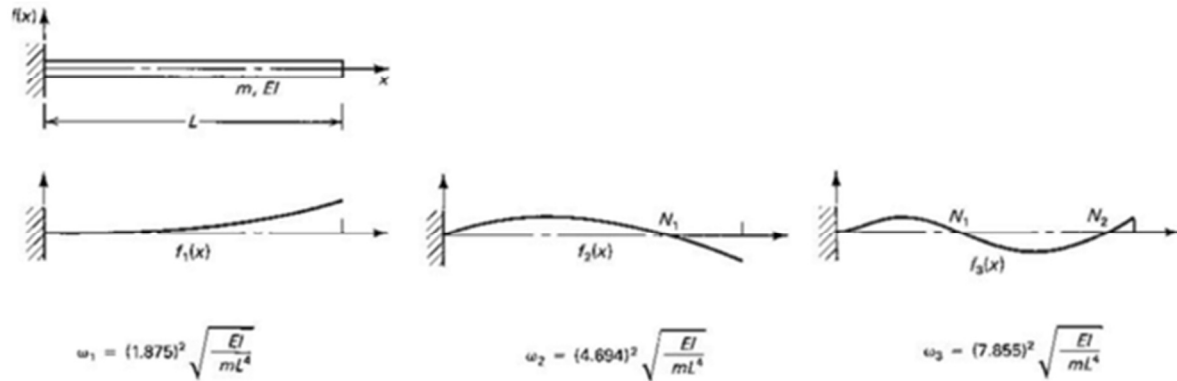
Figure 9.2.1: The first three undamped natural frequencies and mode shape of cantilever beam

The jam has the following **properties**:

- $Length\ L$ $4\ m$
- $Mass\ m$ $47.2\ kg$
- $Elastic\ modulus\ E$ $0.7 \cdot 10^{11}\ N/m^2$
- $Second\ moment\ of\ area\ I$ $4.726 \cdot 10^{-5}\ m^4$

First natural frequency:

$$\boldsymbol{\omega_1} = (1.875)^2 \cdot \sqrt{\frac{EI}{mL^4}} = (1.875)^2 \cdot \sqrt{\frac{0.7 \cdot 10^{11} \cdot 4.726 \cdot 10^{-5}}{47.2 \cdot 4^4}} = 58.17\ rad/sec$$

$$f = \frac{\omega}{2\pi} = 9.26\ Hz$$

Where:

- $\omega\ =\ angular\ frequency$

9.2.2. The Gaussian distribution function

In this thesis, Dirlik's approach method will be considered for counting the stress cycles of the response of the structure, which will be considered in section 9.2.9. As mentioned in [6], the Dirlik's approach is validated for the cases when the random load follows a Gaussian or nearly Gaussian distribution, and becomes less accurate when the random load is a non-Gaussian distribution. Therefore, for an accurate determination of the total damage of the structure a Gaussian distribution is considered for the acting wind loading.

To make a realistic comparison with the static calculation, it is important to make a dynamic analysis for the mean wind speed as considered in the static calculations, namely with a mean wind speed of 17 m/s. Since it is not possible to obtain the 10 minutes mean wind speed measurements from the KNMI database, the standard deviation is based on the available hourly mean wind speed measurement from the KNMI data. The used standard deviation is equal to 3.1 m/s. This makes it possible to assume that this system is under a load F that follows a Gaussian distribution with a mean value of 17 m/s, and a standard deviation of 3.1 m/s. The Gaussian distribution [15] has the following probability density function for the random variable X:

$$f_X(x) = P\left[x < X \leq x + dx\right] = \frac{1}{\sqrt{2\pi}\sigma_X} \exp\left[-\frac{1}{2}\left(\frac{x - \mu_X}{\sigma_X}\right)^2\right]$$

With:

- Mean wind speed $\mu_X = 17\ m/s$ and the standard deviation $\sigma_X = 3.1\ m/s$.

Figure 9.2.2. shows a normal distribution with a mean of 17 m/s and a standard deviation of 3.1 m/s. The density of the Gaussian distribution is shown in Figure 9.2.2.
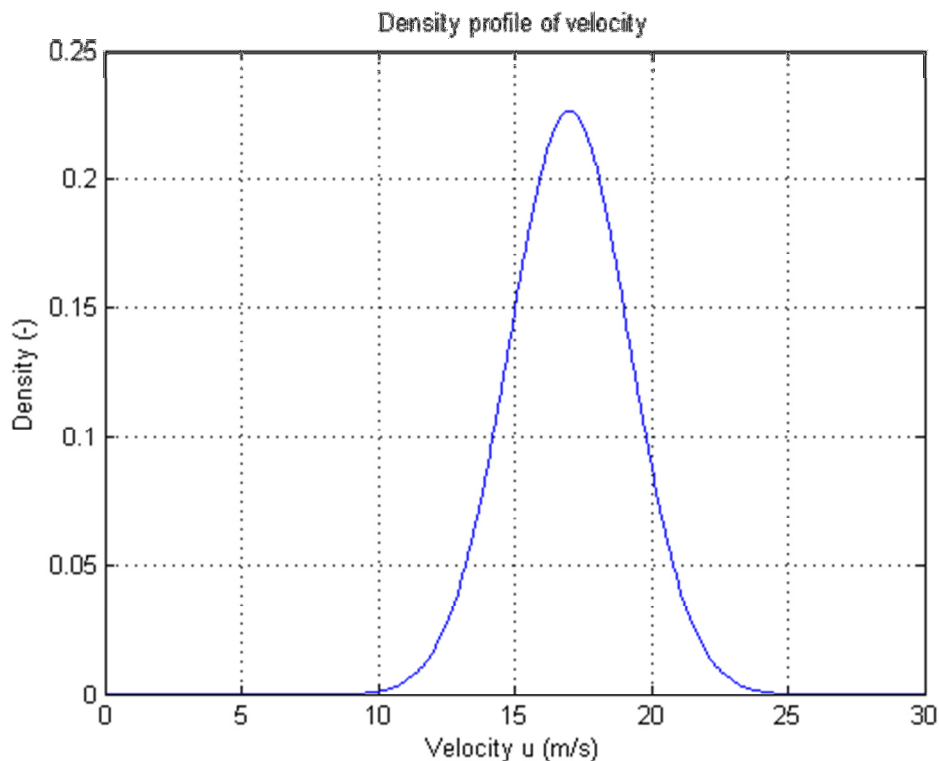

Figure 9.2.2: the Gaussian distribution function

Because of the symmetry around the center, the Gaussian distribution has 50% of its values less than the mean wind speed and 50% greater than the mean wind speed. It is also useful to mention that 68% of the area of a normal distribution is within one standard deviation of the mean and approximately 95% if the area is within two standard deviations of the mean.

9.2.3. Power spectral density function of the wind gusts

The wind distribution over the frequencies is expressed by the non-dimensional power spectral density (PSD) function of Kaimal $S_{vv}(f)$, which is determined using the following expression:

$$S_{vv}(f) = \frac{6.8 \cdot \sigma_v{}^2 \cdot (L_k/v_m)}{(1 + 10.2 \cdot f \cdot L_k/v_m)^{5/3}}$$

Where:

- $L_k = integral\ length\ scale$;
- $v_m = mean\ velocity$;
- $f = frequency\ of\ the\ structure$.

The fluctuating contribution, turbulence, is best described stochastically as a process with a mean value of 0 m/s and a standard deviation of σ_v m/s. The variance $\sigma_v{}^2$ gives information about the fluctuations in terms of wind speed, the Kaimal spectrum describes the distribution of wind speed fluctuations over frequencies and this is important in order to assess the dynamic effects of wind on the structure. Resonance may occur if the frequency of the wind fluctuations (loading frequency) is close to the natural frequency of the structure, which can damage the structure.

To express the PSD function in a function of the angular velocity (angular frequency) ω, the expression "$f = \omega/2\pi$" will be implemented in the formula of $S_{vv}(f)$. Now, the PSD function of Kaimal can be rewritten as:

$$S_{vv}(\omega) = \frac{6.8 \cdot \dfrac{\omega \cdot L_k}{2 \cdot \pi \cdot v_m}}{(1 + 10.2 \cdot \dfrac{\omega \cdot L_k}{2 \cdot \pi \cdot v_m})^{5/3}}$$

This form of the formula corresponds to the non-dimensional power spectral density function given in NEN-EN-1991-1-4 Annex B [1] as shown in Figure 9.2.3.
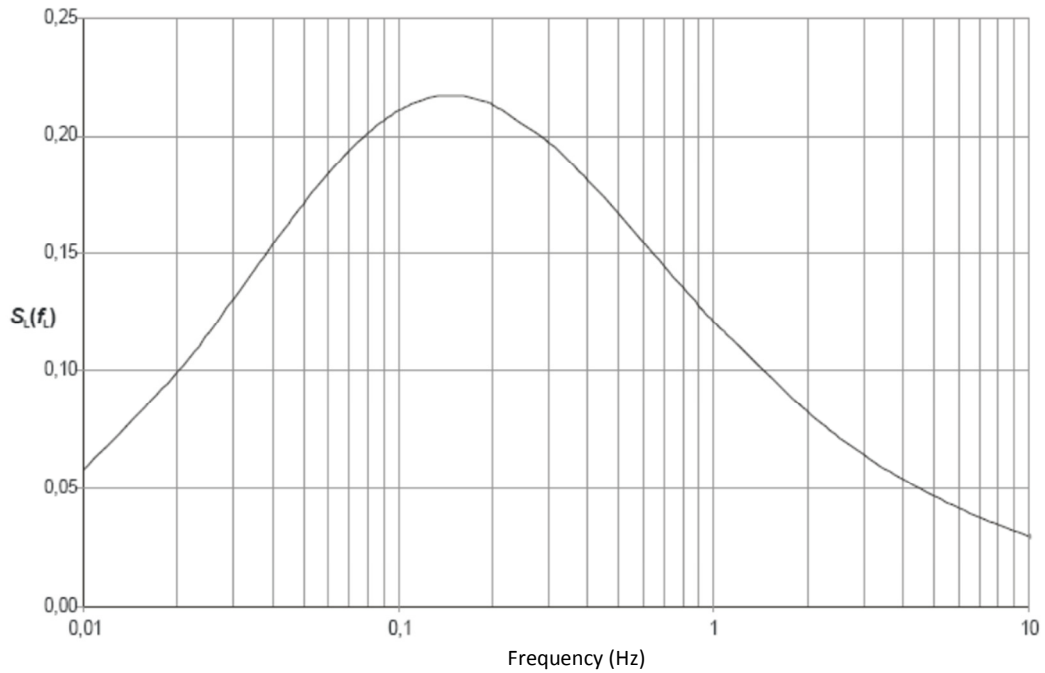
Figure 9.2.3: Power spectral density function of the gusts

Implementing the values of the $integral\ length\ scale, mean\ velocity$ and the $angular\ frequency$ as shown in table 9.2.1. in the Kaimal formula, the graph given in Figure 9.2.4 will be obtained.
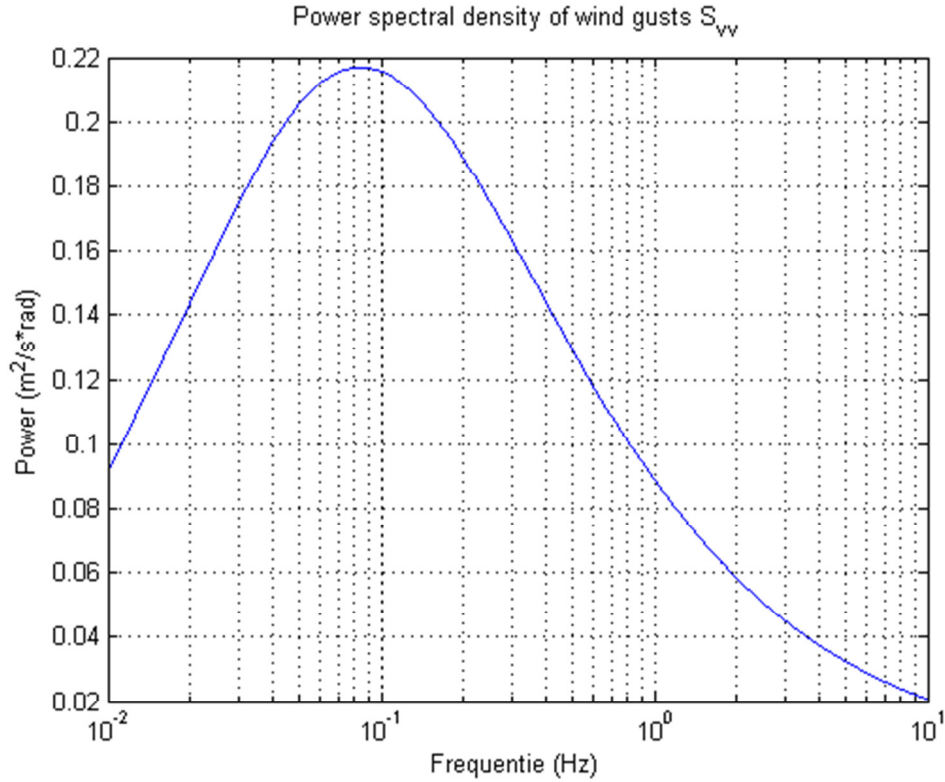
Figure 9.2.4: Power spectral density function of the gusts obtained from MATLAB

It is clearly shown that the obtained spectrum (Figure 9.2.4) corresponds closely with the spectrum given in NEN-EN-1991-1-4 Annex B [1] (Figure 9.2.3).

Power spectral density functions (PSD) show the strength of the variations (energy) as a function of frequency. In other words, it shows at which frequencies variations are strong and at which frequencies variations are weak.

The wind gusts consist of a large number of frequencies. As mentioned before, the distribution of the magnitude of the gusts over the frequencies is given by the variance spectrum S_{vv}. In other words, this spectrum shows how wind speed fluctuations are distributed over the frequencies.

9.2.4. Power spectral density function of the wind force

For a realistic determination of the structural fatigue lifetime due to wind exerted vibrations it is important to consider all aspects which can influence the response of the structure. This involves the aerodynamic and mechanic parameters. The parameters can be considered by using admittance functions [12].

The power spectral density function of the wind forces can be obtained by multiplying the power spectral density function of the wind gusts by the squared aerodynamic admittance function as given in the following expression [16]:

$$S_{\tilde{F}_i\tilde{F}_j}(\omega) = \int_A \int_A \left(c_f \cdot \rho_{air} \cdot \bar{v}_i\right)\left(c_f \cdot \rho_{air} \cdot \bar{v}_j\right) \cdot S_v(\omega) \cdot dA_i dA_j = \left[c_f \cdot \rho_{air} \cdot \bar{v}_m \cdot A\right]^2 \cdot S_{vv}(\omega)$$

Where $\left[\rho_{air} \cdot \bar{v} \cdot c_f \cdot A\right]$ is the aerodynamic admittance function and:

- ρ_{air} is the density of air (=1,25 kg/m^2);
- $\bar{v}$ is the mean wind speed [m/s];
- c_f is the form-factor [-];
- A is the loaded area of the structure [m^2].

The spectrum is given in Figure 9.2.5. It shows to what degree the wind speed fluctuations affect the structure. For high frequencies the low wind gusts, and for low frequencies the high wind gusts.
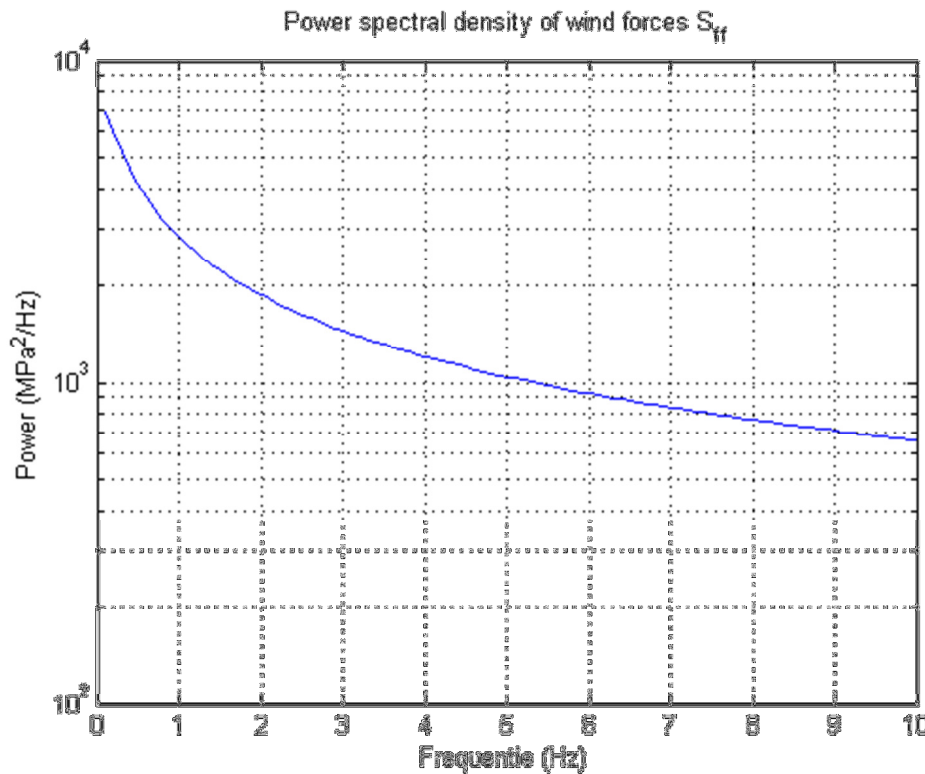

Figure 9.2.5: Power spectral density function of the wind force obtained from MATLAB

9.2.5. Bode plots & Mechanical admittance function

Before it is possible to introduce the mechanical admittance functions (or transfer function) of the system, it is necessary to obtain more clarification about Bode plots. Bode plots are graphs which are very useful to represent the frequency response of a system. On the horizontal axis of the Bode plot the frequency is given. On the vertical axis the magnitude and phase of the frequency response are plotted on a logarithmic scale. Bode plots consider a periodic (sinusoidal) signal with a frequency ω and an amplitude A, an example of such a signal is given in the following expression:

$$u(t) = A \cdot sin(\omega t)$$

Using the periodic signal as the input signal for the linear SDOF system gives the following output signal:

$$y(t) = |H(j\omega)| \cdot A \left(sin\ \omega t + \angle H(j\omega) \right)$$

The output signal consists of an amplitude A multiplied by an amplification factor $|H(j\omega)|$ which is the magnitude (or gain) of the system. Using a transfer function, which will be introduced in the following section, the magnitude can be determined using the following expression:

$$|G(j\omega)| = \sqrt{\{Re[H(j\omega)]\}^2 + \{Im[H(j\omega)]\}^2}$$

In contrast to the phase of the signal, the frequency does not change; the angular frequency ω in this expression has the same value as the angular frequency ω of the input signal. In the output signal a phase shift, $\angle H(j\omega)$ is obtained, which can be determined using the following expression:

$$\angle G(j\omega) = \tan^{-1} \left(\frac{Im[H(j\omega)]}{Re[H(j\omega)]} \right)$$

To gain more insight in the Bode plots two different signals are given with an equal input signal but a different value for the angular frequency ω. In this example the focus will be put on the magnitude and the phase of the signals.
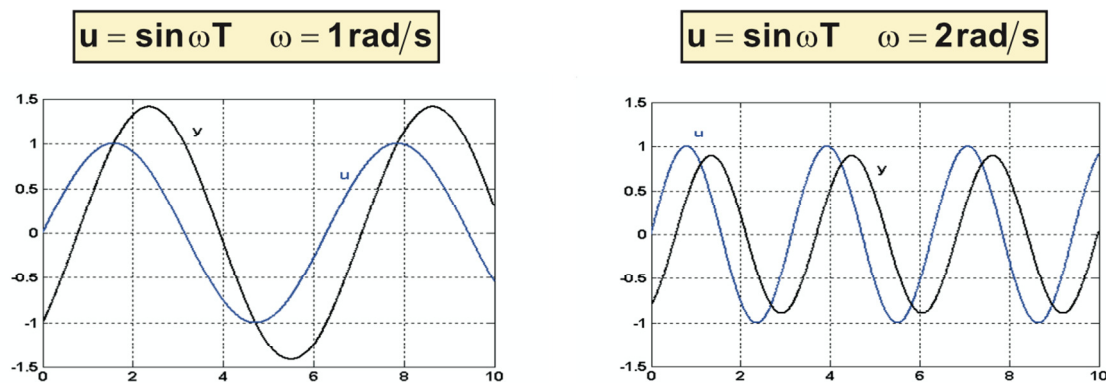
Figure 9.2.6: Two different sinusoidal input signals u with their out signals y.

Figure 9.2.6 clearly shows that the frequency does not change. In contrast to the right-hand Figure, the amplitude in the left-hand Figure of the output signal is larger than the amplitude of the input signal. This means that the magnitude (the amplification factor) in the left-hand Figure is greater than 1 and in the right-hand Figure less than 1. There is also a phase delay obtained in both Figures.

In other words, for different values of the angular frequencies different values will be obtained for the magnitude and the phase shift of a system.

In order to get structural response in the time domain, a transient structural analysis would be required, before the fatigue analysis is done. In the frequency domain a transfer function would first be computed for the structural model. This is completely independent of the input load and is a fundamental characteristic of the system. The PSD response, caused by any PSD of the input load, is then obtained by multiplying the transfer function by the input loading PSD. Once the response PSD has been computed the remaining task is to estimate the fatigue damage using Dirlik's method.

According to [12] the structure may be considered as a linear dynamic system. This means that the equation of motion is linear differential equation first order. The equation for a forced ($p(t)$) damped SDOF system will be determined step by step in this section.

Figure 9.2.7. shows the structural system which will be considered for determining the equation of motion for linear SDOF system.
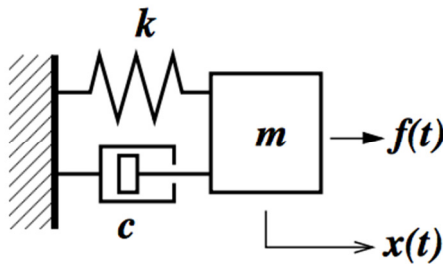
Figure 9.2.7 linear structural system   Figure 9.2.8: cantilever beam with a concentrated load P at the free end
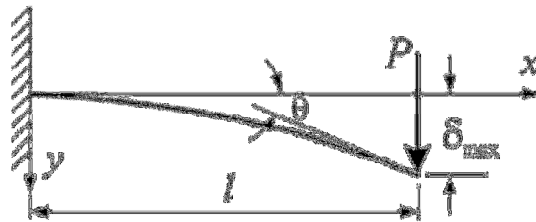
The general equation of motion for a forced damped SDOF system can be given as follows:

$$m\ddot{x} + c_v\dot{x} + kx = p(t)$$

Where:

- x is the displacement of the moving object[m];
- $\dot{x}$ is the velocity of the moving object [m/s];
- $\ddot{x}$ is the acceleration of the moving object [m/s^2];
- m is the mass of the moving object [kg];
- c_v is the linear viscous damping;
- k is the linear elastic stiffness coefficient;
- $p(t)$ is the external excitation force acting on the structure [kN];

For further elaboration of the general equation of motion, the oscillating of a cantilever beam with a concentrated load P at the free end is assumed to be as shown in Figure 9.2.8. Using this Figure the equation of motion can be derived as follows:

The natural frequency of the system ω_0 is given by:

$$\omega_0 = \sqrt{\frac{k}{m}}$$

To simplify the equation of motion, the critical damping c_c and the damping ratio ξ are defined as follows:

$$c_c = 2\,m\sqrt{\frac{k}{m}} = 2m\omega_0 \qquad \text{and} \qquad \xi = c_v/c_c$$

Substituting the critical damping c_c into the equation of the damping ratio ξ the following expression for c_v is acquired:

$$\xi = c_v/2m\omega_0 \;\longrightarrow\; c_v = \xi\,2m\omega_0$$

Substituting this into the general equation of motion can be rewritten as:

$$m\ddot{x} + \xi\,2m\omega_0\dot{x} + kx = p(t)$$

Dividing this equation by m gives:

$$\ddot{x} + \xi\,2\omega_0\dot{x} + \frac{kx}{m} = \frac{p(t)}{m}$$

Now, squaring the expression of the natural frequency of the system ω_0 we can express the spring stiffness in the angular velocity:

$$\omega_0 = \sqrt{\frac{k}{m}} \;\rightarrow\; \omega_0{}^2 = \frac{k}{m} \;\rightarrow\; k = \omega_0{}^2\,m$$

The final expression of the equation of motion is given by the following expression:

$$\ddot{x} + \xi\,2\omega_0\dot{x} + \omega_0{}^2\,mx = \frac{p(t)}{m}$$

As mentioned before, the force spectrum (PSD) describes the actual aerodynamic forces exerted on the structure. The structure's response depends on its resonant characteristics which must be accounted for via the mechanical admittance function. The final result of the technique gives the spectrum of displacements.

The solution of the differential equation above naturally depends on the excitation of the system, and analytical solutions for the special cases where $f(t) = 0$, or where $f(t)$ is some harmonic function. This is given by Erwin Kreyszig [17]. This thesis deals with arbitrary non-periodic excitation functions. In such cases, the response of the system could be calculated in the frequency domain using the frequency response function, $H(j\omega)$, or in the time domain using the impulse response function $h(t)$.

From the equation of motion, the following mechanical admittance function $H(j\omega)$ can be given for the SDOF dynamic system:

$$H(j\omega) = \frac{1}{m(\omega_0^2 - \omega^2) + i\omega\xi}$$

Where:

- $j\omega$ is the frequency of the response [rad/s].

It is useful to mention that the complex admittance function $H(j\omega)$ is the inverse of the impedance function. The frequency response characteristics of a system are obtained from the mechanical

admittance function by replacing $j\omega$ by s. The Bode plot will be created using MATLAB, see Annex A for the script. The Bode plot is given in the Figure 9.2.9.
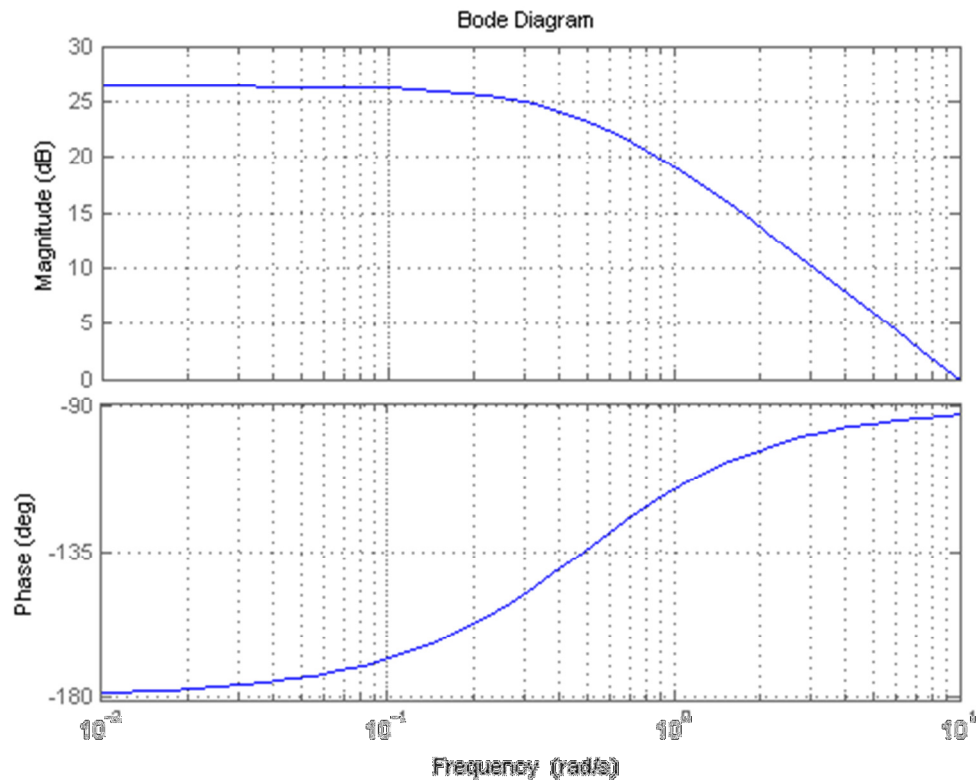
Figure 9.2.9. Bode plot of the structural system

Magnitude response:

- Low-frequency asymptote ($\omega \rightarrow 26$), flat
- Breakpoint at $\omega = a$
- High frequency asymptote +10 dB/decade

Phase response:

- Low frequency asymptote = $-180°$
- $-135°$ at breakpoint ($\omega = a$)
- High frequency asymptote = $-90°$

In this specific case the magnitude slowly decreases as the frequency increases up to a frequency of 0.2. From this point the magnitude decreases rapidly to 0. The phase-angle plot starts at $-180°$ at the low-frequency asymptote and increases to $-90°$ at the high-frequency asymptote.

Having gained more insight into the behaviour of the system allows the usage of MATLAB again to draw the graph of the frequency response of the mechanical admittance function, which will be used when determining the PSD of displacements from the PSD of wind forces. The PSD of displacements (S_{aa}), is simply the PSD of wind forces (S_{ff}) times the admittance function ($|H(j\omega)|^2$).

The square admittance function can thus be derived as such:

$$|H(j\omega)|^2 = H \cdot H^* = \frac{1}{m(\omega_0^2 - \omega^2) + j\omega\xi} \cdot \frac{1}{m(\omega_0^2 - \omega^2) - j\omega\xi} = \frac{1}{m^2(\omega_0^2 - \omega^2)^2 + (\omega\xi)^2}$$

The maximum of $|H(j\omega)|^2$ is the natural frequency of the construction. To avoid resonance the natural frequency should not be too close to the loading frequency S_{ff}. For $\xi = 0$ the natural frequency is ω_0, for $\xi > 0$ it is a value of ω for which the derivative of $|H(j\omega)|^2$ is equal to 0.

$$\frac{d}{dx}(|H(j\omega)|^2) = \frac{4m^2\omega(\omega_0^2 - \omega^2) - 2\xi^2\omega}{(m^2(\omega_0^2 - \omega^2)^2 + (\omega\xi)^2)^2} = 0$$

$$\Rightarrow 4m^2\omega(\omega_0^2 - \omega^2) - 2\xi^2\omega = 0$$

$$\Rightarrow \omega = 0 \lor \omega = \pm\sqrt{\omega_0^2 - \frac{\xi^2}{2m^2}}$$

The derivative of $|H(j\omega)|^2$ is positive for $\omega > 0$ and negative for $\omega > \omega_1 = \sqrt{\omega_0^2 - \frac{\xi^2}{2m^2}}$, so the natural frequency is ω_1. See Figure 9.2.10. Note that $\omega_0 = 58.17$, $\xi \leq 1$, and $m = 47.2$. The term $\frac{\xi^2}{2m^2}$ is smaller than 1, while $\omega_0^2 \approx 3384$. Therefore the natural frequency's dependency on ξ is negligible.
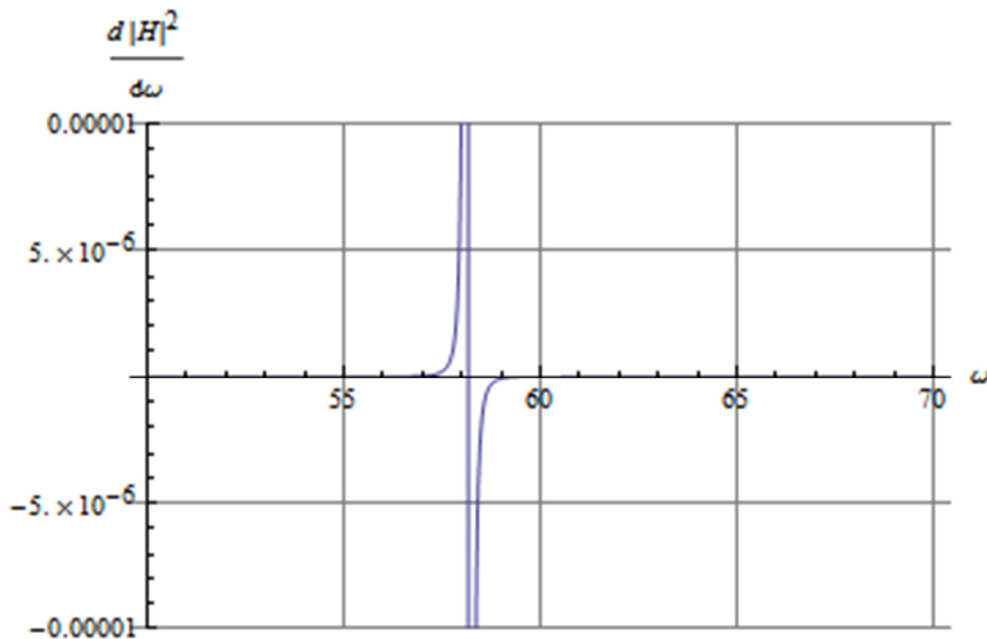
Figure 9.2.10: Plot of the derivative of the square admittance for $\xi = 0.01$.

The obtained PSD of the squared mechanical admittance function is shown in Figure 9.2.11. This graph shows the peak of the response which is the natural frequency of the system. The admittance function may be seen as the dynamic amplification factor, or dynamic magnification factor. It clearly shows that the natural frequency of the system is between 9 Hz and 10 Hz.
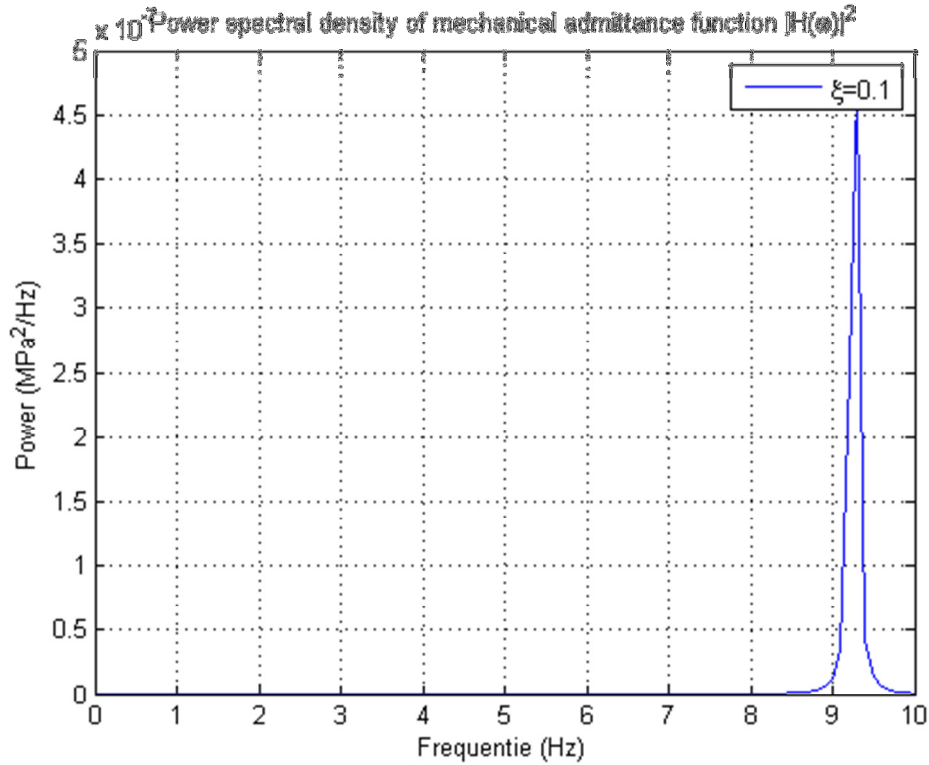
Figure 9.2.11: Power spectral density function of the absolute value squared of the mechanical admittance function obtained from MATLAB

9.2.6. Power spectral density function of the displacements

For a SDOF system, the PSD of the structural displacements can be computed as a product of the PSD of the stochastic loading $S_{ff}(\omega)$ and the complex mechanical admittance function $H(j\omega)$ as shown in the following expression:

$$S_{aa}(\omega) = |H(j\omega)^* \cdot H(j\omega)| \cdot S_{ff}(\omega)$$

Where:

- $H(j\omega)^*$ is the conjugated value of $H(\omega)$, can also be given as: $\overline{H(j\omega)}$

The absolute value of $H(j\omega)^*$ is the same as the absolute value of $H(j\omega)$. Rewriting the expression of the PSD of the structural displacements gives:

$$S_{aa}(\omega) = |H(j\omega)|^2 \cdot S_{ff}(\omega)$$

The power spectral density of the response of the structure can be obtained by multiplying the power spectral density of wind forces by the squared mechanical admittance function, see Figure 9.2.12. The area under the spectrum represents the variance of the response (displacements) of the structure as a result of the wind load. In contrast to a structure that reacts completely static, a peak is added in this spectrum.
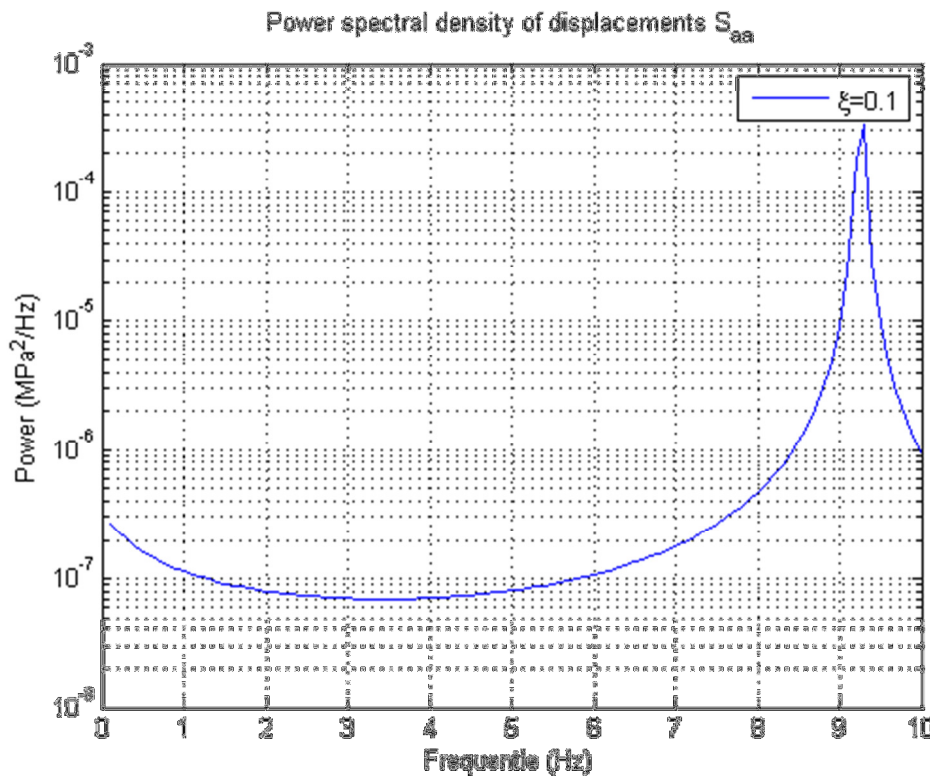
Figure 9.2.12 Power spectral density function of the displacements obtained from MATLAB

9.2.7. Comparison of the frequency of the loading and the response

To be able to compare the natural frequency and the frequency of the loading to each other, the relative values are considered. In Figure 9.2.13 the relative values have been taken to be able to see the natural frequencies, which are invariant through vertical scaling. The goal is to Figure out at which frequencies peaks are present, making the degree of vertical scaling irrelevant.
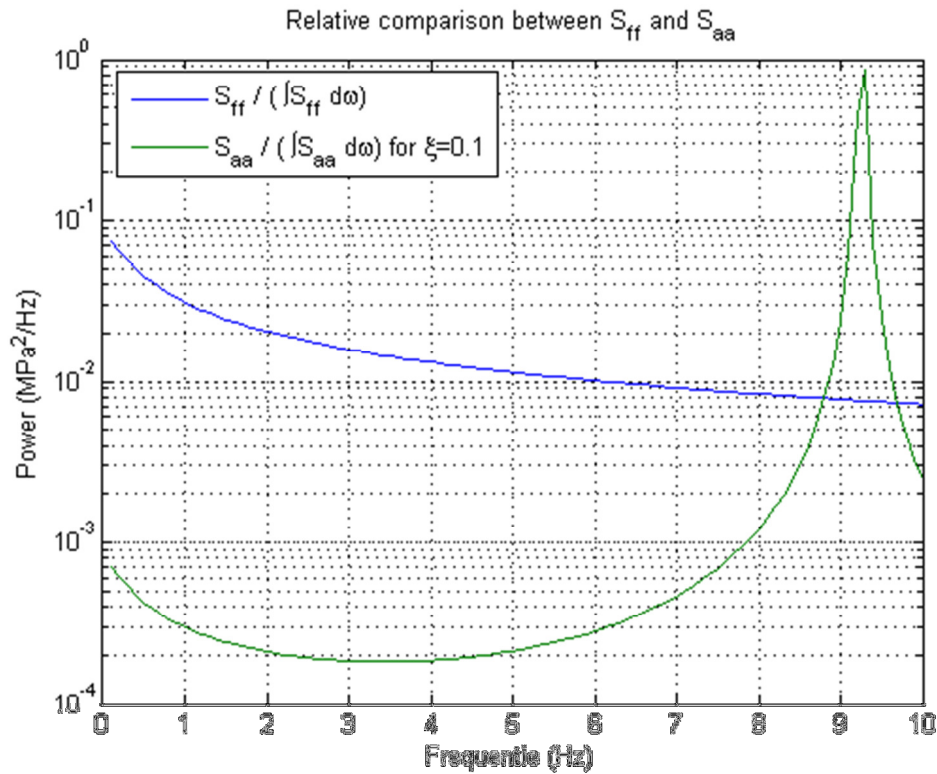
Figure 9.2.13: Comparison of the power spectral density function of the loading Sff and the respons Saa obtained from MATLAB

9.2.8. Power spectral density function of the stresses

Now, the goal is to obtain the PSD of stresses from the PSD of displacements. To be able to do this a multiplication factor is derived from two equations. The derivation is given below.

The determination of the multiplication factor between PSD of displacements and PSD of stresses

Structure properties

- Young's modulus E $70\,000\ MPa$;
- Second moment of inertia I $47261600\ mm^4$;
- Section modulus W $370099\ mm^3$;
- Length l $4000\ mm$.

The following expressions will be used describing the multiplication factor:

$$1 \rightarrow \quad u = \frac{F \cdot l^3}{3 \cdot E \cdot I} \quad \rightarrow \quad F = \frac{3 \cdot u \cdot E \cdot I}{l^3}$$

$$2 \rightarrow \quad \sigma = \frac{M}{W} = \frac{F \cdot l}{W}$$

Substituting 1 into 2 leads to:

$$3 \rightarrow \quad \sigma(u) = \frac{M}{W} = \frac{3 \cdot u \cdot E \cdot I}{l^2 W}$$

Filling in the structure properties gives:

$$\sigma(u) = \frac{3 \cdot u \cdot (70\,000\ \cdot 47261600)}{4000^2 \cdot 370099} = 3 \cdot u \cdot \frac{3308312}{5921584} = u \cdot 1.7\ (N/mm^2)/m$$

$$= u \cdot 1.7 \cdot 10^6 (N/m^2)/m$$

Assuming a linear relationship between the displacements and the stresses of the structure [18], the following expression to calculate the PSD of stress can now given by:

$$S_{\sigma\sigma}(\omega, \bar{u}) = \sigma(u)^2 \cdot S_{aa}(\omega, \bar{u})$$

9.2.9. Dirlik's formulation

From the PSD of stresses $S_{\sigma\sigma}(\omega, \bar{u})$, the number of stress cycles of range σ $[N/mm^2]$ expected in time T $[sec]$ can be determined using Dirlik's formula. This section describes the approach of Dirlik for computing fatigue life, or damage, directly from the PSD of stress as opposed to a time history. Based on extensive Monte-Carlo Simulations, Dirlik derived an empirical formula which allows for PDF estimations of stochastic processes. It defines the stress-range probability distribution as a function of the first four main spectral moments, (m_0, m_1, m_2 and m_4) of the power spectral density function [12]. The mean error in fatigue damage is typically better than 10%. The moments are considered in section 10.2.11. meaning of the moments is as follows:

4. n=0, 0th-orde moment = expectation;
5. n=1, 1st-orde moment = mean;
6. n=2, 2nd-orde moment = standard deviation;
7. n=3, 3rd-orde moment = skewness parameter;
8. n=4, 4th-orde moment = peaked of parameter.

The approximation of the probability density function of rain flow ranges σ is given in the following expression, it consists of an exponential density function and two Rayleigh functions:

$$p(\sigma) = \frac{\frac{D_1}{Q} \cdot e^{\frac{-Z}{Q}} + \frac{D_2 \cdot Z}{R^2} \cdot e^{\frac{-Z^2}{2 \cdot R^2}} + D_3 \cdot Z \cdot e^{\frac{-Z^2}{2}}}{2 \cdot \sqrt{m_0}}$$

Five parameters, namely D_1, D_2, D_3, Q, and R, in the probability density function are determined by imposing the normalization on $p(\sigma)$, by finding the "best fit" of this assumed probability function with that from extensive simulations. This procedure leads to the following empirical relationships between the density parameters and the spectral moments of the original stress process [19]. The empirical factors are given in table 9.2.2 .

Table 9.2.2: Empirical factors of Dirlik's formula

$D_1 = \dfrac{2 \cdot (x_m - \gamma^2)}{1 + \gamma^2}$	$D_3 = 1 - D_1 - D_2$	$R = \dfrac{\gamma - x_m - D_1{}^2}{1 - \gamma - D_1 + D_1{}^2}$
$D_2 = \dfrac{1 - \gamma - D_1 + D_1{}^2}{1 - R}$	$Q = \dfrac{1.25 \cdot (\gamma - D_3 - D_2 \cdot R)}{D_1}$	

The dimensionless mean frequency is defined by Dirlik as: $x_m = \dfrac{m_1}{m_0} \cdot \sqrt{\dfrac{m_2}{m_4}}$ and Z is a normalized variable equal to: $Z = \dfrac{\sigma}{2 \cdot \sqrt{m_0}}$

Two of the most important statistical parameters are the number of so-called zero crossings and number of peaks in the signal which will be used for determining the irregularity factor γ. Figure 9.2.14 shows a 1 second piece cut out from a typical wind band signal.
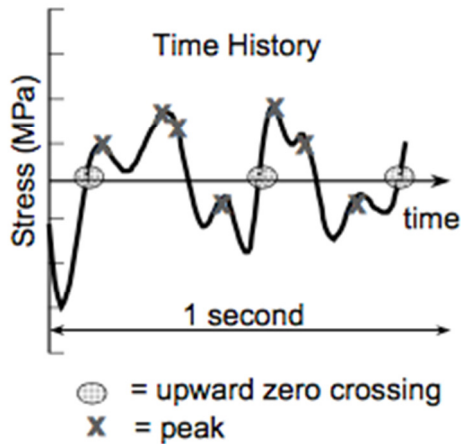
Figure 9.2.14: Zero and peak crossings

SO Rice developed the very important relationships for the numbers $E[0]$ and $E[P]$. $E[0]$ represents the expected number of (upward) zero crossings, or mean level crossings for a signal with a non-zero mean. $E[P]$ represents the expected number of peaks in the same sample. The expected number of mean crossings per second and the expected number of peaks are expressed using following formulas [20]:

$$E[0] = \sqrt{\frac{m_2}{m_0}} \quad and \quad E[P] = \sqrt{\frac{m_4}{m_2}}$$

The irregularity factor is defined as the expected number of upward zero crossings divided by the expected number of peaks, as shown in the following formula:

$$\gamma = \frac{E[0]}{E[P]} = \frac{m_2}{\sqrt{m_0 \cdot m_4}}$$

Moments from a PSD

Since we are concerned with structural systems analysed in the frequency domain, a method is required for extracting the PDF of rainflow ranges, directly from PSD of stress. The characteristics of the PSD that are used to obtain this information are the nth moments of the PSD function (Figure 9.2.14). The relevant spectral moments are easily computed from the following expression:

$$m_n = \int f^n G(f) \cdot df = \int \left(\frac{\omega}{2\pi}\right)^n S_{\sigma\sigma}(\omega, \bar{u}) \, d\omega$$

Using MATLAB the integral will be solved numerically. Numerical integration consist of finding numerical approximation for the value S (the area under the curve) as shown in Figure 9.2.15. The integrals are approximated with the composite trapezoidal rule which is described below.
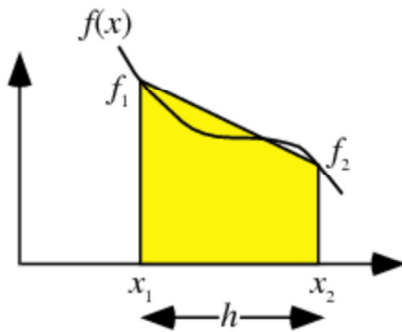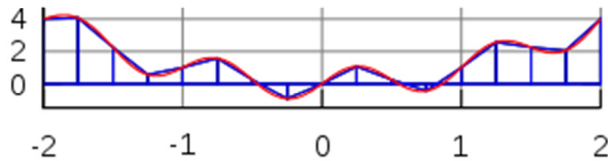
Figure 9.2.15: area under the curve

Figure 9.2.16: Illustration of the trapezoidal rule.

Integration can be approximated by a weighted summation of function values. The interval of integration is divided in small subintervals. In each of these subintervals the surface under the graph is approximated by the surface of a rectangle with a width equal to the interval length. The accuracy of the approximation depends on your choice of the length of the rectangle, which should depend on the function values within the interval. One approximation is the trapezoidal rule, in which the length of the rectangle is the average of the function values on the boundaries of the interval. Hence on the interval $[x_1, x_2]$ the approximation of the surface under the graph is given by [21]:

$$A = (x_2 - x_1) \frac{f(x_1) + f(x_2)}{2}$$

Where:

- $x_1 = lower\ bound\ value;$
- $x_2 = upper\ bound\ value;$
- $f(x), h = seperation\ between\ the\ points$

The composite trapezoidal rule used on a grid of equidistant points $(x_1, x_2, \dots, x_N)$ yields the following approximation for an integral [21]:

$$\int_a^b f(x)\ dx \approx \sum_{n=1}^{N-1} \Delta x \frac{f(x_n) + f(x_{n+1})}{2} = \Delta x \left(-\frac{f(x_1)}{2} - \frac{f(x_N)}{2} + \sum_{n=1}^{N} f(x_n) \right)$$

Number of stress cycles

Now, using the following expression, the number of stress cycles of range $\sigma\ [N/mm^2]$ expected in time $T\ [sec]$ can be determined.

$$N(\Delta\sigma, u) = E[P] \cdot T \cdot p(\sigma)$$

9.2.10. Weibull distribution function

The final step is to combine the stress range spectra expected in time T with a stress range spectra for the life-time of the structure. As mentioned in the literature survey (Annex B) and [12], the stress range spectra for the life-time of the structure can be computed using the following expression:

$$N(\Delta\sigma)_{Life} = \int_0^{\bar{u}} \frac{T_{Life}}{T_{ref}} \cdot f(\bar{u}) \cdot N(\Delta\sigma, u) du$$

In this formula the Weibull probability distribution function is included, namely $f(\bar{u})$. For a life-time assessment of wind excited structural responses, the usual wind conditions with lower velocities has to be taken into account. The frequency distribution of the natural wind flow at a specific location can be well approximated by the two parametric density function of the Weibull distribution. These two parameters are determined from the European Wind Atlas [22]. The Weibull distribution function is given by the following expression [15]:

$$f(\bar{u}) = \frac{k}{A} \cdot \left(\frac{\bar{u}}{A}\right)^{k-1} \cdot e^{-\left(\frac{\bar{u}}{A}\right)^k}$$

- $f(\bar{u})$ is the probability of observing mean wind speed;
- $\bar{u}$ is the mean wind speed [m/s];
- A is the scale parameter, this determines the scale of the curve which is in this case **5.6 m/s**;
- k is the shape parameter (also known as the Weibull slope): This parameter determines the shape of the distribution which is in this case **1.83**.

The Weibull power spectral density function for the specific location of the noise barriers is given in Figure 9.2.17.
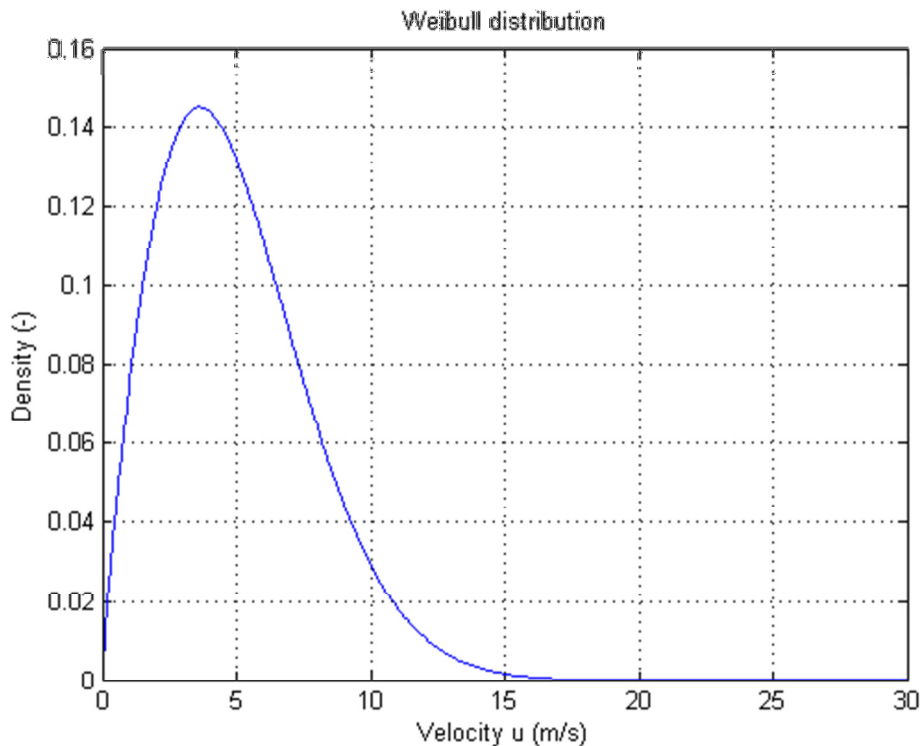

Figure 9.2.17: The Weibull power spectral density function

It should be mentioned that the Weibull function only takes the magnitude of the wind speed into account and ignores the wind direction.

According to Figure 9.2.17, the following aspects of the wind speed at the location can be determined, namely:

- The probability for wind speed 0 m/s is very small, this is typical for the Weibull distribution function;
- The probability becomes larger up to a maximum. At this point, the wind speed is approximately 4 m/s;
- From the maximum the probability decreases for high wind speeds.

9.2.11. The total amount of stress cycles

The expected total amount of stress cycles can be determined using the following formula:

$$N(\Delta\sigma)_{Life} = \int_0^{\bar{u}} \frac{T_{Life}}{T_{ref}} \cdot f(\bar{u}) \cdot N(\Delta\sigma, u) du$$

The graph for the total number of cycles which is obtained by MATLAB is shown Figure 9.2.18.

Figure 9.2.18: The Weibull power spectral density function
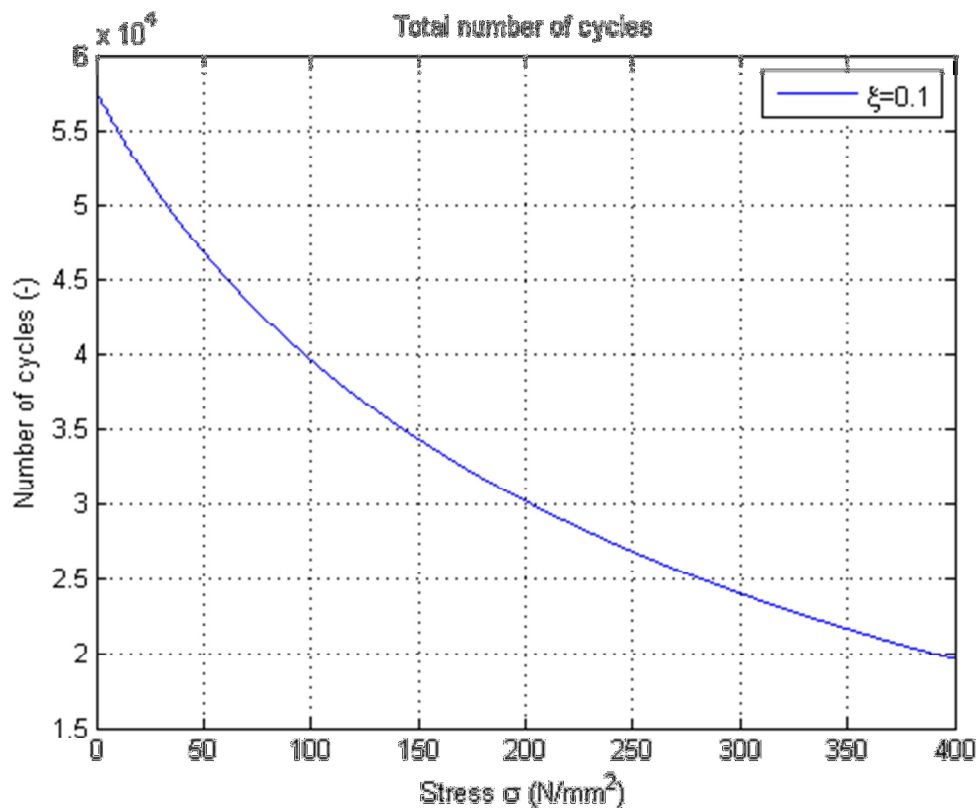
As given in this graph, the number of cycles decreases if the stress increases. This corresponds to the graphs which are given in the static analysis, section 8.6.2. The stress cycles for the same values of α (as in the static analysis) are determined using MATLAB. The total damage of steel and aluminium according to the different analyses is given in table 9.2.3.

Table 9.2.3: Comparison between the different analyses

Comparison between the different analyses

NEN-EN 1991-1-4	α	GCW-2012	Stress bolt	Resistance Steel	Resistance Aluminium
1	1	1	163	27079	8123
8	0.85	6	138	44623	13387
48	0.73	60	118	71376	21413
350	0.60	600	98	124601	37380
2 800	0.48	6 000	73	301463	90438
350 000	0.26	60 000	42	1582906	474871
120 00 000	0.12	600 000	18	234186898	70256069
120 00 00 000	0.05	6 000 000	5	infinite	infinite

DAMAGE EUROCODE		DAMAGE GCW-2012		DAMAGE DYN. ANALYSIS	
Steel	**Aluminium**	**Steel**	**Aluminium**	**Steel**	**Aluminium**
3.69283E-05	0.000123094	3.69283E-05	0.000123094	0.05589769	0.19635030
0.000179277	0.000597589	0.000134458	0.000448192	0.05173416	0.18172449
0.000672487	0.002241625	0.000840609	0.002802031	0.04777254	0.16764289
0.002808945	0.009363149	0.004815334	0.016051113	0.03700700	0.14922562
0.009288029	0.030960096	0.019902919	0.066343062	0,02358108	0.12937972
0.221112274	0.737040912	0.037904961	0.126349871	0,01227687	0.08283223
0	0.170803748	0	0.008540187	0	0.04329211
0	0	0	0	0	0

Total damage

0.23409794	0.951130214	0.063635209	0.220657551	0.22826934	0.95044736

Conclusion: Steel satisfies the following condition:

$$\sum \frac{n_i}{N_i} < 1.0 \rightarrow 0.23 < 1.0$$

Conclusion: Also the aluminium satisfies the following condition:

$$\sum \frac{n_i}{N_i} < 1.0 \rightarrow 0.95 < 1.0$$

9.2.12. Comparison of the static and dynamic analysis

Now, according to table 9.2.3 it is possible to compare the different analyses with each other. Once again, the obtained damages from the analyses are given below.

- GCW-2012 [5]   Steel: 0.06   Aluminium 0.22
- NEN-EN 1991-1-4 [1]   Steel: 0.23   Aluminium 0.95
- Dynamic analysis   Steel: 0.23   Aluminium 0.95

It is clearly shown that there is no difference obtained of the damage between the method given by NEN-EN 1991-1-4 [1] and the dynamical analysis. However, a difference around 75% is obtained between the method given in GCW-2012 [5] and the other two methods that are considered.

Now, based on the static and dynamic analysis the questions given in the problem statement can be answered. The main question will be considered at the end of this report after comparing the steel and aluminium jams. The three sub-questions will be answered below.

Sub-questions from the problem statement

How do the frequencies of the stress responses of the structure relate to the frequencies of the dynamic wind loads?

This is shown in Figure 9.2.13. In this Figure it is clearly shown that the frequency of the stress response of the structure varies from the frequency of the dynamic loading.

How to the dynamic- and statistical fatigue calculations compare, and what is the reliability of the methods?

The dynamic analysis also takes the dynamical properties of the specific structure into account. It is mentioned in NEN-EN 1991-1-4 [1] that this static analysis also takes some of the dynamical properties of structures into account, but it should be mentioned that this method cannot universally determine these dynamic properties for each structure. This static analysis has determined the contribution of dynamics based on different dynamical analysis of structures.

In GCW-2012 it is mentioned that the fatigue analysis are based on the fatigue analysis given in NEN-EN 1991-1-4 [1]. However, this is in contrast with the different value, which is obtained for the damage check. Because the obtained damage varies too much from the other two methods, there are some doubts about the reliability of this method. The difference was expected according to the conclusion given in section 8.6.7.3.

Based on the obtained damages from the dynamic analysis, the conclusion can be given that the fatigue analysis given in NEN-EN 1991-1-4 [1] has the same accuracy and reliability as the dynamic analysis.

Should it be mandatory for structural engineering to conduct a dynamic analysis, or does it suffice to perform the analysis as described in NEN-EN 1991-1-4 [1]?

In this report, it has been shown that all considered methods satisfy the requirements. However, a difference has been found between the GCW-2012 [5] and the other two methods. When taking the vibration behaviour of the jam into account, the design guide GCW-2012 [5] is obviously unsafe. We can conclude that for these types of structures, structural engineers who use this design guide should conduct a dynamic analysis.

10. Comparison between a noise barrier with a steel and aluminium jam

In this section the following main question, from the problem statement, will be answered:

The problem statement is as follow: is it possible to develop a viable aluminium alternative to replace the steel variant, which has a fatigue life of 50 years?

To answer this question more insight in the steel variant is required. After getting more insight a comparison between the designed aluminium variant and the current steel variant is possible. For this comparison a steel jam with the same conditions will be selected from standard profiles (with the same height, angle, location and loading). In the comparison a special focus will be put on the weight of the jam and the assembly time of the noise barrier.

10.1. The steel variant:

Since the stiffness is the leading factor in the calculation of the jam, the choice for the profile will be made using a simple stiffness calculation.

The structure has a height of 4000 mm, which means that the permissible deflection in the serviceability limit state (SLS) according to GCW-2012 [5] is given by 4000/150=26.67 mm. The minimum required value of the second moment of area can now calculated using the following expression:

- $\delta_{max} = \dfrac{M_{max} \cdot l^2}{8 \cdot E \cdot I} = \dfrac{2.56 \cdot 4000^4}{8 \cdot 210000 \cdot 15800000} = 24.70 \ mm$

Using steel profile table containing the options for the profiles, the IPE200 profile has been chosen. The shields will be connected to the jams using clamping profiles. The jam will be connected to the footing plate through welding. The weight of a IPE200 profile is equal to 22,9 kg/m, which means that the total weight of the jam without the footing plate and clamping profiles is equal to $22,9 \cdot 4 = 91,6 \ kg$. The system is shown in Figure 10.1.1. The clamping profile is shown in Figure 10.1.2. The assembly thereof is shown in 10.1.3 – 10.1.8.
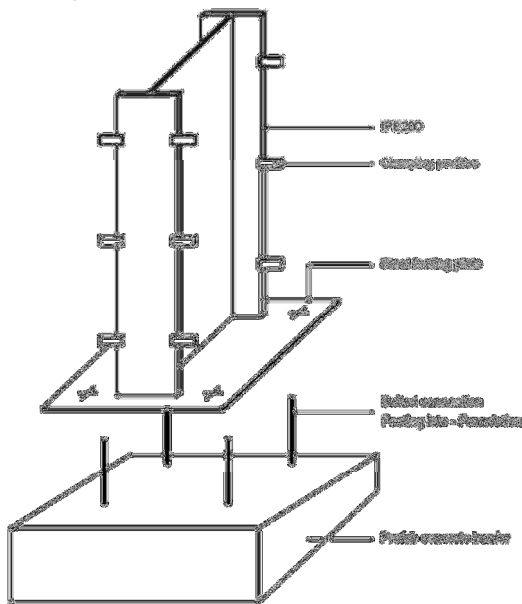

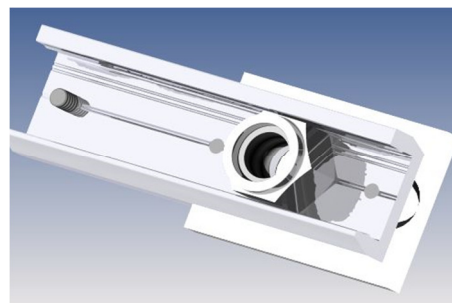*Figure 10.1.1: Principle steel variant*

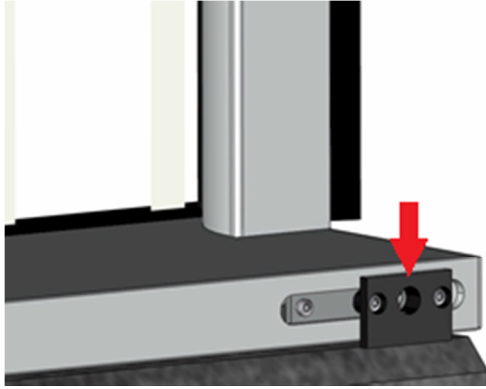*Figure 10.1.2.: 3D clamping profile*

Figure 10.1.3: clamping profile

Figure 10.1.4: clamping profile

The jams are delivered with a clamping profile which comes with a block (made of plastic, nylon, or glass) which is placed between the post and the jam as shown in Figure 10.1.3. One side of this block is attached to the clamping profile, the other side can move freely. The steel jams have a hole to attach the post to the jam using the bolt as shown in Figure 10.1.4.

Figure 10.1.5: clamping profile

Figure 10.1.6: clamping profile

The following components are required to attach the clamping profiles to the jams: Nylon ring M12, stainless steel A4 ring M12, and a stainless steel A4 bolt M12X50, as shown in Figure 10.1.5. The posts contain slots which allow the assembler to reach the screw in the clamping profile as shown in Figure 10.1.6.
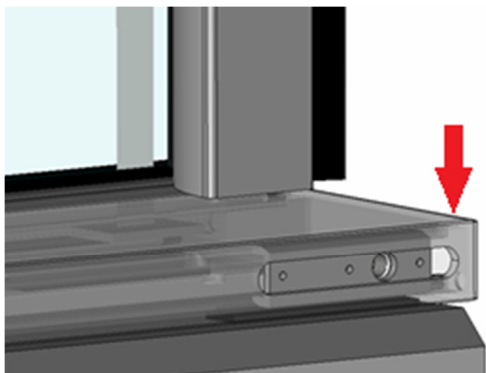
Figure 10.1.7: clamping profile

Figure 10.1.8: clamping profile
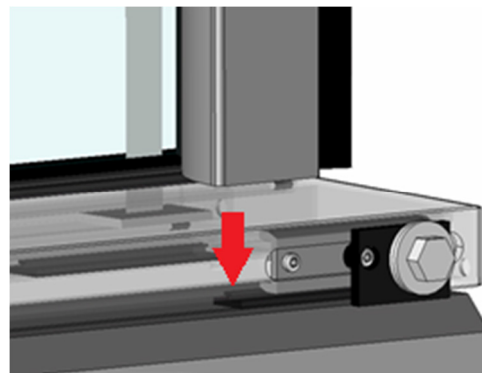
Plastic profiles (caps) are placed at each end of the aluminium posts. These profiles are equipped with drainage holes, this is visible in Figure 10.1.7.

In Figure 10.1.8 EPDM blocks with a length of 100mm are shown. These are placed between the aluminium posts and the concrete barrier to avoid direct contact. However, these are not closed due to the capillary effect and fluid imbalance.

10.2. Comparison steel and aluminium variant

Table 10.2.1. shows the comparison between the two materials with the focus on the assembly and the total weight of the structure (without the shields).

Table 10.2.1: Comparison between the aluminium and steel variant

	Aluminium variant	Steel variant
Self weight	47.2 kg incl. footing plate	91.6 kg excl. footing plate
Structure elements	Jam, footing plate and concrete barrier	Jam, footing plate, clamping profiles and concrete barrier
Structure shields	Consists only of glass panels	Consists of glass panels with an aluminium frame where the clamping profile will be confirmed
Connection between jam and shields	No connector needed	Clamping profiles needed
Connection between jam and footing plate	Bolts, which can easily be attached to the screw tubes.	Welding technique needed
Crane required for connecting jam to concrete barrier?	The jam's light dead load (less than 50kg) allows the jam to be installed manually at the construction site.	Heavy weight, crane required
Assembly time and location of the connection between the jam and concrete barrier	Location: in fabric (total weight less than 50 kg, no installation required on site) which allows for quick assembly on site. On site the jam needs to be attached to the concrete barrier by using nuts.	Location: fabric or on site, preferably fabric because welding is an intensive, sensitive, and slow process.
Assembly time of the connection between the jam and the shields	It is possible to slide the glass-panels in the profile without using any connecting elements, which makes a quick assembly time possible.	First the gaps will be made in the jam after which the shields, where the clamping profile is placed in the posts of the shields, will be attached to the jams. Which is a slow process.

Conclusion

Now, we are able answer to answer the main question of the problem statement which is given above, namely:

Is it possible to develop a viable aluminium alternative to replace the steel variant, which has a fatigue life of 50 years?

It is clearly shown in table 10.2.1 that the aluminium variant is more attractive based on the assembly time and the self-weight of the structure. The fatigue life-time is extensively discussed in the statistical and dynamic analysis. In these analyses it is shown that the structure meets the requirement of a fatigue life of 50 years.

11. Recommendations

GAUSSIAN DISTRIBUTION FUNCTION

In this research the mean wind velocity is selected to make the comparison between the static and dynamic analyses possible. The standard deviation is determined from the KNMI data base with the available wind measurements. To get a more accurate damage check for a location, it should be noted that the usage of measured wind speeds at location and additionally a check whether these measurements are Gaussian distributed is required.

THE CONSIDERED α-FACTORS

The considered α factor in this research is taken from the design guide of noise barriers (GCW-2012 [5]). However, no validation of the reliability of this value are available. Considering other α factors will lead to a different damage of the structure. Thus, more research is required in order to verify the reliability of these factors.

MULTIPLICATION FACTOR BETWEEN THE PSD OF DISPLACEMENTS AND THE PSD OF STRESSES

The multiplication factor is based on the structural properties of the structure. According to [18] a linear relationship between the displacements and the stresses is assumed. Because of the weak underpinnings in several papers, more research is required for determining the PSD of stresses from the PSD of displacements.

DIRLIK'S FORMULA

The formula of Dirlik is given in many papers. However, a universal approach for this method is still missing. There is no information given, except for the fact that it is sufficient and most accurate for loads which follow a normal distribution, about the calculation methods which can be used to calculate Dirlik's formula. Also boundry conditions are missing for this method. From an other MATLAB script [23] an attempt was made to gain as much as possible explanations about the methods to derive the unknowns for Dirlik's formula. It seems that this is done in a proper way, but in order to make this method clear for other cases a universal script or approach is required.

12. Bibliography

In this section the list of literatures 12.1 and the list of the Figures 12.2. is shown which are used during this research.

12.1. List of Literature

[1]   NEN-EN 1991, including national Annex, December 2011;

[2]   NEN-EN 1992, including national Annex, December 2011;

[3]   NEN-EN 1993, including national Annex, December 2011;

[4]   NEN-EN 1999, including national Annex, December 2011;

[5]   I.W. Koster (2012), *richtlijnen geluidbeperkende constructies langs wegen (GCW-2012)*, CROW;

[6]   Dirlik, T. (1985). *Application of computers in fatigue analysis.* Department of Engineering. Coventry: University of Warwick.

[7]   The Aluminum Association, Incl. (1998, 12). *Aluminum Alloys.* Retrieved 03 12, 2015, rom www.calm-aluminium.com.au: http://www.calm-aluminium.com.au/documents/aluminium-alloy.pdf

[8]   Fastenal Engineering & Design Support. (2009, 04 03). *Corrosion & Corrosion Resistance.* Retrieved 09 21, 2015, from www.fastenal.com: https://www.fastenal.com/content/feds/pdf/Article%20-%20Corrosion.pdf

[9]   Maljaars, J. (2008). *Local buckling of slender aluminium sections exposed to fire.* Delft: Netherlands Institute for Metal Research

[10]   Hobson Technical. (2007, 08). *Hex Bolts minimal tensile stress.* Retrieved 03 07, 2015, from www.hobson.com.au: https://www.hobson.com.au/files/technical/htd-hxb-met-properties.pdf

[11]   Menzemer, D. C., Deliwala, J., & Kissel, J. R. (10-2008). *Pull-Out Strength of Self Tapping Fasteners in Aluminum Screw Slot Connections.* University of Akron, Boyer & Lonestar Prestress Mfg, TGB Partnership.

[12]   Kemper, F., & Feldmann, M. (06-2011). *Fatigue life prognosis for structural elements under stochastic wind loading based on spectral methods, Part I: Linear structures .* Institute for Steel Structures . Germany: RWTH Aachen University.

[13]   Bishop, N., & Woodward, A. *Fatigue Analysis of a Missile Shaker Table Mounting Bracket.* RLD Limited, UK and MSC Software, UK, UK.

[14]   iitg.vlab.co.in. (2011). *Free vibration of a cantilever beam (continuous system)*. Retrieved 11 07, 2015, from http://iitg.vlab.co.in/: http://iitg.vlab.co.in/?sub=62&brch=175&sim=1080&cnt=1

[15]   ReliaSoft Corporation. (2002, 04 13). *Characteristics of the Weibull distribution*. Retrieved 05 03, 2015, from www.weibull.com: http://www.weibull.com/hotwire/issue14/relbasics14.htm

[16]   Hembre, J. *Stochastic Analysis of an Offshore Wind Turbine Using a Simplified Dynamic Model.* Norwegian Universirt of Science and Technology, Department of civil and transport engineering. Norwegian Universirt of Science and Technology.

[17]   Erwin Kreyszig. *Advanced Engineering Mathematics*. Willey, New York, 8th edition, 1999.

[18]   Paulissen, J. (2014). *Dynamisch gedrag van verkeersportalen - fase 2.* Delft: TNO innovation for life

[19]   Sun, J.-Q. (2006). *Stochastic Dynamics and Controls.* Amsterdam: Elsevier B.V.

[20]   Bishop, N., & Woodward, A. *Fatigure Analysis of a Missile Shaker Table Mounting Bracket.* UK: RLD Limited, UK and MSC Software, UK.

[21]   Wikipedia. (2015, 12 05). *Numerical integration*. Retrieved 12 20, 2015, from www.en.wikipedia.org: https://en.wikipedia.org/wiki/Numerical_integration

[22]   Riso National Laboratory Denmark. (1989). *European Wind Atlas.* Commision of th European Communities Directorate-General for Science, Research of the Development Brussels, Belgium, Denmark.

[23]   Irvine, T. (2013, 11 08). *Dirlik Rainflow Counting Method from Response PSD*. Retrieved 05 23, 2015, from www.vibrationdata.wordpress.com: https://vibrationdata.wordpress.com/2013/11/08/dirlik-rainflow-counting-method-from-response-psd/

12.2. List of Figures

Figure 5.1.3. The Aluminum Association, Incl. (1998, 12). *Aluminum Alloys.* Retrieved 03 12, 2015, rom www.calm-aluminium.com.au: http://www.calm-aluminium.com.au/documents/aluminium-alloy.pdf

Figure 7.1.2. Woodward, R. (1994). *Aluminium Extrusion: Alloys, Shapes and Properties.* Retrieved 04 08, 2015, from www.core.materials.ac.uk: http://core.materials.ac.uk/repository/eaa/talat/1302.pdf

Figure 7.1.7. Nedal Aluminium. (n.d.). *Extrusion possibilities.* Retrieved 03 08, 2015, from www.nedalextrusion.com: http://www.nedalextrusion.com/e/aluminium-profiles/extrusion-possibilities

Figure 7.1.12. Soetens, F., Maljaars, J., van Hove, B., & Pawiroredjo, F. *Aluminium structural design.* Eindhoven University of Technology, Architecture, Building and Planning. Eindhoven: Eindhoven University of Technology.

Figure 7.1.16. Fastenal Engineering & Design Support. (2009, 04 03). *Corrosion & Corrosion Resistance.* Retrieved 09 21, 2015, from www.fastenal.com: https://www.fastenal.com/content/feds/pdf/Article%20-%20Corrosion.pdf

Figure 7.1.17. Fastenal Engineering & Design Support. (2009, 04 03). *Corrosion & Corrosion Resistance.* Retrieved 09 21, 2015, from www.fastenal.com: https://www.fastenal.com/content/feds/pdf/Article%20-%20Corrosion.pdf

Figure 8.2.1. NEN-EN 1991-1-4, article 7.

Figure 8.6.2. NEN-EN 1991, article 6.

Figure 8.6.4. Maljaars, J. (2008). *Local buckling of slender aluminium sections exposed to fire.* Delft: Netherlands Institute for Metal Research

Figure 8.6.11. Menzemer, D. C., Deliwala, J., & Kissel, J. R. (10-2008). *Pull-Out Strength of Self Tapping Fasteners in Aluminum Screw Slot Connections.* University of Akron, Boyer & Lonestar Prestress Mfg, TGB Partnership.

Figure 8.6.15. NEN-EN 1993-1-9, article 8.

Figure 8.6.16. NEN-EN 1993-1-9, article 7.

Figure 8.6.17. NEN-EN 1991-1-4, Annex B.3.

Figure 9.1.1. Bishop, N., & Woodward, A. *Fatigue Analysis of a Missile Shaker Table Mounting Bracket.* RLD Limited, UK and MSC Software, UK, UK.

Figure 9.1.2. Bishop, N., & Woodward, A. *Fatigue Analysis of a Missile Shaker Table Mounting Bracket.* RLD Limited, UK and MSC Software, UK, UK.

Figure 9.1.3. Bishop, N., & Woodward, A. *Fatigue Analysis of a Missile Shaker Table Mounting Bracket.* RLD Limited, UK and MSC Software, UK, UK.

Figure 9.1.4. Bishop, N., & Woodward, A. *Fatigue Analysis of a Missile Shaker Table Mounting Bracket.* RLD Limited, UK and MSC Software, UK, UK.

Figure 9.1.5. Bishop, N., & Woodward, A. *Fatigue Analysis of a Missile Shaker Table Mounting Bracket.* RLD Limited, UK and MSC Software, UK, UK.

Figure 9.1.6.   Paulissen, J. (2014). *Dynamisch gedrag van verkeersportalen - fase 2.* Delft: TNO innovation for life.

Figure 9.2.1.   iitg.vlab.co.in. (2011). *Free vibration of a cantilever beam (continuous system).* Retrieved 11 07, 2015, from http://iitg.vlab.co.in/: http://iitg.vlab.co.in/?sub=62&brch=175&sim=1080&cnt=1

Figure 9.2.3.   NEN-EN 1991-1-4, Annex B.3.

Figure 9.2.6.   Babuska, R. (2015). Frequency response, and Bode plots. Delft: Centre for systems and control faculty of Mechanical Engineering. Delft University of Technology, The Netherlands

Figure 9.2.8.   Elliott, R. (2000, 04). *Deflection of Beams*. Retrieved 10 11, 2015, from www.clag.org.uk: https://www.clag.org.uk/beam.html/

Figure 9.2.14.   Bishop, N., & Woodward, A. *Fatigue Analysis of a Missile Shaker Table Mounting Bracket.* RLD Limited, UK and MSC Software, UK, UK.

Figure 9.2.15.   Weisstein, Eric W. (2016). *Trapezoidal rule*. Retrieved 02 14, 2016, from www. mathworld.wolfram.com: http://mathworld.wolfram.com/TrapezoidalRule.html

Figure 9.2.16.   Wikipedia. (2015, 12 05). *Numerical integration*. Retrieved 12 20, 2015, from www.en.wikipedia.org: https://en.wikipedia.org/wiki/Numerical_integration

ANNEX A. the MATLAB script

Clear variables and command window

```matlab
% clear variables and command window
clear all
clc
format('long')
```

Input values

```matlab
% input
disp('height z in meters:')
z=input('');
disp('roughness length z0 in meters:')
z0=input('');

% characteristics velocity
vm=17.0; % mean velocity
sigma=3.1; % standard deviation velocity
T=1000; % running time in minutes
TLife=50; % TLife in years

% conversion to seconds
T=60*T;
TLife=TLife*31556926;

% frequency
df=0.1; % sampling frequency
fmax=10; % highest frequency
nf=round(fmax/df);
fmax=nf*df;
f=0:df:fmax;
w=2*pi.*f;
dw=2*pi*df;
nf=nf+1;

% velocity
du=0.1;
umax=30;
nu=round(umax/du);
umax=du*nu;
u=0:du:umax;
nu=nu+1;

% constants from table
ksi=[0.1] %[0.01 0.1 1]; damping ratio
nksi=length(ksi);
kshape=1.83; % shape parameter
A=5.6; % scale parameter
rho=1.25; % density air
cf=2.1; % force coefficient
Area=4; % loaded area
w0=58.17; % angular frequency
m=47.2; % mass
c=159712.9; % stiffness
```

```matlab
% constants for determining Lk
zt=200;
Lt=300;


% dependent variables
Iref=sigma/vm; % turbulence intensity
alpha=0.67+0.05*log(z0);
Lk=Lt*(z/zt)^alpha;
```

Power spectral density of gusts

```matlab
% power spectral density of gusts
Sv=6.8*Lk/(2*pi*vm).*w./(1+10.2*Lk/(2*pi*vm).*w).^(5/3);


% power spectral density of wind force
Sff=(cf*rho*vm*Area)^2.*Sv;
```

Mechnical admittance function

```matlab
% index 1: (angular) frequency, index 2: damping ratio
for k=1:nksi
    for n=1:nf
        H2(n,k)=1/(m^2*(w0^2-w(n)^2)^2+(ksi(k)*w(n))^2); % |H(iw)|^2, in
which H(iw) is the mechanical admittance
        Hangle(n,k)=180/pi*angle(1/(m*(w0^2-w(n)^2)+j*ksi(k)*w(n))); %
phase of H in degrees
        Saa(n,k)=H2(n,k)*Sff(n); % power spectral density of displacements
    end
end
```

Gaussian distribution function

```matlab
% density profile for velocity u
fu=1/sqrt(2* pi* sigma).* exp(-1.*(u-vm).^2./sigma^2);
```

Plots

```matlab
% Svy
figure;
semilogx(f,Sv)
xlabel('Frequentie (Hz)')
ylabel('Power (m^{2}/s*rad)')
title('Power spectral density of wind gusts S_{vv}')
grid on

% Sff
figure;
semilogy(f,Sff)
xlabel('Frequentie (Hz)')
ylabel('Power (MPa^{2}/Hz)')
title('Power spectral density of wind forces S_{ff}')
grid on

% |H(iw)|^2
figure;
plot(f,H2)
xlabel('Frequentie (Hz)')
ylabel('Power (MPa^{2}/Hz)')
title('Power spectral density of mechanical admittance function
|H(\omega)|^{2}')
```

```matlab
% creating legend
for i=1:nksi
    strings(i)={strcat('\xi=',num2str(ksi(i)))};
end
legend(strings)
clear('strings');
grid on

% Saa
figure;
semilogy(f,Saa)
xlabel('Frequentie (Hz)')
ylabel('Power (MPa^{2}/Hz)')
title('Power spectral density of displacements S_{aa}')
for i=1:nksi
    string=strcat('\xi=',num2str(ksi(i)));
% creating legendksi(i)));
    strings(i)={string};
end
legend(strings)
clear('string','strings');
grid on

% density profile of velocity
figure;
plot(u,fu)
xlabel('Velocity u (m/s)')
ylabel('Density (-)')
title('Density profile of velocity')
grid on
```

Relative comparison between the load and the natural frequency

```matlab
% relative Sff and relative Saa
figure;
sumSff=numInt(Sff,dw);
sumSaa=numInt(Saa,dw);
semilogy(f,Sff./sumSff,f,Saa./sumSaa)
title('Relative comparison between S_{ff} and S_{aa}')
xlabel('Frequentie (Hz)')
ylabel('Power (MPa^{2}/Hz)')
clear('sumS_{ff}','sumS_{\sigma\sigma}');
% creating legend
strings=cell(1+nksi,1);
strings(1)={'S_{ff} / ( \int_{}^{}S_{ff} d\omega)'};
for i=1:nksi
    string=strcat('S_{aa} / ( \int_{}^{}S_{aa} d\omega) for
\xi=',num2str(ksi(i)));
    strings(i+1)={string};
end
legend(strings,'Location','best');
clear('string','strings')
grid on
```

Bode plots (two types)

```matlab
% Bode plot of H (not using bode or bodeplot command)
figure;
subplot(2,1,1)
plot(f,sqrt(H2)) % |H|=sqrt(|H|^2)
title('Bode plot of H(i\omega)')
ylabel('|H|')
grid on
subplot(2,1,2)
plot(f,Hangle)
ylabel('Arg(H) [degree]')
xlabel('Frequency [Hz]')
grid on

%% Bode plot H (using bode command)
s=tf('s');
H=abs(1)/(((-w0^2*m)+(s*ksi)+(c)))

bode(H)
grid on
```

Dirlik's approach

```matlab
%% Dirlik
% wind speed Weibull
fuBull= kshape/A.*(u./A).^(kshape-1).*exp(-(u./A).^kshape);
uBullmax=round(vm/du)+1;

% plot
figure;
plot(u,fuBull)
title('Weibull distribution')
xlabel('Velocity u (m/s)')
ylabel('Density (-)')
grid on

m0=zeros(uBullmax-1,nksi);
m1=zeros(uBullmax-1,nksi);
m2=zeros(uBullmax-1,nksi);
m4=zeros(uBullmax-1,nksi);

for i=1:nksi
    for k=2:uBullmax
        m0(k-1,i)=numInt(Sss(:,k,i),dw);
        m1(k-1,i)=numInt(Sss(:,k,i).*f',dw);
        m2(k-1,i)=numInt(Sss(:,k,i).*f'.^2,dw);
        m4(k-1,i)=numInt(Sss(:,k,i).*f'.^4,dw);
    end
end

clear('S_{vv}','S_{ff}','S_{\sigma\sigma}','S_{ss}') % to preserve memory

EP=sqrt(m4./m2);
xm=m1./m0.*sqrt(m2./m4);
gamma=m2./sqrt(m0.*m4);
D1=2*(xm-gamma.^2)./(1+gamma.^2);
R=(gamma-xm-D1.^2)./(1-gamma-D1+D1.^2);
D2=(1-gamma-D1+D1.^2)./(1-R);
D3=1-D1-D2;
```

```matlab
Q=1.25.*(gamma-D3-D2.*R)./D1;


Smax=400;
dS=0.1;
n=round(Smax/dS);
dS=Smax/n;
n=n+1;
N=zeros(n,uBullmax-1,nksi);
S=zeros(n,1);


for i=1:n
    S(i)=(i-1)*dS;
    for k=1:nksi
        for l=1:uBullmax-1
            Z=S(i)/(2*sqrt(m0(l,k)));
%
            t1=(D1(l,k)/Q(l,k))*exp(-Z/Q(l,k));
            a=-Z^2;
            b=2*R(l,k)^2;
%
            t2=(D2(l,k)*Z/R(l,k)^2)*exp(a/b);
            t3=D3(l,k)*Z*exp(-Z^2/2);
%
            pn=t1+t2+t3;
            pd=2*sqrt(m0(l,k));
            p=pn/pd;
%
            N(i,l,k)=p;
        end
        N(i,:,k)=N(i,:,k).*EP(:,k)'.*T;
    end
%
end
```

Total number of cycles

```matlab
% total number of cycles
Ntotal=zeros(n,nksi);
for i=1:n
    for k=1:nksi
        Ntotal(i,k)=numInt((TLife/T)*fuBull(2:uBullmax).*N(i,1:uBullmax-
1,k),du);
    end
end


% plot of number of cycles versus stress
figure;
plot(S,Ntotal)
title('Total number of cycles')
xlabel('Stress \sigma (N/mm^{2})')
ylabel('Number of cycles (-)')
% creating legend
for i=1:nksi
    string=strcat('\xi=',num2str(ksi(i)));
    strings(i)={string};
end
legend(strings)
clear('string','strings');
grid on
```

Numerical integration

```matlab
%%%% Num. Int.

% calculates the integral f(x) dx for x=a to x=b=a+n*dx.
function [fnew]=numInt(f,dx)
    n=length(f);

    % we use the composite trapezoidal rule as an approximation
    % integral f(x) dx = f(x(1))*dx/2+f(x(N))*dx/2+sum(n=2 to n=N-1)
f(x(n))*dx
    % integral f(x) dx = -f(x(1))*dx/2-f(x(N))*dx/2+sum(n=1 to n=N)
f(x(n))*dx
    fnew=-f(1)*dx/2-f(n)*dx/2;

    for i=1:n
        fnew=fnew+f(i)*dx;
    end
end
```

ANNEX B: LITERATURE SURVEY